LBL-2708
c.2

# COHERENCE IN EXCITED TRIPLET STATES OF MOLECULAR CRYSTALS

Michael David Fayer

(Ph. D. Thesis)

RECEIVED
LAWRENCE
RADIATION LABORATORY

JUL 16 1974

LIBRARY AND
DOCUMENTS SECTION

May 1974

Prepared for the U. S. Atomic Energy Commission
under Contract W-7405-ENG-48

TWO-WEEK LOAN COPY

*This is a Library Circulating Copy which may be borrowed for two weeks. For a personal retention copy, call Tech. Info. Division, Ext. 5545*

LAWRENCE BERKELEY LABORATORY
UNIVERSITY OF CALIFORNIA
BERKELEY

LBL-2708
c.2

## DISCLAIMER

This document was prepared as an account of work sponsored by the United States Government. While this document is believed to contain correct information, neither the United States Government nor any agency thereof, nor the Regents of the University of California, nor any of their employees, makes any warranty, express or implied, or assumes any legal responsibility for the accuracy, completeness, or usefulness of any information, apparatus, product, or process disclosed, or represents that its use would not infringe privately owned rights. Reference herein to any specific commercial product, process, or service by its trade name, trademark, manufacturer, or otherwise, does not necessarily constitute or imply its endorsement, recommendation, or favoring by the United States Government or any agency thereof, or the Regents of the University of California. The views and opinions of authors expressed herein do not necessarily state or reflect those of the United States Government or any agency thereof or the Regents of the University of California.

## PREFACE

The following is an excerpt from Werner Heisenberg's book Physics and Beyond which relates a conversation between Heisenberg and Niels Bohr.

> *After we had been looking for possible experimental mistakes for some time, I said to Niels: "Isn't it odd that, throughout this discussion, no one should have mentioned quantum theory? We behave as if the electrically charged particles were an object like an electrically charged oil droplet, or like a pith ball in an old electroscope. We quite unthinkingly used the concepts of classical physics, as if we had never heard of the limitations of these concepts and of uncertainty relations. Isn't that bound to lead to errors?"*
>
> *"No, certainly not," Neils replied. "After all, it is almost the essence of an experiment that the observations can be described with the concepts of classical physics. That is the whole paradox of quantum theory. On the one hand, we establish laws that differ from those of classical physics; on the other, we apply the concepts of classical physics quite unreservedly whenever we make observations, or take measurements or photographs. And we have to do just that because, when all is said and done, we are forced to use language if we are to communicate our results to other people. A measuring instrument is a measuring instrument only when the observations it yields enable us to arrive at*

*unequivocal conclusions about the phenomenon under observation, only when a strict causal connection can be assumed to exist. Yet when it comes to the theoretical description of an atomic phenomenon, we must make a distinction between the phenomenon and the observer or his apparatus. The demarcation line may be subject to choice, but on the observer's side of the split we are forced to use the language of classical physics, simply because we have no other language in which to express the results. We know that the concepts of this language are imprecise, that they have a limited area of application, but we have no other language, and, after all, it does help us to grasp the phenomenon at least indirectly."*

# COHERENCE IN EXCITED TRIPLET STATES OF MOLECULAR CRYSTALS

## Contents


Preface . . . . . iii

Contents . . . . . v

Abstract . . . . . vii

I. Boltzmann Equilibrium Between Exciton States and Single Traps . 1

A. Introduction . . . . . 1

B. Thermal Equilibria between Exciton States and Single Traps 4

C. Exciton Group Velocities and Thermal Equilibrium . . . . . 19

D. The Effects of Multiple Bands . . . . . 26

1. Zero-Field Splitting of the Exciton Band and Trap States . . . . . 26

2. Two and Three Dimensional Bands . . . . . 30

II. Equilibrium between exciton States and Multiple Traps . . . . . 34

A. Boltzmann Equilibrium . . . . . 34

B. Non-Boltzmann Distributions between Exciton and Trap States 44

1. Non-Boltzmann Low Temperature Limit . . . . . 47

2. Non-Boltzmann Intermediate Temperatures . . . . . 50

C. Other Considerations . . . . . 53

D. Qualitative Features of TCB in the Non-Boltzmann Region . . 56

E. Experimental . . . . . 61

III. Decay of Localized States into Delocalized Band States . . . . 65

A. Introduction . . . . . 65

B. Discussion . . . . . 66

C. Experimental . . . . . 68

D. Results . . . . . 72

E. Model for the Decay of Localized States into Delocalized Band States . . . . . 74

F. Conclusions . . . . . 81

G. Summary of Chapters I, II and III . . . . . 85

IV. Coherent Coupling with Feeding and Decay . . . . . 87

A. Introduction . . . . . 87

B. Mathematical Development . . . . . 89

1. Equation of Motion in the Absence of Feeding and Decay . . . . . 92

2. Solution of the Equation of Motion with Decay . . . . 95

3. Inclusion of Entering Population into the Geometrical Representation . . . . . 100

C. Physical Applications . . . . . 108

1. Transient Nutation . . . . . 109

2. The CW Spectrum . . . . . 114

3. Kinetic Coherence . . . . . 117

4. The Optical Case: Long Term Superradiance . . . . . 122

D. Summary of Chapter IV . . . . . 127

Acknowledgements . . . . . 128

Appendix. Computer Programs . . . . . 129

1. Program Traps . . . . . 129

2. Program Deep2 . . . . . 131

3. Program GVELO . . . . . 134

4. Program TWODI . . . . . 136

References . . . . . 138

# COHERENCE IN EXCITED TRIPLET STATES OF MOLECULAR CRYSTALS

Michael David Fayer

Inorganic Materials Research Division, Lawrence Berkeley Laboratory
and Department of Chemistry; University of California,
Berkeley, California 94720

## ABSTRACT

Presented in this thesis are two distinct topics; the effects of coherent Frenkel-exciton migration and exciton detrapping on band-trap equilibria in solids and the coherent coupling of two excited state energy levels by an applied radiation field for a system which undergoes incoherent feeding and decay of population. Both of these topics will be discussed in terms of excited triplet states of molecular crystals, although the considerations presented are quite general.

A model is developed which relates the dynamics of energy migration in crystals to the mechanisms by which thermal equilibrium between delocalized band states and localized trap states is achieved. Central to this model is the requirement that coherent energy migration must be the dominant mode of migration at low temperatures in order to achieve Boltzmann equilibrium between band and trap states within the lifetime of the excited electronic state. The relation between detrapping and the ability of a crystal to achieve thermal equilibrium within the excited-state lifetime is developed and applied to one-dimensional crystals. Experimental results on molecular crystals representing examples of one-dimensional exciton bands are presented. Specifically, the temperature dependence of phosphorescence from excited triplet trap states is interpreted in terms of the above considerations. From these experiments, one can obtain both the sign of the intermolecular

interaction matrix element and the dispersion of the first excited triplet band in addition to an estimate of the coherence length associated with exciton migration in the Frenkel limit.

A technique for measuring the decay of localized excited triplet states into delocalized band states of a solid utilizing the optical detection of electron spin coherence is described. Specifically, the use of optically detected electron spin locking for measuring kinetic phenomena in the presence of fluctuating triplet spin sublevel populations is presented and illustrated. In addition, preliminary experimental data is reported which yields the temperature dependence of the phonon assisted promotion of a localized isotopic excited state to an energy equal to that associated with the energies of the host exciton band. A stochastic model for the detrapping is developed which is based on an irreversible radiationless relaxation process of a phonon-trap intermediate into the density of delocalized band states. Explicit account is taken of trap-phonon interactions in the formation of the excited trap intermediate.

Finally, coherent coupling of two excited triplet spin sublevels by an applied microwave field is treated with the effects due to population entering and leaving the ensemble of excited triplet states included. The problem is set up in terms of the time dependent Schrödinger equation and solved using the Laplace transform technique. The case in which the wavelength of the radiation field is large relative to the sample size is discussed. This is the case which applies to microwave coupling of excited triplet spin sublevels. An interesting new effect is predicted, i.e., it is possible to maintain a coherent

component for extended periods of time, in fact, for times longer than the lifetimes of the excited states involved. This kinetic coherent component is continually replenished by the incoherent feeding process under certain experimental conditions. The extension of this treatment to the optical case is discussed and the possibility of producing long term superradiance is pointed out.

# I. BOLTZMANN EQUILIBRIUM BETWEEN EXCITON STATES AND SINGLE TRAPS

## A. Introduction

In the first three chapters, the relation between energy migration in solids and the populations of localized and delocalized states will be discussed in terms of a model which includes explicit features of the exciton band, the sign of the intermolecular interaction in the nearest neighbor approximation, the number of wave vector states comprising the band, and a mechanism for Frenkel[1] exciton migration in solids including the effects of coherent and incoherent propagation. Although the theoretical and experimental details which will be presented here pertain to the triplet state of molecular solids, identical considerations are also applicable to singlet states and transport phenomena in non-molecular solids. The model will be applied specifically to the temperature dependence of the intensity of trap emission in molecular crystals although the approach is applicable to a wide variety of related problems.

The necessity of considering the above features of exciton migration in solids in a model which attempts to explain some straightforward observations on the temperature dependence of the intensity of the trap states can readily be seen by the paradoxes which are created if exciton dynamics are not treated properly. For illustration consider the simplest case where it is tacitly assumed that the excited states of the host are degenerate and that the different types of traps which may be due either to impurities or crystal lattice defects may be regarded as independent but describable by Boltzmann statistics. The problems

created by this oversimplified treatment can readily be seen. In the absence of intermolecular interactions between an excited host molecule and its unexcited neighbors, an excitation is an isolated molecular state as opposed to a mobile crystal state, and hence it cannot migrate to a trap. The difficulty of this model is not so much in the trivial assumption that the host states are degenerate (i.e., no intermolecular interactions) but in failing to provide the mechanism whereby thermal equilibration between the host and trap states can be achieved which permits the use of Boltzmann statistics.[2] This latter consideration requires that a distinction be made between coherent and incoherent migration insofar as the dynamics of achieving trap-exciton equilibration determine whether or not Boltzmann statistics is a valid assumption. Intermolecular interactions break the degeneracy of the host excited states and produce a band of mobile exciton states with width $4\beta$, where $\beta$ is the intermolecular interaction matrix element. These mobile excitons can migrate between traps in one limit (the low temperature limit) as coherent wave packets whose properties are determined by the wave vectors of the crystals or in another limit (high temperature limit) by a random walk diffusional process characterized by a hopping frequency proportional to the intermolecular interaction.[3] If the migration is rapid, equilibration of the excited state populations can be established among the exciton and trap states within the lifetime of the excited electronic state. The populations of the various energy levels can then be determined using a Boltzmann statistical model. The width of the exciton band and the sign of the intermolecular interaction, the location of the exciton energy levels relative to the trap depth, and the mode of

exciton migration all determine whether or not the equilibrium condition can be established within the lifetime of the state and hence determine the functional form of the temperature dependence of the trap emission. Indeed we shall demonstrate that the measurement of trap phosphorescence, which reflects the triplet trap population, provides a tool capable of investigating the mode of migration in triplet Frenkel excitons in addition to the magnitude and sign of intermolecular interaction $\beta$.

Specifically in the following, the temperature dependence of trap phosphorescence will be discussed using a model which primarily treats the exciton band as one-dimensional although multidimensional bands are considered briefly. A method for determining the exciton band width and the sign of $\beta$ from the trap emission temperature dependence is presented. Systems composed of both single and multiple traps in equilibrium with an exciton band will be considered where the effect of coherent vs random walk exciton migration on the temperature dependence of the trap emission intensity is central to the model. Next we will discuss isotropically mixed crystals where the effects of trapping result in both a Boltzmann equilibration and non-Boltzmann equilibration in different temperature regions. Solutions to the non-Boltzmann steady state between trap and band states also allow a measure of the coherence to be estimated. In addition, a model for the decay of localized states into delocalized band states based on radiationless relaxation is developed
Finally, experimental results on "one-dimensional" molecular crystals will be presented and interpreted in terms of the above considerations. These include optically detected magnetic resonance experiments on trap states in which the electron spin coherence in the rotating frame is used to measure absolute detrapping rates.

B. Thermal Equilibria between Exciton States and Single Traps

The formal features of one-dimensional Frenkel excitons in the absence of phonon exciton coupling are well understood.[4] A finite linear array of n independent molecules in which one molecule of the chain is in an excited electronic state will have an energy $E^o$ corresponding to the "isolated" molecule excited state energy. The system, however, is n fold degenerate, since the excitation may be on any one of the n molecules in the linear array. If the molecules are allowed to interact through a nearest neighbor interaction $\beta$, the degeneracy is destroyed and a band of energies is formed. In the nearest neighbor approximation the energy dependence of the exciton band on the quantum number k which labels the levels is given by

$$E(k) = E_o + 2\beta \cos k\bar{a} \qquad (I.1)$$

where $\bar{a}$ is the distance between translationally equivalent molecules along the axis of delocalization. The quantum number k can take on n values from zero to $\pm\pi/a$ in the first Brillouin Zone giving a band width of $4\beta$.

The temperature dependence of the intensity of trap emission in the temperature region where Boltzmann statistics is applicable can be understood in terms of the partition function, z, for the systems consisting of one excitation found in the trap energy level or in one of the levels of the exciton band. We adopt as a model for "real" one-dimensional crystals, a crystal composed to a set of independent exciton chains, each chain being separated by one or more impurities or trap sites. The gaussian distribution of chain lengths in a crystal is

sharply peaked, and therefore the average length is employed. This is a valid assumption for most bands provided the number of molecules in a chain exceeds ~100. Each chain may be labeled by a set of molecular indicies which specify its location in the crystal and thus make it distinguishable from the other chains in the crystal. This, in addition to the fact that there are many energy levels available to each excitation in the crystal, allows Boltzmann statistics to be employed in writing the partition function provided the trap and band states are in thermal equilibrium. Such a partition function has the form

$$z = 1 + e^{-\Delta/kT} + \sum_{k=\pi/an}^{(n-1)(\pi/an)} 2e^{-(\Delta-2\beta(1-\cos ka))/kT} \quad . \qquad (I.2)$$

The zero of energy is taken at the energy of the trap while the trap depth, $\Delta$, is taken to be the difference in energy between the trap level and the $k = 0$ level of the exciton band in the approximation that the wave vector of the radiation field has zero momentum.[5] This is the depth which can be measured spectroscopically from absorption or emission experiments at low temperatures. The first term in z is simply the Boltzmann factor for the trap level while the second term is associated with the nondegenerate $k = 0$ level of the band. Appart from $k = 0$, k can take on values greater than zero to $\pm\pi/a$, and thus, all non $k = 0$ states in the band are doubly degenerate. If there are (2n) states in the band plus the $k = 0$ state, corresponding to $(2n + 1)$ molecules in a linear chain, then the final term in the partition function is a summation over n doubly degenerate states where k takes on values $\pi/an$, $2\pi/an$, $3\pi/an$ . . . $n\pi/an = \pi/a$. The energy dependence of the band

on quantum number k is given by Eq. (I.1), and the partition function has been written so that the k = 0 level has energy $\Delta$.

In terms of the partition function, z, the probability that an excitation of the system is in the trap is simply

$$P_{trap} = 1/z \quad . \tag{I.3}$$

The intensity of emission, I, from the trap is

$$I_{trap} = K^r_{trap} N_{trap} \tag{I.4}$$

where $K^r_{trap}$ is the radiative rate constant and $N_{trap}$ is the number of trap states populated. If the total number of states excited in the system is $N_{total}$, then

$$N_{trap} = P_{trap} N_{total} \tag{I.5}$$

and

$$I_{trap} = K^r_{trap} N_{total} P_{trap} = K^r_{trap} N_{total} z^{-1} \quad . \tag{I.6}$$

Since $K^r_{trap}$ is essentially temperature independent[6] and the $N_{total}$ is usually constant, the temperature dependence of the trap intensity is determined by the temperature dependence of the normalized trap probability, $P_{trap} = z^{-1}$ which includes explicit features of the band states.

By varying $\beta$ and the number of states in the band while keeping the trap depth $\Delta$ constant, the relationship between the "real" partition function and a partition function using the degenerate approximation for calculating the trap probability can be seen. Two cases arise depending upon the sign of $\beta$ as illustrated in Fig. 1. If $\beta$ is negative the exciton band spans an energy range from $\Delta$, the k = 0 energy, to $\Delta + 4\beta$,

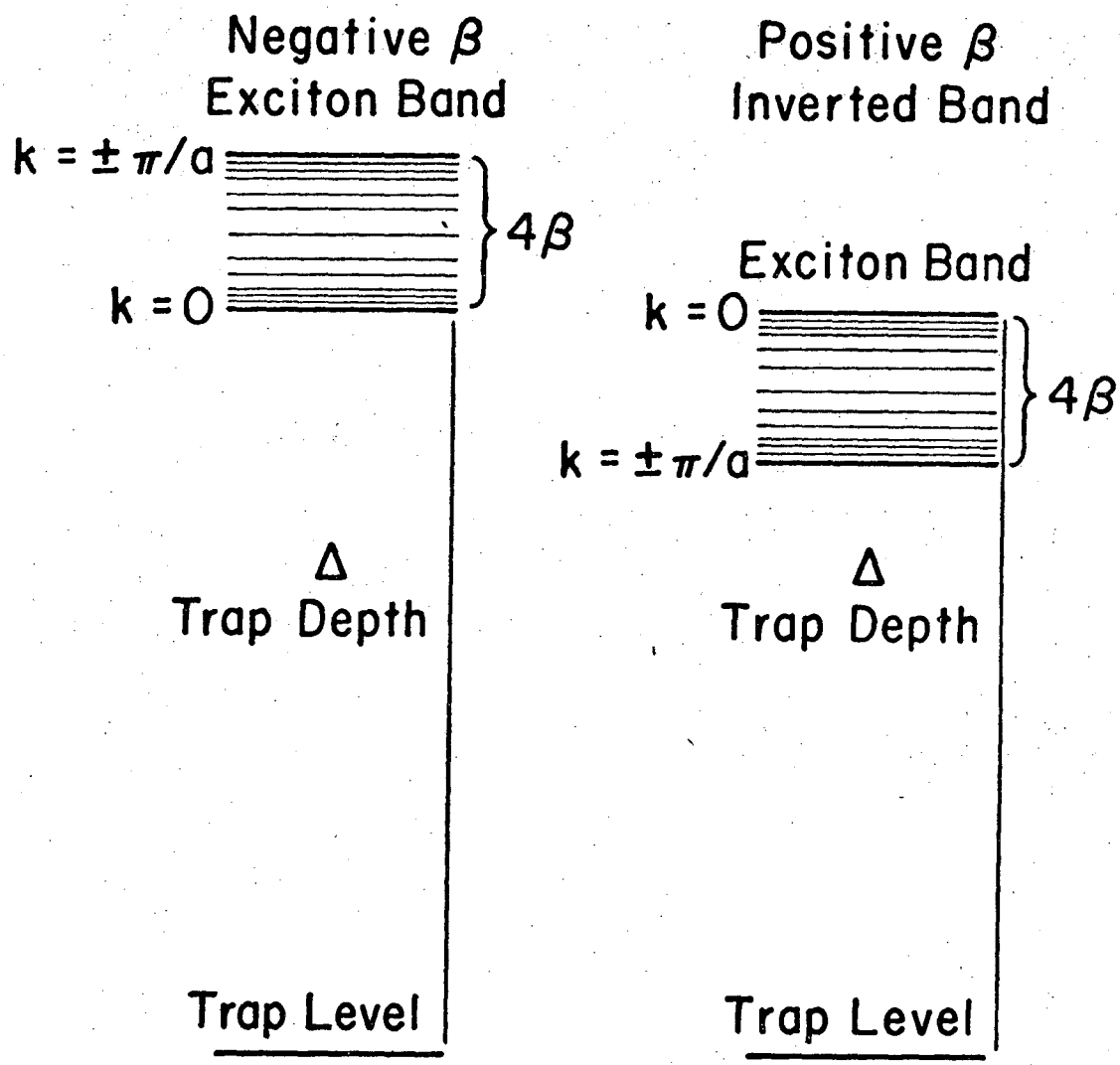


XBL 737-904

Fig. 1. Trap and exciton energy levels for both negative and positive signs of the intermolecular interaction, β. For negative β, the exciton band extends 4β to higher energy than the trap depth Δ, and for positive β the band is inverted and extends 4β to lower energy than Δ.

the $k = \pm\pi/a$ energy. On the other hand, if $\beta$ is positive the band is inverted and it spans an energy range from $\Delta$ to $\Delta - 4\beta$. The approximation that all the states in the band are given the energy of the $k = 0$ state corresponds to the limiting case of a band with zero band width. In cases where $\beta$ is finite however, most states accumulate at the top and bottom of the band where the density of states function for one-dimensional systems[7] is sharply peaked. One might expect a significant effect on the trap emission due to the dispersion of the band, particularly when the band width to trap depth ratio, $4\beta/\Delta$, takes on reasonable values. Such is indeed the case.

Recently 1,2,4,5-tetrachlorobenzene (TCB) and 1,4-dibromonapthalene have been shown to exhibit the properties of one-dimensional excitons. Francis and Harris[8] measured the band width of TCB by an optically detected magnetic resonance experiment[9] and found it to be 1.25 $cm^{-1}$. Hochstrasser and Whiteman[10] in an isotopically mixed crystal experiment measured 1,4-dibromonapthalene band width to be 29.6 $cm^{-1}$. These two values will be used as examples of narrow and broad triplet exciton bands respectively although it should be kept in mind that singlet bands can be one or more orders of magnitude greater in width. In Figs. 2a through 2e the trap probability, $P_{trap}$, vs temperature is plotted for several different negative values of $4\beta$ using the experimental value of $\Delta$ (21.3 $cm^{-1}$) determined for one of the intrinsic traps here after referred to as the X-trap in $H_2$-TCB.[11] In each figure curves resulting from several different ratios of number of states in band to number of traps is plotted. Figure 2a is the degenerate case. Figure 2b uses the small value of $\beta$

Fig. 2. Calculated trap probabilities, which are proportional to trap intensities are shown as a function of temperature for various negative values of $\beta$. The numbers to the right of each set of curves give the number of exciton k states (number of molecules per chain) per trap state used to calculate the curve. The trap depth $\Delta$ used is the tetrachlorobenzene trap depth, 21.3 $cm^{-1}$. (a) illustrates the limiting case of a band with zero width, $4\beta = 0$. (b) uses the band width previously reported for tetrachlorobenzene. (c) and (d) are for intermediate band widths, and (e) is calculated using the reported 1,4-dibromonaphalene band width. As the band width becomes more negative, the energy differences between the trap and states in the band become greater and the temperature dependence of the trap probability becomes more gradual.

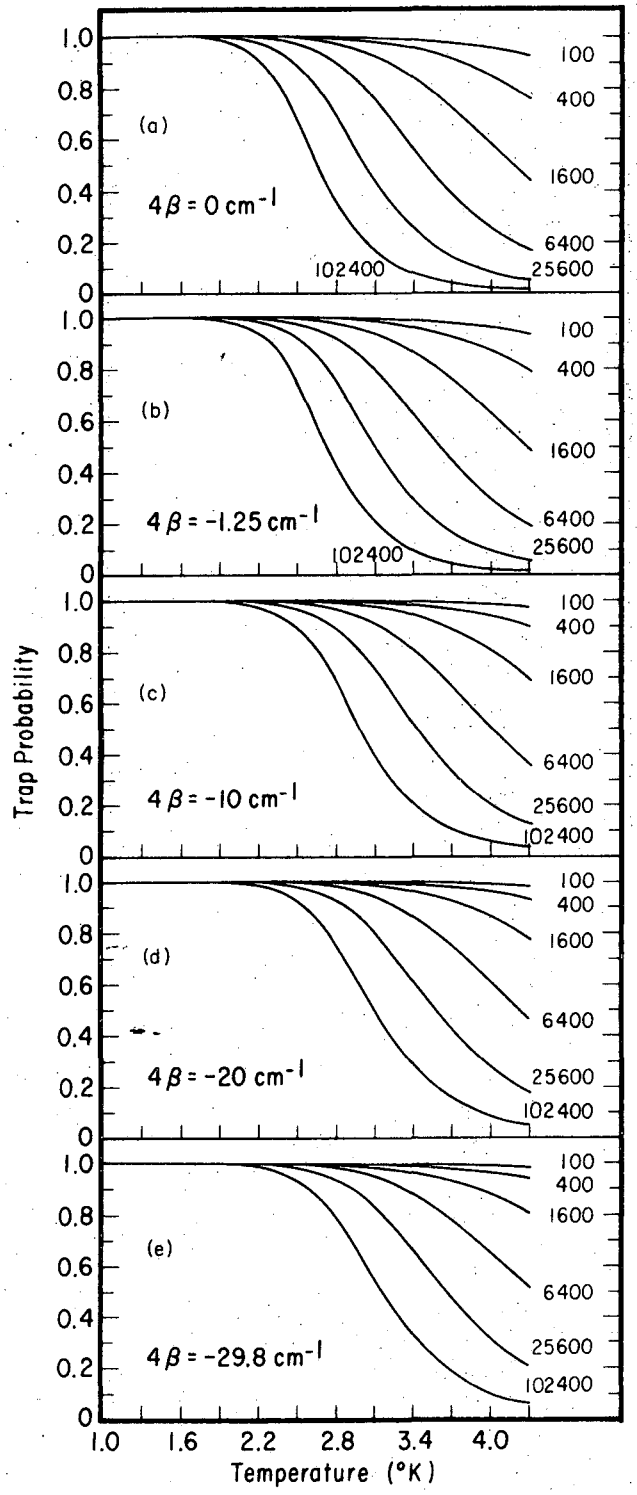


XBL 7210-5700

Fig. 2

taken to be the narrow band example. Figures 2c and 2d are calculated using intermediate values, and Fig. 2e uses a value associated with a broader band. In Fig. 3, one line from each of the Fig. 2 drawings is shown so that the differences can be more clearly seen. The number of k states (i.e., the number of molecules in the chain) has been kept constant in Fig. 3. Figures 4a through 4e are similar plots, however a positive sign of $\beta$ is considered. As illustrated in Fig. 1, as $\beta$ becomes more negative the energy differences between the trap and all the states in the band, except the $k = 0$ state, become greater. For a given number of states the temperature dependence of the trap probability and therefore the change in emission is more gradual. As $\beta$ takes on larger positive values, the energy differences between the states in the band and the trap become smaller. This causes the trap probability (and the trap intensity) to have a steeper temperature dependence. Figure 4e is an example where $4\beta$, the band width, is greater than $\Delta$, and hence the bottom of the band extends below the trap. When the trap and exciton states become degenerate it is necessary to consider additional perturbations. In particular, a realistic treatment should include the localization of band states by the trap impurity and the delocalization and energy shift of the trap state via interactions with band states.[12a] Furthermore, when the number of impurity states becomes significant relative to the number of band states amalgamation must be considered in detail.[12b] This would cause deviation from the zeroth order temperature dependence illustrated in Fig. 4e. In Fig. 5 one curve from each of the Fig. 4 drawings is plotted so that the change in the temperature dependence with $\beta$ can be more clearly seen. One notes

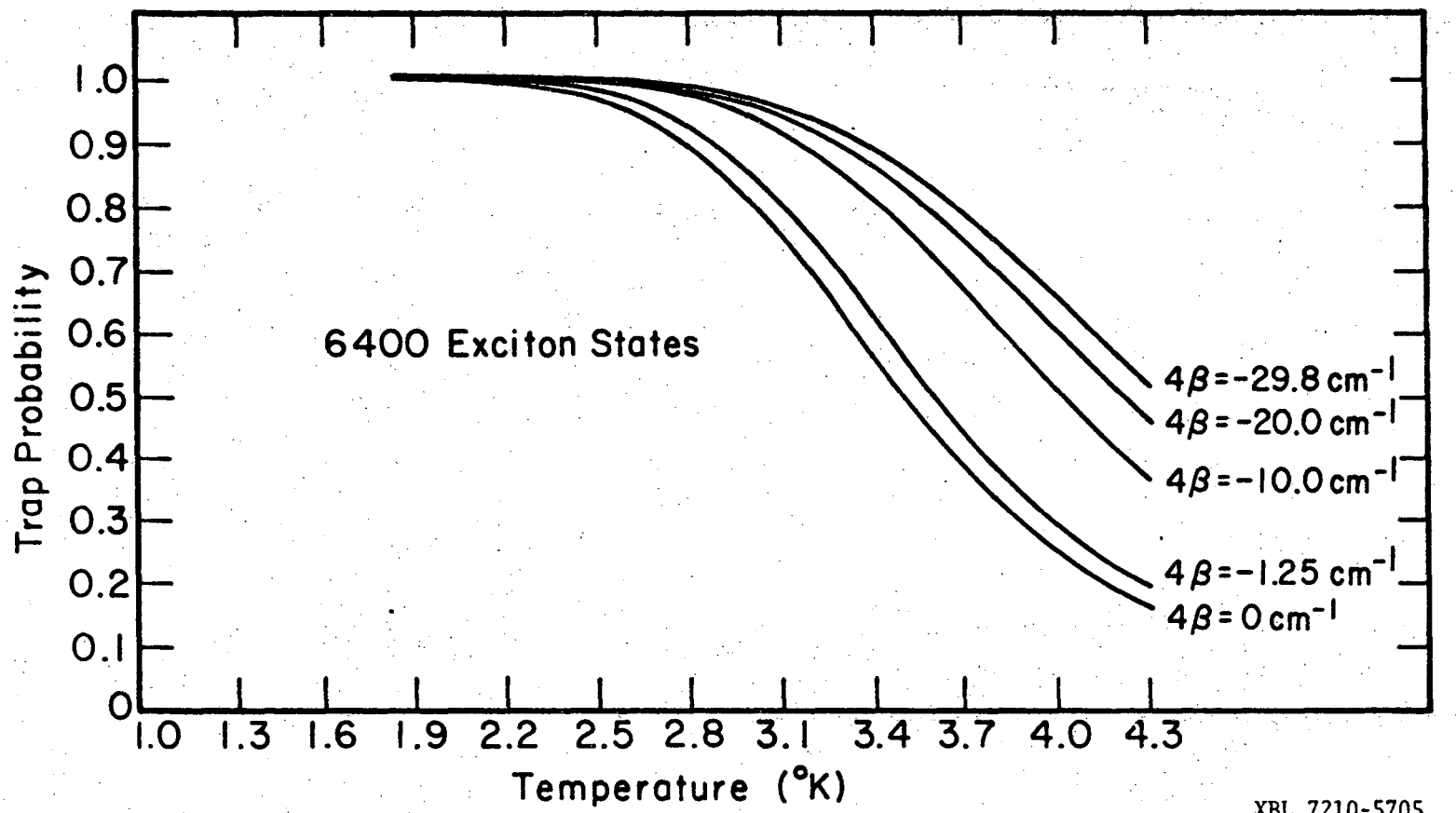


XBL 7210-5705

Fig. 3. One curve from each of the five sets of curves of Fig. 2 is displayed so that the temperature dependence of the trap probability as a function of β can be more clearly seen. The curves are for 6400 exciton k states per trap using the negative value of 4β from Fig. 2.

Fig. 4. Calculated trap probabilities, which are proportional to trap intensities are shown as a function of temperature for various positive values of $\beta$. The number next to each curve gives the number of exciton states per trap states. The 21.3 $cm^{-1}$ tetrachlorobenzene trap depth $\Delta$ is used. The band width, $4\beta$, used to calculate the curves is given in each section of the drawing. It should be noted that the scale changes in (d) and (e). As the band width $4\beta$ becomes increasingly more positive the energy differences between the trap and the levels of the band become smaller resulting in a steeper temperature dependence of the trap probability. (e) is an example of the amalgamation limit where the bottom of the band extends below the trap level.

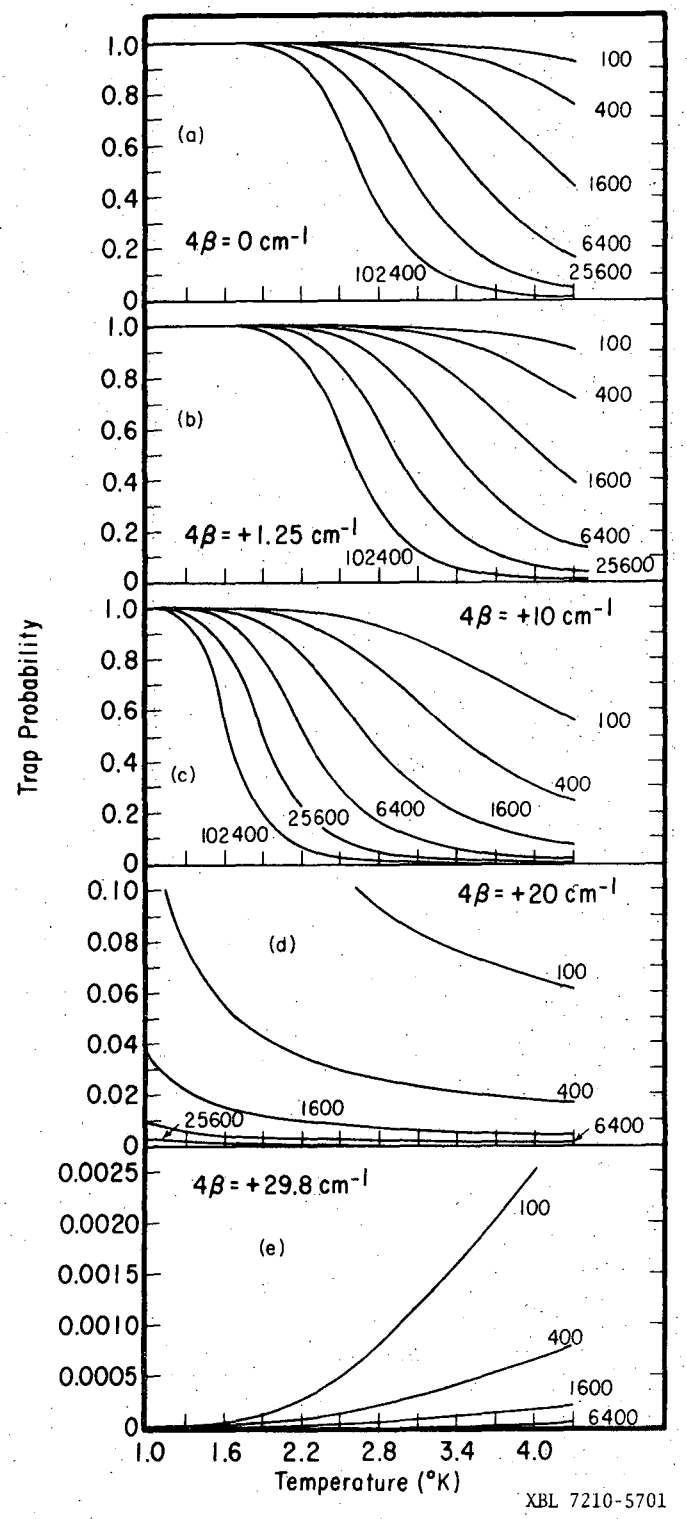
Trap Probability
(a)
4β = 0 cm⁻¹
100
400
1600
6400
25600
102400
(b)
4β = +1.25 cm⁻¹
(c)
4β = +10 cm⁻¹
(d)
4β = +20 cm⁻¹
(e)
4β = +29.8 cm⁻¹
Temperature (°K)
XBL 7210-5701

Fig. 4

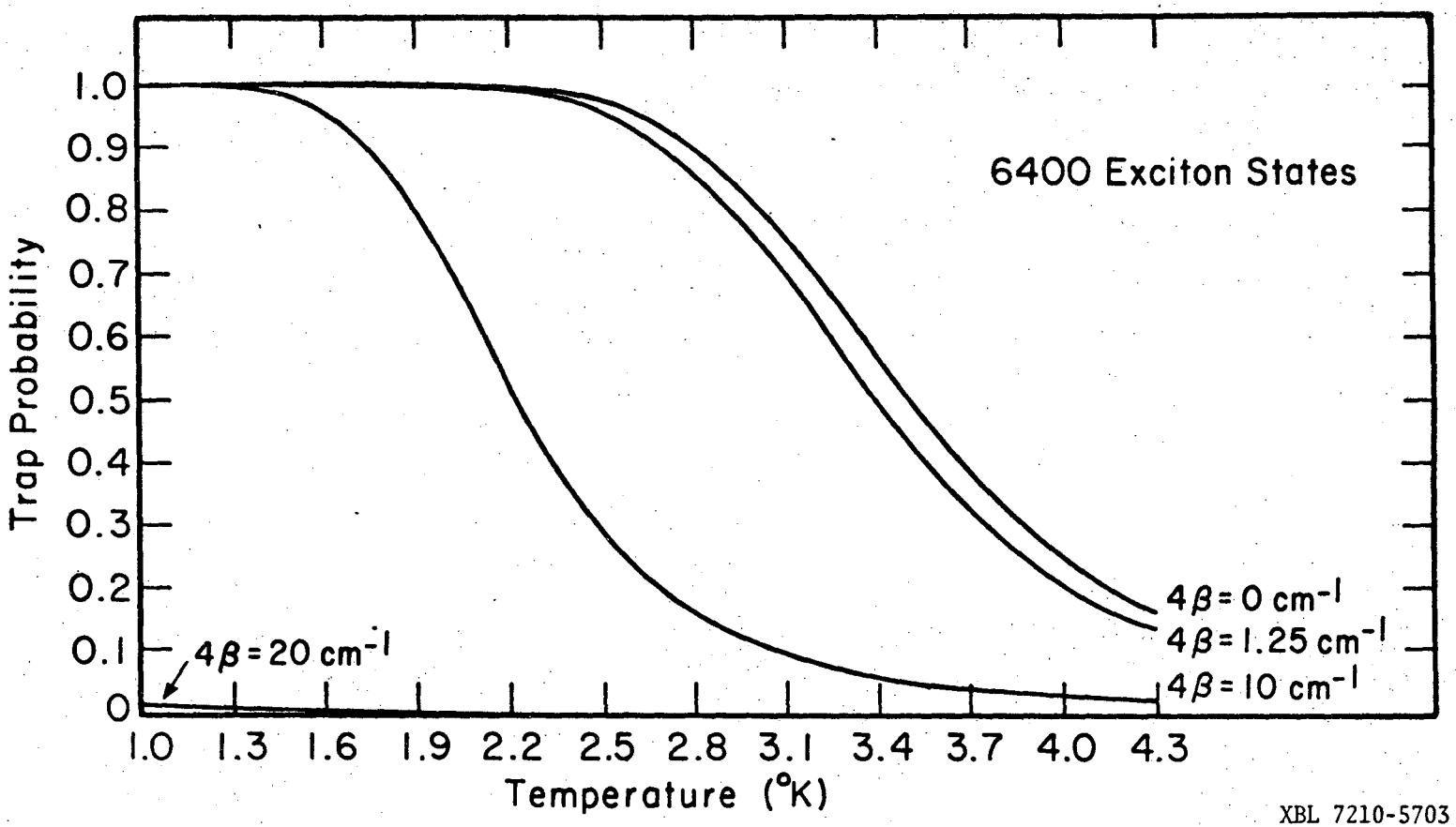


XBL 7210-5703

Fig. 5. One curve from each of the sets of curves in Fig. 4(a) through 4(d) is displayed so that the temperature dependence of the trap probability as a function of $\beta$ can be more clearly seen. The curves are for 6400 exciton k states per trap using the positive values of $4\beta$ from Fig. 4.

that the temperature dependence of trap emission, in addition to being dependent on the trap depth and trap concentration, is significantly governed by the detailed structure of the exciton band. In the case of degenerate trap and band states in the absence of trap-band interactions, for example, a reversal in the temperature dependence results (cf. Fig. 4e). In other cases, each value of the chain length and band width generates a unique temperature dependence in the trap phosphorescence. Indeed, this interrelationship between the band width, exciton chain length and trap depth can be exploited to give an experimental measure of these parameters in crystals representative of one-dimensional systems. The temperature dependence of trap emission can also be used to determine (via inference) whether or not the band and trap states are in Boltzmann equilibrium. An example of this is illustrated in Fig. 6, where the experimental temperature dependence of the intensity of the intrinsic $H_2$-TCB X-trap is plotted as a function of temperature. The best calculated fit to the experimental data is also shown along with values of the parameters which are well outside of the limits of the accuracy of the results. Since the trap is intrinsic, the trap concentration was unknown; consequently, both $\beta$ and the trap concentration were varied in order to obtain the calculated curve. The best values are $3.5 \pm 2$ $cm^{-1}$ for the band width $4\beta$ with $\beta$ <u>positive</u> and a trap concentration of one part in 90,000. If the trap concentration is known from an independent measurement, the uncertainty in the band width measured in this type of experiment can be greatly reduced. Although the $H_2$-TCB band width measured by this method is somewhat larger than that reported[8] (1.25 $cm^{-1}$) from an independent method, the essential features of these results are in agreement with the

Fig. 6. The solid circles are the experimentally determined intensity vs temperature data for the 21.3 $cm^{-1}$ trap in 1,2,4,5-tetrachlorobenzene. The center solid line is the theoretically determined best fit of the data to the bandwidth, $4\beta$, and the number of exciton k states which corresponds to the number of molecules in the average exciton chain. The two additional curves labeled 1.25 $cm^{-1}$ and 6.0 $cm^{-1}$ correspond to values well outside the standard deviation of the data and are illustrated to demonstrate the uniqueness of the data in the variables $4\beta$ and the number of k states. The best value of the bandwidth is $3.5 \pm 2$ $cm^{-1}$ with $\beta$ positive.

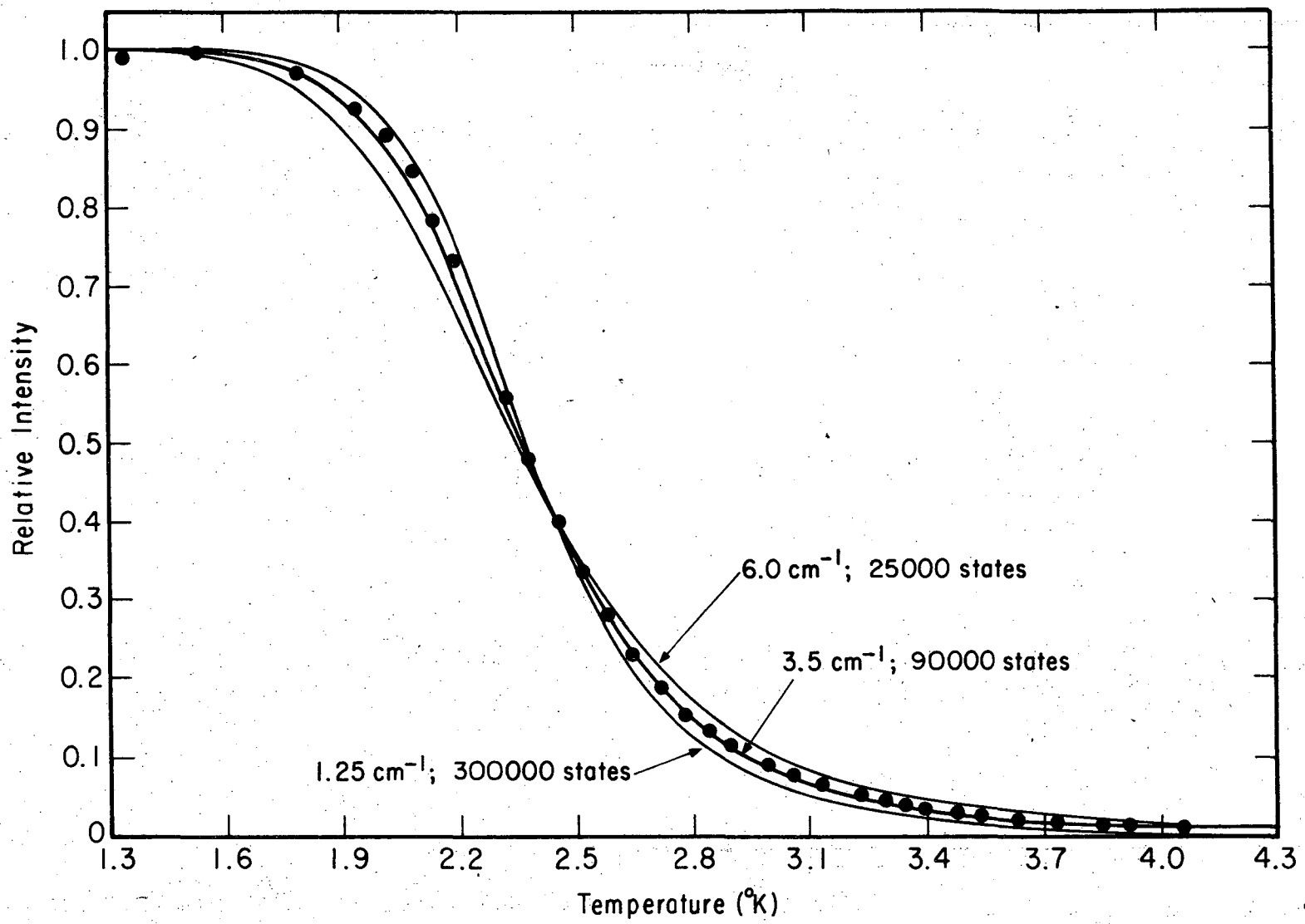


XBL 737-905

Fig. 6

interpretation of the earlier results. It is important to note that the earlier experiments[8] and the above experiment can only be fully understood and interpreted in terms of a model which is dependent upon coherent migration being the principal mode of exciton transport in the TCB crystal at low temperatures. The importance of coherent migration in the above results is discussed in detail in the next section. The discussion in this and following sections is primarily concerned with excited triplet states; however, it should be kept in mind that identical considerations also apply to singlets and transport properties in general.

### C. Exciton Group Velocities and Thermal Equilibrium

In the Frenkel limit once a molecule is excited it cannot transfer its excitation to another molecule without an intermolecular interaction which destroys the degeneracy of the states. In a finite band, the velocity with which an excitation propagates in the crystal with a particular momentum in a coherent model is the group velocity, $V_g(k)$, which is given by the slope of the energy dispersion of the band

$$V_g(k) = \frac{1}{\hbar} \frac{\partial E(k)}{\partial k} \tag{I.7}$$

and is proportional to the change in exciton energy with k. For a non-degenerate band at temperatures above 0°K, the group velocity will be nonzero because of the population of non $k = 0$ or $\pm\pi/a$ wave vector states; the excitation will be able to migrate. The average velocity of this migration, and certain details of phonon-exciton scattering determines whether or not the system can reach thermal equilibrium. If during the lifetime of the excited state the excitations do not travel far enough to reach traps, the trap probability cannot be described by

Boltzmann statistics. On the other hand, if the excitations during their lifetime can travel on the average many times farther than the average distance between traps, then all the excitations will be able to "sample" traps, the system will be able to reach thermal equilibrium, and the trap probability will be determined by the partition function of the previous section. The importance of phonon-exciton scattering in the equilibration process cannot be underestimated, for it is what ultimately limits the mean free path of coherent propagation.[13,14] If we assume that there is no memory between phonon-exciton scattering events and restrict the scattering to stochastic first order Markoffian processes[15] one can assign a coherence time, $\tau(k)$, to the wavepackets propagating at velocities $V_g(k)$. The distance, $\ell(k)$, a coherent state propagates between "random" scattering events is then given by

$$\ell(k) = V_g(k)\,\tau(k) \tag{I.8}$$

and is thus equivalent to a mean free path.

At intermediate temperatures where the principal limitation on $\tau(k)$ is phonon-exciton scattering, Frenkel excitons initially in a state k (or a linear combination of k states) scatter to other k' states in a time short compared to the radiative or radiationless lifetime, but in a time long compared to the intermolecular interaction time ($\beta^{-1}$). As a result the coherence time, $\tau(k)$, is shortened, the mean free path reduced and the ability to equilibrate trap and exciton states is attenuated. It is shown in work not contained in this thesis that scattering is principally to adjacent k states and hence the average group velocity is relatively unaffected until one approaches the high

temperature limit.[16] Diffusion or random walk is simply the limit where the change in k occurs on a time scale short compared to $\beta^{-1}$. These features will be dealt with in far greater detail in a subsequent paper[16] where a method for observing the dynamics of individual k states will be presented. In the present case however only manifestations of the average velocities (and/or $\tau(k)$'s) are easily measurable and therefore we restrict the discussion to these features. The importance of $\langle V_g(T) \rangle$ is easily seen by comparison of coherent and incoherent migration.

Treating the exciton band as one-dimensional, the average group velocity at a given temperature, $\langle V_g(T) \rangle$, is given by the normalized sum over the velocities of the k states in the band with each velocity weighted by the probability of finding the system in that k state at a particular temperature, T, i.e.,

$$\langle V_g(T) \rangle = \frac{1}{\hbar} \left\langle \frac{\partial E(k)}{\partial K} \right\rangle_T = \frac{2\beta a}{\hbar} \frac{\sum_k \sin(ka)\, e^{-(2\beta \cos ka/kT)}}{\sum_k e^{-(2\beta \cos ka/kT)}} \tag{I.9}$$

We will restrict the summation in Eq. (I.9) to positive wave vector states only so that $\langle V_g(T) \rangle$ is physically related to a scalar velocity in one direction. In the limit that the number of k states becomes large, the summations in Eq. (I.9) converge to integral form which can be evaluated using modified Bessel functions. The resulting expression for the average group velocity is given by

$$\langle V_g(T) \rangle = (2\beta a/\hbar)(2kT/\pi\beta)^{1/2} \left(I_{1/2}(z)/I_o(z)\right) \tag{I.10a}$$

where $z = (2\beta/kT)$ and $I_o(z)$ and $I_{1/2}(z)$ are given by

$$I_o(z) = (1/\pi) \int_0^{\pi} \exp(z \cos\theta)\, d\theta \qquad \text{(I.10b)}$$

and

$$I_{1/2}(z) = (1/2\ z/\pi)^{1/2} \int_0^{\pi} \exp(\pm z \cos\theta) \sin\theta d\theta \qquad \text{(I.10c)}$$

where $\theta = ka$. In Table I, group velocities, calculated using Eq. (I.9), for a narrow, intermediate and broad triplet band are listed as a function of temperature. The average group velocity is not very sensitive to the number of states in the band when the number of states in the band is greater than 100. It can be seen from Table I, that even for the narrow band width of 1.25 $cm^{-1}$ which Francis and Harris[8] have reported for TCB, at 1°K an excitation traveling completely coherently will be able to sample $10^9$ lattice sites in ten milliseconds which is the order of the lifetime of the TCB triplet state.[11] (The exciton will of course travel even further given the 3.5 $cm^{-1}$ band reported here.) This is sufficient to enable a system with trap concentrations as low as 1 part per $10^7$ to come to thermal equilibrium. For the larger band widths, systems with even smaller trap concentrations will be able to equilibrate. Only very pure samples with nearly degenerate bands will be unable to come to thermal equilibrium when the excitons migrate coherently.

Attenuation of this long range migration occurs when phonon-exciton scattering limits the coherence time and hence the coherence length. When this length becomes less than the average trap-to-trap separation, thermal equilibrium becomes progressively more difficult to achieve. In the high temperature limit, phonons destroy the translational symmetry

Table I. Average group velocities (cm/sec) for a band of 25,000 k states as a function of temperature.

| °K | Band Width | | |
|---|---|---|---|
| | 1.25 $cm^{-1}$ | 15 $cm^{-1}$ | 29.6 $cm^{-1}$ |
| 1.0 | 2652 | 12747 | 18075 |
| 1.6 | 2750 | 15996 | 22781 |
| 2.2 | 2782 | 18592 | 26611 |
| 2.8 | 2797 | 20762 | 29902 |
| 3.4 | 2804 | 22601 | 32814 |
| 4.0 | 2809 | 24161 | 35436 |

of the lattice and tend to scatter an excitation at each lattice site, and hence the group velocity is replaced by a diffusion rate as the excitation executes a random walk at every lattice site. In one-dimensional diffusion, the exciton can move with equal probability to either of the two molecules adjacent to it. The average time, $\tau$, it takes an exciton undergoing a random walk migration to take one step is on the order of[17]

$$\tau = \frac{h}{4\beta} \tag{I.11}$$

Hence, the median distance traveled in cm is given by

$$\langle d \rangle = 1/3\ N^{1/2}\ \bar{a} \tag{I.12}$$

where N is the number of hops taken per unit time and $\bar{a}$ is the distance traveled in one hop, one lattice translation, in centimeters. In Table II, the median random walk distances are listed for the three band widths used in Table I for a variety of times. The value of $\bar{a}$ used is 3.76Å which is the translational spacing of molecules along the $\bar{a}$ direction in TCB.[18] Table III also gives the ratio of the distances traveled by an exciton moving in the coherent limit vs random walk migration for the three band widths at 2.8°K.

It is seen that random walk migration is a factor of $10^4$ to $10^6$ slower than coherent migration. While a $H_2$-TCB exciton traveling completely coherently could sample approximately $10^9$ lattice sites during its lifetime (10 ms), an exciton undergoing random walk migration on the average will only sample $10^3$ to $10^4$ lattice sites. The number of excitons able to migrate larger distance falls off very rapidly

Table II. Median distance traveled in a random walk process.

| Time | Band Width | | |
|---|---|---|---|
| | 1.25 $cm^{-1}$ | 15 $cm^{-1}$ | 29.6 $cm^{-1}$ |
| 1 ms | $7.6\times10^{-5}$ cm | $2.7\times10^{-4}$ cm | $3.7\times10^{-4}$ cm |
| 10 ms | $2.4\times10^{-4}$ cm | $8.4\times10^{-4}$ cm | $1.2\times10^{-3}$ cm |
| 100 ms | $7.6\times10^{-4}$ cm | $2.7\times10^{-3}$ cm | $3.7\times10^{-3}$ cm |
| 1 ms | $2.4\times10^{-3}$ cm | $8.4\times10^{-3}$ cm | $1.2\times10^{-2}$ cm |

Table III. Ratio of the coherent migration distance to the random walk distance at 2.8°K.

| Time | Band Width | | |
|---|---|---|---|
| | 1.25 $cm^{-1}$ | 15 $cm^{-1}$* | 29.6 $cm^{-1}$* |
| 1 ms | $3.7\times10^{4}$ | $7.8\times10^{4}$ | $7.8\times10^{4}$ |
| 10 ms | $1.1\times10^{5}$ | $2.5\times10^{5}$ | $2.5\times10^{5}$ |
| 100 ms | $3.7\times10^{5}$ | $7.8\times10^{5}$ | $7.8\times10^{5}$ |
| 1 s | $1.1\times10^{6}$ | $2.5\times10^{6}$ | $2.5\times10^{6}$ |

*Differences between the 15 $cm^{-1}$ and 29.6 $cm^{-1}$ ratios are less than 1% because of insufficient population in k states at the center of the band at this low temperature.

because one-dimensional random walk processes are describable by a Gaussian distribution of distances around some initial starting point.[19] In the case of $H_2$-TCB only 3 excitons out of 1000 traveling completely by random walk migration would be able to cover a distance of $5\times10^4$ lattice sites which is half the average distance between traps in these crystals. The conclusion to be drawn is that the observation that the temperature dependence of the $H_2$-TCB trap intensity obeys Boltzmann statistics provides strong evidence that coherent migration is the principal mode of exciton transport at liquid helium temperatures. Indeed the coherence time must be at least several orders of magnitude longer than the intermolecular exchange time.

## D. The Effects of Multiple Bands

### 1. Zero-Field Splitting of the Exciton Band and Trap States

To this point, the triplet exciton band and trap have each been considered as consisting of a single magnetic sublevel. This is an accurate description for singlet states, but both the triplet exciton band and trap are split into three energy sublevels by the zero-field spin dipolar interaction of the unpaired triplet electron spins.[20] The intensity of trap emission, $I_{trap}$, for the three level system is given by

$$I_{trap} = K^r_{x\ trap} N_{x\ trap} + K^r_{y\ trap} N_{y\ trap} + K^r_{z\ trap} N_{z\ trap} \qquad (I.13)$$

where $K^r_{i\ trap}$ is the radiative rate constant for the $i^{th}$ sublevel and $N_{i\ trap}$ is the population of the $i^{th}$ sublevel. In the absence of a spin-lattice relaxation processes in the band states, the trap states, and between trap and band states, the population of a triplet sublevel

is independent of the populations of the other sublevels and hence the total population of a particular magnetic spin component is the sum of the populations in the particular spin sublevel of exciton band and the trap. Thus, the trap population of the $i^{th}$ sublevel can be given by

$$N_{i\ trap} = N_{i\ total} \frac{1}{Z_i} \tag{I.14}$$

where $Z_i$ is the partition function for the $i^{th}$ spin sublevel. Under these conditions the total trap intensity can be written as

$$I_{trap} = K^r_{x\ trap} N_{x\ total} \frac{1}{Z_x} + K^r_{y\ trap} N_{y\ total} \frac{1}{Z_y} + K^r_{z\ trap} N_{z\ total} \frac{1}{Z_z} \tag{I.15}$$

In the absence of spin-orbit coupling the dispersion of each of the three triplet bands will be identical when the zero-field spin dipole interaction is much smaller than the band dispersion. Thus, the three spin sublevel partition functions, $Z_x$, $Z_y$ and $Z_z$ are essentially the same and the trap intensity is given by

$$I_{trap} = (K^r_{x\ trap} N_{x\ total} + K^r_{y\ trap} N_{y\ total} + K^r_{z\ trap} N_{z\ total}) \frac{1}{Z} \tag{I.16}$$

The net result is that the temperature dependence, as in the single spin sublevel case, is determined only by the change in Z with temperature.

In general, however, spin-orbit coupling must occur in order to give allowed transition character from the triplet excited state to the ground singlet manifold.[21] In most cases the spin eigenfunctions have different symmetry properties resulting in admixture of different singlet states into three individual spin sublevels.[22] The dispersion of the three

triplet spin sublevel bands can differ in such cases giving each sublevel a slightly different partition function and therefore in principle a different intensity temperature dependence. However, the changes in the dispersions of the bands due to spin-orbit coupling are, in almost all cases, so small that the temperature dependence of the intensity of trap phosphorescence is unaffected by these small energy differences. In $H_2$-TCB spin-orbit coupling produces only one part in $10^6$ difference in the dispersion of the three spin sublevel bands.[8]

A more serious consideration for molecular systems in some temperature regions is the effect of spin lattice relaxation on the temperature dependence of trap emission. In the above discussions the steady state population in the band and trap, $N_{total}$, in a particular magnetic sublevel was assumed to be independent of temperature and independent of the populations of the other two sublevels. However, spin lattice relaxation couples the sublevels, allowing population to be transferred from one to another. Since this is in general highly temperature dependent,[23] the total steady state population of a particular magnetic sublevel can change significantly with temperature. To account for these variations is in principle straightforward. The population of a trap, and therefore its intensity, at any one temperature is determined by the partition function as before, but as the temperature changes, the change (via $T_1$) in the total sublevel population as well as the change in the partition function must be determined. The change in the total sublevel populations can be determined by measuring the change in the

lifetimes of the three sublevels as a function of temperature, and thereby assessing the amount of spin lattice relaxation.[24] The trap probability is determined as before using the partition function, but now it must be multiplied by the relative sublevel population for each temperature, i.e.,

$$I_{trap} = \left[ \sum_{i=x,y,z} K^{r}_{i\ trap} N_{i\ total}(T) \right] \frac{1}{z} \quad . \qquad (I.17)$$

Although the effects of spin lattice relaxation between the magnetic sublevels of the triplet band in one-dimensional bands can complicate the evaluation of the trap phosphorescence intensity, in most crystals this does not present any real difficulty. It is only when there is a significant temperature dependence to the <u>effective</u> spin lattice relaxation process over the temperature range of interest that difficulty arises. Usually, small two-dimensional exchange interactions between translationally inequivalent molecules in the unit cell result in an effective averaging of the spin sublevel populations in band states on a time short compared to the lifetime of the state. Thus, the exciton dynamics keep <u>the individual spin-sublevels</u> close to Boltzmann equilibria, and hence the temperature dependence of spin lattice relaxation is ineffective in causing large deviations in the individual spin sublevel populations over the range of temperature of interest. This is the case at least for $H_2$-TCB and $D_2$-TCB between 1-4°K.

## 2. Two and Three Dimensional Bands

The above considerations can be readily extended to systems in which a trap interacts with a multidimensional exciton band. For one molecule per unit cell the most general form is given by the three-dimensional partition function z:

$$z = 1 + \sum_{k_a=0}^{\pi/a} \sum_{k_b=0}^{\pi/a} \sum_{k_c=0}^{\pi/a} G(k)\, e^{-(\Delta-2\beta_a(1-\cos k_a\bar{a})-2\beta_b(1-\cos k_b\bar{b})-2\beta_c(1-\cos k_c\bar{c})/kT} \tag{I.18}$$

where $k_a$, $k_b$, and $k_c$ are the wave vectors associated with the crystallographic translational directions $\bar{a}$, $\bar{b}$ and $\bar{c}$ and $\beta_a$, $\beta_b$ and $\beta_c$ are the nearest neighbor intermolecular interaction matrix elements along these three axes. G(k) is a degeneracy factor which takes on the value 1 when the values of all three k wave vectors are zero, 2 when any two k wave vectors are zero, 4 when only one k wave vector is zero, and finally, 8 when all three k wave vectors are greater than zero. The partition function for the case in which the exciton band is two-dimensional is obtained by setting $\beta_c$ equal to zero, and the one-dimensional partition function given in Eq. (I.2) follows naturally from Eq. (I.18) by setting $\beta_c$ and $\beta_b$ equal to zero.

To simplify the discussion, only the two-dimensional case will be explicitly considered. For illustration $\beta_b$ is set equal to 1/2 of $\beta_a$ and the two-dimensional exciton band is limited to four hundred states corresponding to a square array of 400 molecules. An energy level diagram for the trap and exciton system is given in Fig. 7. As in the

Fig. 7. Trap and exciton energy level diagrams for a one dimensional exciton band $\beta_b = 0$ and a two dimensional band with $\beta_b = \frac{1}{2}\beta_a$. The spectroscopically determinable trap depth is the difference in energy between the trap level and the $k_a = 0$, $k_b = 0$ level of the two dimensional exciton band. The trap depth can have one of the four possible values, $\Delta_1$ to $\Delta_4$ shown in the figure, depending upon the signs of $\beta_a$ and $\beta_b$. If both $\beta_a$ and $\beta_b$ are negative, $\Delta_1$ will be observed. If $\beta_a<0$ and $\beta_b>0$, $\Delta_2$ will be observed. If $\beta_a>0$ and $\beta_b<0$, $\Delta_3$ will be observed, and if $\beta_a$ and $\beta_b$ are both positive, $\Delta_4$ will be the spectroscopically measured value of the trap depths.

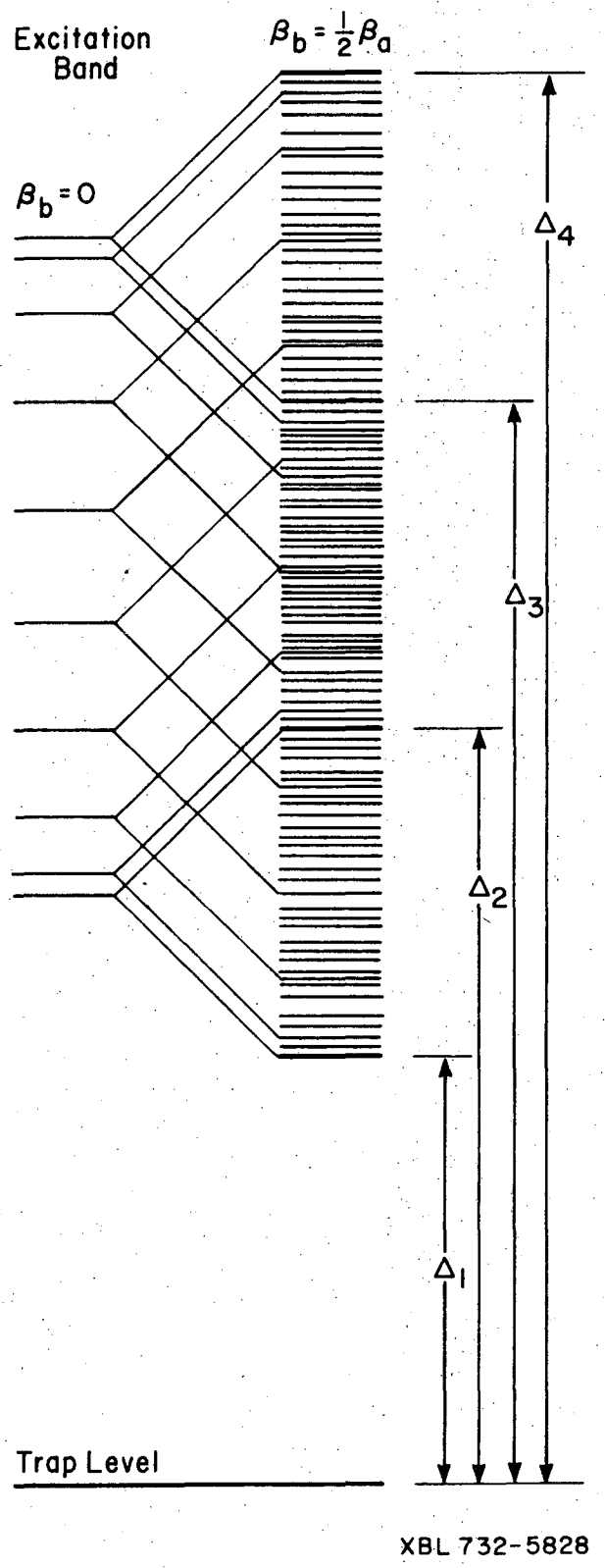
Excitation Band
$\beta_b = \frac{1}{2}\beta_a$
$\beta_b = 0$
$\Delta_4$
$\Delta_3$
$\Delta_2$
$\Delta_1$
Trap Level
XBL 732-5828

Fig. 7

one-dimensional case, the 0-0 absorption must obey the selection rule $\Delta k = 0$; thus, the 0-0 transition is associated with the $k_a = 0$, $k_b = 0$ level. Depending upon the signs of $\beta_a$ and $\beta_b$, the $k_a = 0$, $k_b = 0$ exciton level can occur at four different energies relative to the trap energy. As indicated in Fig. 7, if $\beta_a$ and $\beta_b$ are both negative, $\Delta_1$ will be the observed trap depth. If $\beta_a$ is negative and $\beta_b$ is positive, $\Delta_2$ will be the trap depth. If $\beta_a$ is positive and $\beta_b$ is negative, $\Delta_3$ will be the trap depth. If both $\beta_a$ and $\beta_b$ are positive, $\Delta_4$ will be the spectroscopically measured trap depth.

For a given trap concentration, the average number of states in the exciton band is known, the trap depth, $\Delta$, can be measured, and the temperature dependence of the trap intensity can be fit by varying the signs and magnitudes of $\beta_a$ and $\beta_b$ in the multidimensional partition function (Eq. (I.18)). For systems in which the number of states in the band is large, i.e., low trap concentration, the density of states in the band becomes so large that the partition function is not sensitive to $\beta_a$ and $\beta_b$ separately but depends only upon the total bandwidth, $4|\beta_a| + 4|\beta_b|$; thus, a measure of the bandwidth can be experimentally determined, even in multidimensional crystals, but details of the band along specific crystallographic axes are lost. The above discussion has been restricted to systems containing trap levels of only one energy. Systems with two or more traps of different energies present a different problem but provide additional and unique information on the exciton dynamics and will be considered in detail below.

## II. EQUILIBRIUM BETWEEN EXCITON STATES AND MULTIPLE TRAPS

### A. Boltzmann Equilibrium

The extension of the above treatment to systems in which there are two or more types of traps having different energies would be straightforward if it were not for the fact that the excitons and traps have finite lifetimes. If the excited state lifetimes were long enough, the system would come to thermal equilibrium and a statistical treatment would always be proper for any temperature or trap depth. However, given the finite lifetimes of the states involved, a statistical approach is only possible above a certain characteristic temperature, hereafter termed $T_c$, which is determined by the trap depths, the trap concentrations, and the exciton band width.

The inability of the system to achieve thermal equilibrium below the characteristic temperature is due in part to the spacial separation of the traps of different energies and in part due to different trap-phonon interactions at the different trap sites in the lattice. This can be seen more clearly by considering the energy level diagram in Fig. 8 for a system consisting of an exciton band, a shallow trap, $\tau_s$, and a deep trap, $\tau_d$. The dashed arrows indicate the possible paths electronic excitation can travel in the system in the absence of direct long range energy exchange between traps. Basically, an excitation cannot be transferred to another trap site without first being thermally promoted to the exciton band in which it can migrate to another trap site and again be trapped. Equilibrium is only established through a continuous process of detrapping, migration and retrapping. If the process continues long

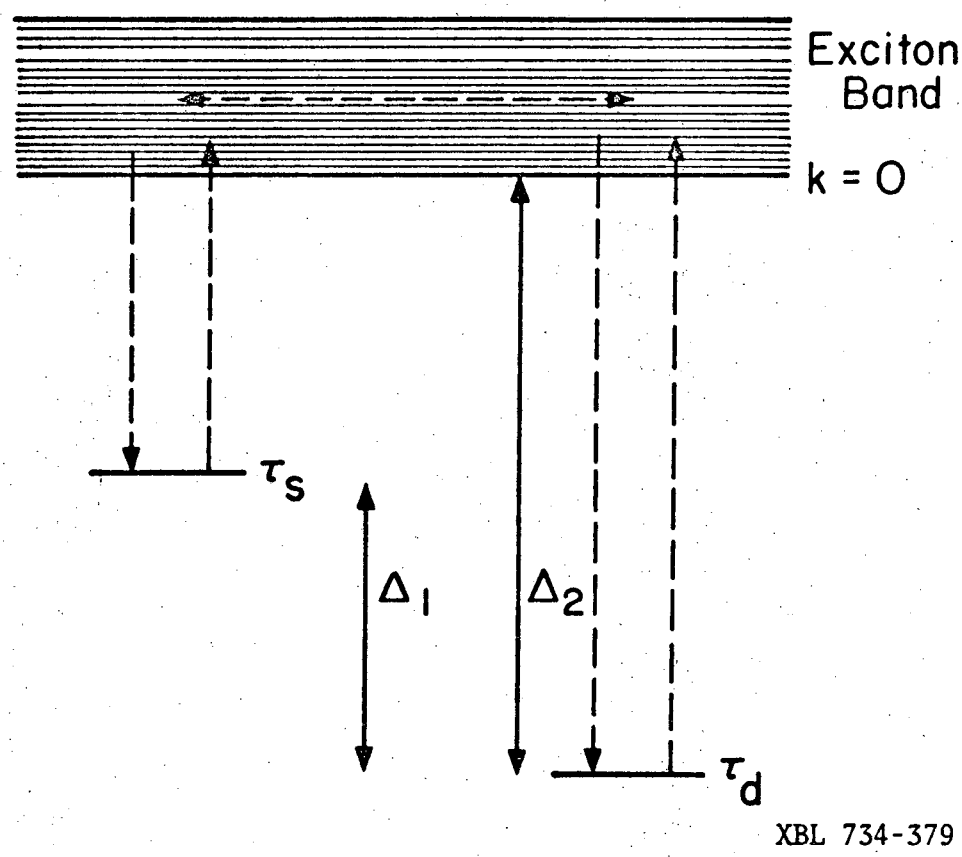


Fig. 8. Energy level diagram for a system containing an exciton band and traps of two different energies. $\tau_s$ labels the shallow traps, and $\tau_d$ labels the deep traps. $\Delta_1$ is the energy difference between $\tau_s$ and $\tau_d$, and $\Delta_2$ is the energy difference between $\tau_d$ and the $k = 0$ level of the exciton band. The dashed arrows indicate the possible paths an excitation can travel in the system.

enough, the system reaches its equilibrium population distribution in spite of the fact that the shallow and deep traps exchange their population with the band states at different rates. Because the exciton and trap states have a finite lifetime, however, the rate of detrapping and retrapping for both traps must be large enough to compete with radiative and radiationless processes. This can only occur above some characteristic temperature $T_c$ where phonon-trap interactions are frequent enough to keep the system in thermal equilibrium.

In the equilibrium temperature region, the temperature dependence of the trap intensities can be determined from the probabilities $P_{\tau_d}$ and $P_{\tau_s}$ that an excitation will be in deep trap, $\tau_d$, or shallow trap, $\tau_s$, respectively. Taking the exciton band to be one-dimensional in the nearest neighbor approximation, the partition function, z, for the system is given by

$$z = 1 + G_1 e^{-\Delta_1/kT} + G_2 e^{-\Delta_2/kT} + \sum_{k=\pi/na}^{(n-1)\pi/na} 2G_2 e^{-[\Delta_2 - 2\beta(1-\cos ka)]/kT} \quad . \qquad \text{(II.1)}$$

The zero of energy is taken as the energy of the deep trap. As shown in Fig. 8, $\Delta_1$ is the energy difference between the deep and shallow traps, and $\Delta_2$ is the energy difference between the deep trap and the k = 0 level of the exciton band. The k = 0 level may be at the top or bottom of the band (as discussed previously) depending upon the sign of $\beta$. The concentration of the traps and excitons are normalized to a unit concentration of the deep trap. The first term in z is due to the deep trap. The second term is the Boltzmann factor for the shallow trap, multiplied by $G_1$, the number of shallow traps relative to a single deep trap. The third

term is the Boltzmann factor for the non-degenerate k = 0 level of the exciton band times $G_2$, the number of exciton chains relative to a single deep trap. The final summation is over the remainder of the exciton k states, which are doubly degenerate, giving rise to the factor of two. The total number of host molecule states relative to one deep trap is $G_2 \times (2n)$ where there are 2n states per exciton and $G_2$ exciton chains per deep trap. The trap probabilities $P_{\tau_d}$ and $P_{\tau_s}$ (which are proportional to the trap intensities) are

$$P_{\tau_d}(T) = \frac{1}{Z(T)} \tag{II.2}$$

and

$$P_{\tau_s}(T) = \frac{G_1 e^{-\Delta_1/kT}}{Z(T)} \tag{II.3}$$

respectively. Calculated plots of $P_{\tau_d}$ and $P_{\tau_s}$ vs temperature for systems which contain 99.2% host exciton states, 0.8% shallow traps, and $1.6\times10^{-3}$% deep traps are illustrated in Fig. 9. The trap depths, $\Delta_1$ and $\Delta_2$ are 10 $cm^{-1}$ and 20 $cm^{-1}$, respectively. These values are typical of a single and doubly protonated traps in deutero crystals. The curves are for a range of band widths, $4\beta$, between +8 $cm^{-1}$ and -8 $cm^{-1}$. Several features of the trap phosphorescence intensity in multiple trap systems are particularly noteworthy. First, as $4\beta$ becomes more positive the energy levels in the band become loser to the trap levels. This results in a loss of trap probability and therefore a loss of trap intensity. Although both traps are affected, the change in the deep and shallow trap probability are entirely different. The decrease in the deep trap phosphorescence with increasing temperature results from the

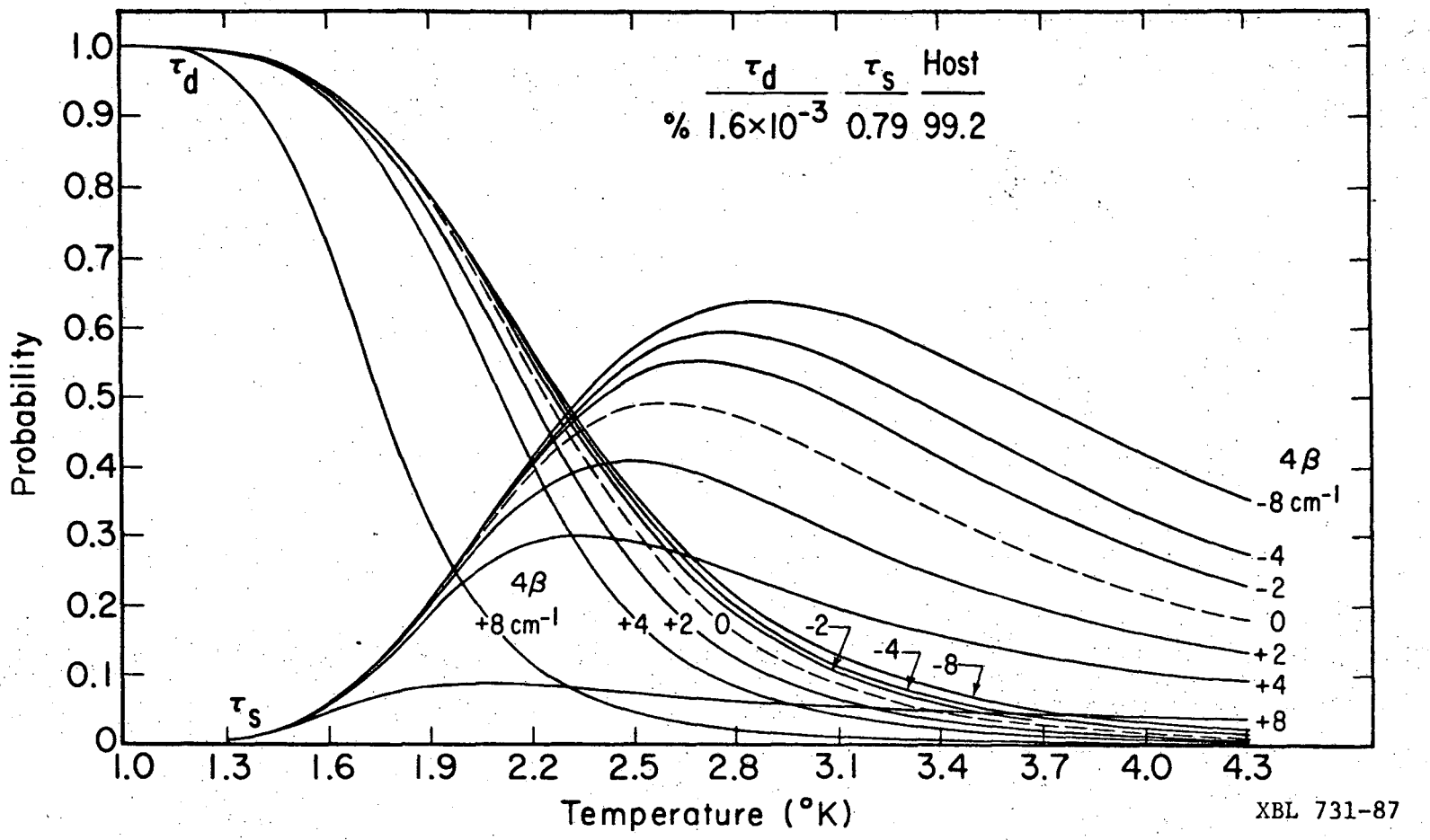


Fig. 9. Trap probabilities, which are proportional to phosphorescence intensities, as a function of temperature are plotted for an exciton and a two-trap type system. $\tau_s$ and $\tau_d$ are 10 cm$^{-1}$ and 20 cm$^{-1}$ below the k = 0 level of the band, respectively. Each pair of lines, one for $\tau_d$ and one for $\tau_s$, is calculated using the indicated exciton band width, 4β. The percent of each of the species are given at the top of the figure.

partitioning of the excitation into the higher energy shallow trap and exciton states. When the number of molecules in an exciton chain (the number of k states in the band) greatly exceeds the number of shallow traps, the form of the deep trap temperature dependence becomes indistinguishable from the single trap problem considered earlier. The temperature dependence of the shallow trap is not as simple. Physically, as the temperature increases from a value where only the deep trap is emitting ($P_{\tau_d} = 1.0$; $P_{\tau_s} = 0.0$) the initial loss in $\tau_d$ results in the onset of $\tau_s$ emission. How rapidly $\tau_s$ increases with increasing temperature, however, is determined by the partitioning of energy from the shallow trap into the band states. If many exciton states are near in energy to the shallow trap, the shallow trap will never acquire a significant intensity because of the ability of the exciton states to partition the energy, i.e., large value of the band partition function. This occurs when the shallow trap depth ($\Delta_2 - \Delta_1$ in Fig. 8) is small and/or the exciton band has a large number of k states at energies near the shallow trap (positive $\beta$). On the other hand, when the shallow trap depth becomes larger and/or the exciton band has a smaller positive dispersion of negative dispersion, the shallow trap emission will continue to increase in intensity at the expense of the deep trap probability until a point when the Boltzmann factor starts to significantly populate the exciton states. At this point the shallow trap will lose intensity with increasing temperature because of partitioning to the band. An important point of the temperature variation of both the deep and shallow traps is that for every curve associated with the deep trap there is a unique shallow trap curve for a specific value of the band

dispersion, number of k states and number of shallow traps. Moreover, the detailed shape of the temperature dependence curve for the shallow traps is determined by the partition function. A variation in $\tau_d$ and $\tau_s$ trap emission as a function of concentration is illustrated in Fig. 10. The value of the band dispersion and trap depth have been fixed at values $4\beta = 4\ cm^{-1}$, $\Delta_1 = 10\ cm^{-1}$, and $\Delta_2 = 20\ cm^{-1}$. As is expected, when the shallow trap concentration increases relative to the band states the intensity peaks at higher temperatures. The values plotted in Fig. 10 are representative of mixed crystals where the band states are the pure deutero ($D_2$) molecule (2 deuteriums/molecule), the shallow trap is a molecule with one D and one H and the deep trap is a molecule with two protons substituted for the two deuteriums of the host. The concentration values listed for cases A through D correspond to statistical mixtures of the various species based upon the total deuterium concentration of the crystals.

The practical use of such an approach to obtain information about the band is straightforward. If a sample is prepared with two traps of known concentration, where $\Delta_1$ and $\Delta_2$ can be measured spectroscopically the the band dispersion and the sign of $\beta$ can be determined from the temperature dependence of the two trap intensities. Figure 11 illustrates this for deutero-proto mixed crystals of TCB. Figure 11a is the temperature dependence of $H_2$-TCB($\tau_d$) and HD-TCB($\tau_s$) trap phosphorescence in a $D_2$-TCB crystal in the temperature range 1.3°K to 3.8°K. Details of the preparation and characterization of the traps are given in Section II-E (Experimental). The data illustrate two

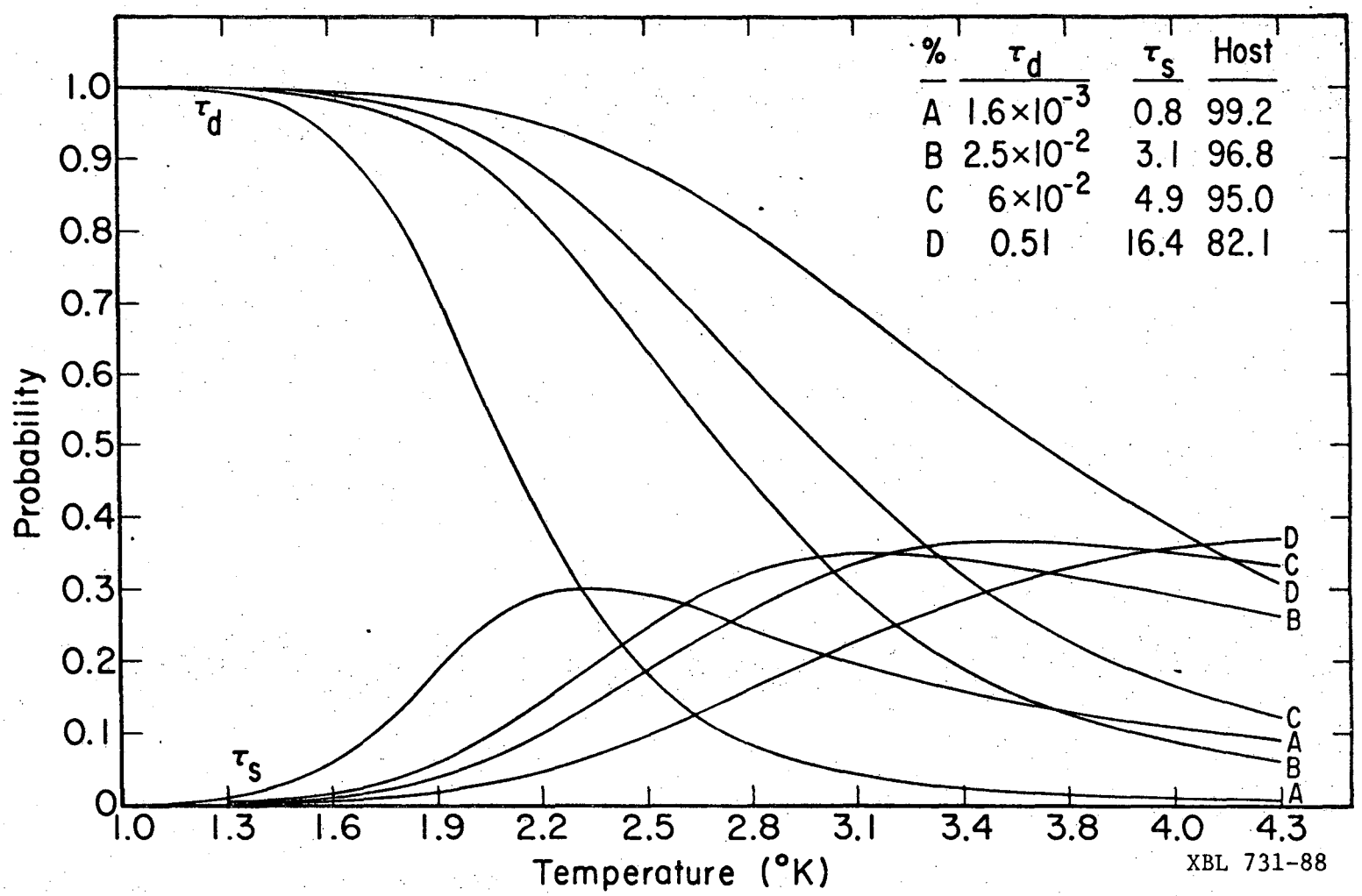


Fig. 10. Trap probabilities as a function of temperature for different percent compositions of the three species in the crystal indicated at the top of the figure. The two traps have 10 $cm^{-1}$ and 20 $cm^{-1}$ trap depths and the exciton band width is 4 $cm^{-1}$ for all curves.

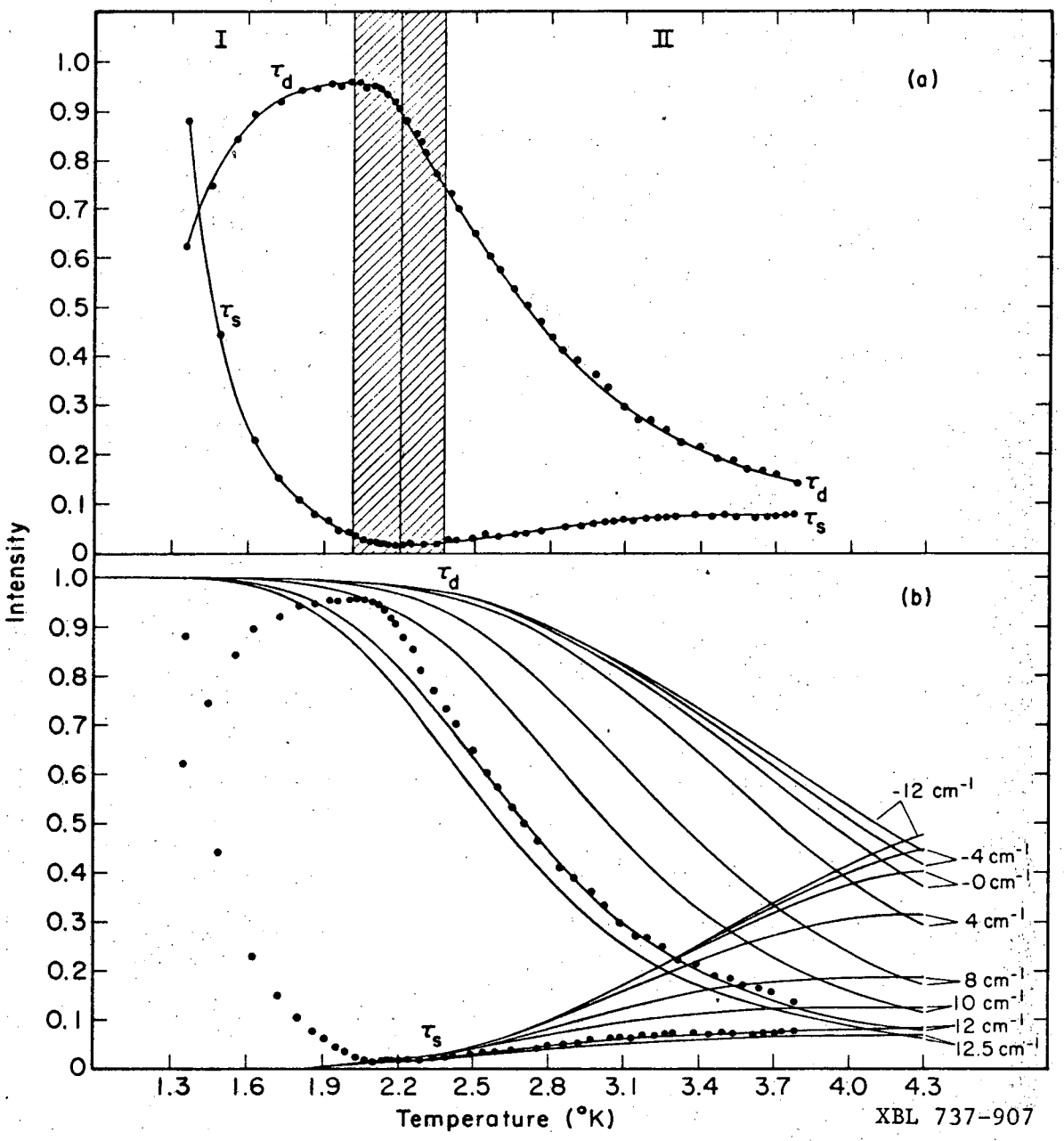


Fig. 11. (a) displays the intensity vs temperature experimental data. The deep trap $\tau_d$ is $H_2$-TCB, the shallow trap $\tau_s$ is DH-TCB, and the host molecules which comprise the exciton chains are $D_2$-TCB. The shallow and deep trap depths are respectively 12.8 $cm^{-1}$ and 23.5 $cm^{-1}$. Region I is the non-Boltzmann temperature region, and Region II is the temperature region in which the system is in thermal equilibrium. The shaded section indicates the transition region. (b) shows the experimental data in addition to curves calculated for various exciton bandwidths, $4\beta$, using the experimental trap depths and trap concentrations. It can be seen that in the Boltzmann equilibrium Region II, both the shallow trap data and the deep trap data fall on the 12 $cm^{-1}$ shallow and deep trap calculated curves.

distinct temperature regions, one below and one above a characteristic temperature $T_c$. These are labeled I and II, respectively, and correspond to regions where Boltzmann statistics are appropriate (II) because the trap and band state are in thermal equilibria and where Boltzmann statistics are inappropriate (I) because the finite lifetime of the excited states are short relative to the time necessary to equilibrate both the deep and shallow traps with the exciton band states.

Using the experimental values for $\Delta_1$, $\Delta_2$, $\tau_s$ and $\tau_d$, an excellent fit for both the deep and shallow trap temperature dependence in region II is simultaneously obtained for the lowest triplet band in $D_2$-TCB. A total band width of 12±2 $cm^{-1}$ and a positive intermolecular exchange interaction for $D_2$-TCB from these experiments (cf. Fig. 11) is to be compared to a total band width of 3.5 $cm^{-1}$ and a positive intermolecular exchange interaction for the same band in $H_2$-TCB (cf. Fig. 6). The relationship between isotope effect, the Born-Oppenheimer approximation and the band dispersion in these crystals will be discussed in a later publication.[25]

In the remainder of this chapter we will discuss the non-Boltzmann region (I) and formulate a general approach to exciton dynamics in this region which is amenable to experimentation. This region is characterized by insufficient phonon-trap interaction to provide thermal equilibrium between trap and band states. We will defer detailed interpretation of TCB in this region until later, but we will demonstrate proof that TCB in this region is not in thermal equilibrium but characterized by considerations of the next section.

B. Non-Boltzmann Distributions Between Exciton and Trap States

Below a characteristic temperature, the system does not come to thermal equilibrium within the lifetimes of the states because the phonon interaction with the trap states does not equilibrate the trap and band states at a fast enough rate. The problem must therefore be treated in terms of a set of coupled rate equations for the processes which are occurring. Differential equations describing the time variation of the states illustrated in Fig. 12 are given in Eqs. (II.4) through (II-7).

$$\frac{d[E]}{dt} = K^{ISC}[S^1] + K_{do}[\tau_d] + K_{so}[\tau_s] - K_{di}[E] - K_{si}[E] - K_E[E] \qquad \text{(II.4)}$$

$$\frac{d[\tau_d]}{dt} = K_{di}[E] - K_{do}[\tau_d] - K_d[\tau_d] \qquad \text{(II.5)}$$

$$\frac{d[\tau_s]}{dt} = K_{si}[E] - K_{so}[\tau_s] - K_s[\tau_s] \qquad \text{(II.6)}$$

$$\frac{d[S^1]}{dt} = P[S^o] - K_{s^1}[S^1] - K^{ISC}[S^1] \qquad \text{(II.7)}$$

[E] is the exciton population; $[S^1]$ is the population of the first excited singlet band, and $[S^o]$ is the ground state concentration; $[\tau_d]$ and $[\tau_s]$ are the deep and shallow trap populations; P is the rate constant for the production of excited singlet excitons, and $K_{s^1}$ is the rate constant for the relaxation of singlets to the ground state manifold, $S^o$, while $K^{ISC}$ is the intersystem crossing rate constant. $K_E$, $K_d$ and $K_s$ are the total rate constants for relaxation to the ground state from the exciton bands, deep traps and shallow traps, respectively;

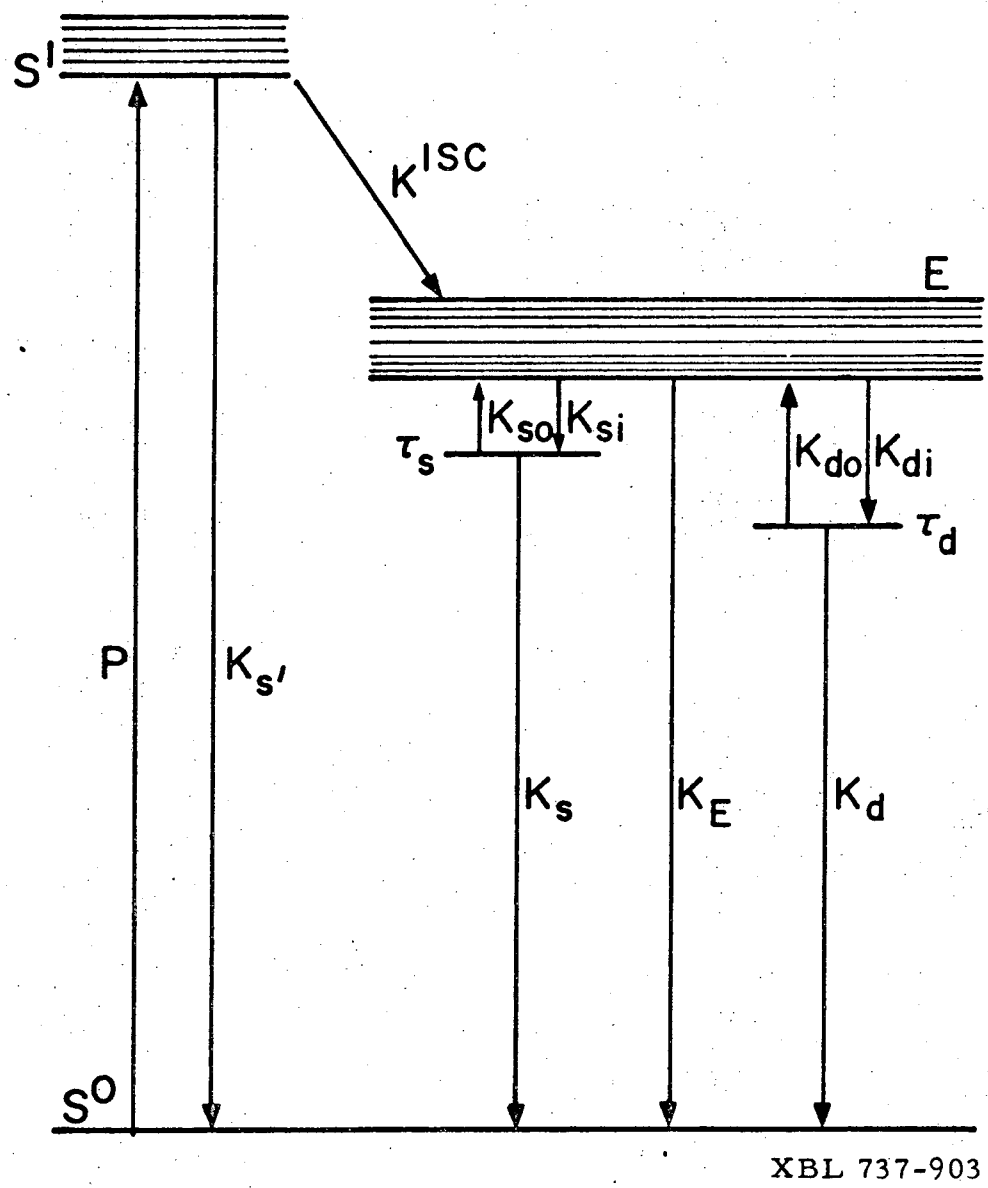


Fig. 12. Energy level diagram for an exciton and two-trap system showing rate constants used in the non-Boltzmann temperature region. $K_s$, $K_E$, $K_d$ and $K_{s1}$ are the total rate constants for relaxation to the ground state, $S^o$, for the shallow trap $\tau_s$, the exciton band E, the deep trap $\tau_d$, and the first excited singlet state $S^1$, respectively. P is the rate constant for the production of excited singlet states and $K^{ISC}$ is the intersystem crossing rate constant. $K_{si}$ and $K_{di}$ are the rate constants for excitations flowing into the shallow and deep traps, respectively, and $K_{so}$ and $K_{do}$ are the rate constants for excitation flowing out of the shallow and deep traps, respectively.

they include radiative and radiationless processes. $K_{si}$ and $K_{di}$ are the trapping rate constants for excitons entering the shallow and deep traps respectively, and $K_{so}$ and $K_{do}$ are the detrapping rate constants of the shallow and deep traps into the exciton bands. Implicit in the kinetic equations is the assumption that the excited state concentrations are low enough to insure that bimolecular annihilation and other non-linear effects may be neglected. The ground state concentration, $[S^o]$, is taken as a constant. If the lifetimes of the excited states are short, then $[S^o]$ will be the concentration of host molecules in the crystal. If the lifetimes of the exciton and trap states are long but are approximately the same, $[S^o]$ will remain constant with changing temperature since transferring population between excited states of the same lifetime will not result in changing $[S^o]$. However, if the lifetimes are long and differ greatly, then $[S^o]$ can change with temperature but will still be constant at any one temperature. Hence, Eqs. (II.4) through (II.7) can be solved for $[\tau_s]$ and $[\tau_d]$ by assuming steady state. The results are:

$$[\tau_s] = \frac{A\, K_{si}(K_d + K_{do})}{(K_d + K_{do})(K_s + K_{so} - C\, K_{si}) - B\, K_{di}(K_s + K_{so})} \qquad \text{(II.8)}$$

and

$$[\tau_d] = \frac{A\, K_{di}(K_s + K_{so})}{(K_d + K_{do})(K_s + K_{so} - C\, K_{si}) - B\, K_{di}(K_s + K_{so})} \qquad \text{(II.9)}$$

where

$$A = \frac{P\, K^{ISC}[S^o]}{(K_{s1} + K^{ISC})(K_E + K_{di} + K_{si})} \qquad \text{(II.10)}$$

$$B = \frac{K_{do}}{(K_E + K_{di} + K_{si})} \tag{II.11}$$

$$C = \frac{K_{so}}{(K_E + K_{di} + K_{si})} \tag{II.12}$$

1. Non-Boltzmann Low Temperature Limit

At some temperature well below the characteristic temperature $T_c$, $K_{so}$ and $K_{do}$ will become insignificant because of the lack of phonons to equilibrate the trap and band states at a rate comparable to the lifetime. Setting these two constants equal to zero in Eqs. (II.8) and (II.9) yields a low temperature limit for $\tau_d$ and $\tau_s$ given by

$$[\tau_d] = A\ K_{di} K_d^{-1} \tag{II.13a}$$

$$[\tau_s] = A\ K_{si} K_s^{-1} \tag{II.13b}$$

where the constants $K_d^{-1}$ and $K_s^{-1}$ are the deep and shallow trap lifetimes. $K_{di}$ and $K_{si}$, the rate constants for excitons flowing into the traps, can be identified in the coherent model with the average group velocity of the excitons, $\langle V_g \rangle$, weighted by distance between traps, i.e.,

$$K_{di} = \langle V_g \rangle\ d_d^{-1} \tag{II.14a}$$

$$K_{si} = \langle V_g \rangle\ d_s^{-1} \tag{II.14b}$$

The average exciton group velocity at a particular temperature is given by Eq. (I.9), and $d_d$ and $d_s$ are the average distances between the deep and shallow trap sites, respectively. It should be noted, however, that

the relationship between $K_{di}$, $K_{si}$ and $\langle V_g \rangle$ need not be restricted solely to coherent migration. The effects of phonon-exciton or impurity-exciton scattering on the average group velocities could be incorporated into $K_{di}$ and $K_{si}$ in cases intermediate between pure coherent migration and random walk migration when the explicit k dependence of these processes are delineated. In the limit that all coherence is lost via these interactions, the average group velocity approaches a temperature independent velocity given by the random walk parameters $\tau$ and $\langle d \rangle$ of Eqs. (I.11) and (I.12), respectively, i.e.,

$$\langle V_g \rangle \rightarrow \langle d \rangle / \tau \quad . \tag{II.14c}$$

Furthermore, the attenuated velocities in the intermediate and high temperature limits could be substituted into the above equations (Eqs. (IV.14a) and (II.14b)) and a kinetic description of energy migration in these limits would be given by substituting the appropriate velocity in the following equations. The trapping rate constants $K_{di}$ and $K_{si}$ are the inverse of the average time it takes an exciton to reach a trap, and hence in the temperature region under consideration, the rate of finding the trap is inversely proportional to the number of trapping sites available. The concentration of populated deep and shallow traps is then simply given by

$$[\tau_s] = A \ \langle V_g \rangle \ K_s^{-1} d_s^{-1} \tag{II.15a}$$

$$[\tau_d] = A \ \langle V_g \rangle \ K_d^{-1} d_d^{-1} \tag{II.15b}$$

or

$$[\tau_s] = A \quad \langle V_g \rangle \quad K_s^{-1} \quad N_s \tag{II.16a}$$

$$[\tau_d] = A \quad \langle V_g \rangle \quad K_d^{-1} \quad N_d \tag{II.16b}$$

where $N_d$ and $N_s$ are the deep and shallow trap site concentrations. When the rate of trapping is large relative to the decay of the exciton through other channels ($K_{di} + K_{si} >> K_E$), the steady state trap concentrations become independent of the average group velocity associated with exciton migration and hence independent of temperature:

$$[\tau_s] \simeq \left(\frac{P\ K^{ISC}}{K_{s1} + K^{ISC}}\right)\left(K_s^{-1}\right)\left(\frac{N_s}{N_s + N_d}\right)[S_o] \tag{II.17a}$$

and

$$[\tau_d] \simeq \left(\frac{P\ K^{ISC}}{K_{s1} + K^{ISC}}\right)\left(K_d^{-1}\right)\left(\frac{N_d}{N_d + N_s}\right)[S_o] \tag{II.17b}$$

and the ratio of the steady state concentrations is simply proportional to their respective total concentrations:

$$\frac{[\tau_s]}{[\tau_d]} = \frac{K_s^{-1} N_s}{K_d^{-1} N_d} \tag{II.18}$$

On the other hand, when the exciton decay competes with or is greater than the rate of trapping ($K_E >> K_{si} + K_{di}$), the steady state trap

concentrations are proportional to the temperature dependent average group velocity of exciton wave packets and are given by

$$[\tau_s] = \left[\frac{P\ K^{ISC}[S_o]}{\left(K_{s1} + K^{ISC}\right) K_E}\right] \langle V_g \rangle \quad K_s^{-1} \quad N_s \tag{II.19a}$$

and

$$[\tau_d] = \left[\frac{P\ K^{ISC}[S_o]}{\left(K_{s1} + K^{ISC}\right) K_E}\right] \langle V_g \rangle \quad K_d^{-1} \quad N_d \tag{II.19b}$$

The ratio of concentrations, however, still remains velocity and therefore temperature independent and is also given by Eq. (II.18).

Since the intensity of emission from the traps is proportional to number of trap sites, the invariance of the ratio over a finite temperature range provides an experimental test of this limit. In addition, since the temperature dependences of $[\tau_s]$ and $[\tau_d]$ result from a change in the average group velocity, the trap emission provides a tool capable of investigating the average velocity distribution in the exciton band and hence the coherence even at the very lowest temperatures.

2. Non-Boltzmann Intermediate Temperatures

As the temperature is increased toward $T_c$, the rate constants for energy transferring from traps to exciton bands are expected to increase. However, if the depths of the traps $\tau_s$ and $\tau_d$ below the bottom of the band are significantly different relative to kT, then excitations will be able to thermalize from the shallow trap $\tau_s$ into the band at temperatures too low for excitations to thermalize from $\tau_d$. The net result is that $K_{so}$ will become significant at temperatures where $K_{do}$ is still negligible.

Setting $K_{do}$ equal to zero in Eqs. (II.8) and (II.9), the concentration of traps is given by

$$[\tau_s] = \frac{A\,K_{si}}{\left[K_s + \left(1 - \frac{K_{si}}{K_E + K_{di} + K_{si}}\right) K_{so}\right]} \tag{II.20a}$$

$$[\tau_d] = \frac{A\,K_{di}(K_s + K_{so})}{K_d\left[K_s + \left(1 - \frac{K_{si}}{K_E + K_{di} + K_{si}}\right) K_{so}\right]} \tag{II.20b}$$

The dependence of these equations on $\langle V_g \rangle$ can be seen by substituting Eqs. (II.14a) and (II.14b) for $K_{di}$ and $K_{si}$. In this region the temperature dependence of $\tau_s$ and $\tau_d$ results from both the temperature dependence of $\langle V_g \rangle$ and the shallow detrapping rate constant, $K_{so}$. Specifically, when the radiative and radiationless decay of the exciton states to the ground state is slow relative to trapping, $K_E \ll K_{di} + K_{si}$, the group velocity dependence contained in $K_{di}$ and $K_{si}$ vanishes and $\tau_s$ and $\tau_d$ are given by

$$[\tau_s] = \left(\frac{P\,K^{ISC}[S_o]}{K_{s1} + K^{ISC}}\right)\left(\frac{N_s}{N_d + N_s}\right)\left(\frac{1}{K_s + \left[1 - \left(\frac{N_s}{N_s + N_d}\right) K_{so}\right]}\right) \tag{II.21a}$$

and

$$[\tau_d] = \left(\frac{P\,K^{ISC}[S_o]}{K_{s1} + K^{ISC}}\right)\left(\frac{K_s + K_{so}}{K_d}\right)\left(\frac{N_d}{N_d + N_s}\right)\left(\frac{1}{K_s + \left[1 - \left(\frac{N_s}{N_d + N_s}\right) K_{so}\right]}\right) \tag{II.21b}$$

respectively. Hence, the only temperature dependence of $\tau_s$ and $\tau_d$ is contained in $K_{so}$. In the other limit, when trapping is slow relative to the radiative and radiationless decay of the exciton states, $K_E >> K_{di} + K_{si}$, the shallow trap population reflects the average group velocity of the excitons via its trapping rate from the band ($K_{si}$); i.e.,

$$[\tau_s] = \frac{P\ K^{ISC}[S_o]}{\left(K_{s1} + K^{ISC}\right)(K_E)} \left(\frac{K_{si}}{K_s + K_{so}}\right) \qquad \text{(II.22a)}$$

The increase in the concentration of $\tau_s$ via the increase in the exciton $\langle V_g \rangle$ may be offset by the increased detrapping rate $K_{so}$ with temperature. By constrast, the deep trap concentration is given by

$$[\tau_d] = \frac{P\ K^{ISC}[S_o]}{\left(K_{s1} + K^{ISC}\right)(K^E)} \left(\frac{K_{di}}{K_d}\right) \qquad \text{(II.22b)}$$

and its temperature dependence results only from the increase in the group velocity of the exciton states with temperature. Finally, the temperature dependence of the <u>ratio</u> of the trap populations is only functionally related to $K_{so}$. This can be seen by combining Eqs. (II.21a) and (II.21b) in one case the Eqs. (II.22a) and (II.22b) in another. In both cases, the ratio is:

$$\frac{[\tau_s]}{[\tau_d]} = \frac{N_s}{N_d} \left(\frac{K_d}{K_s + K_{so}}\right) \qquad \text{(II.23)}$$

This is valid for both conditions, $K_E >> K_{di} + K_{si}$ and $K_E << K_{di} + K_{si}$. The important point of the above equations is that <u>the steady state</u>

concentration of the shallow and deep traps and thus the emission intensity depends implicitly upon both the group velocities in the band and the rate of detrapping of the shallow trap, $K_{so}$. Both of these quantities are measurable and provide, in principle, detailed information on the dynamics of trap-exciton interactions.

Qualitatively, the above processes can be physically viewed as follows. At very low temperatures both $K_{so}$ and $K_{do}$ are zero, and the populations $[\tau_s]$ and $[\tau_d]$ (except for changes caused by variations in $\langle V_g \rangle$) remain constant with increasing temperature. Since the shallow trap is closer in energy to the band than the deep trap, as the temperature is increased $K_{so}$ becomes nonzero before $K_{do}$, and some of the shallow trap's population is thermalized into the exciton band. This additional exciton population migrates in the band at an average group velocity determined by the temperature and band dispersion and is retrapped in deep traps. Contrary to what would have been expected for a thermal equilibrium, the deep trap gains population and intensity at the expense of the shallow trap. The importance of the deep trap concentration in relation to the magnitude of $K_{so}$ cannot be underestimated if a phenomenological understanding of the complexities and variations of impurity effects in crystals are to be properly understood.

## C. Other Considerations

To this point, the effects of possible differences in exciton and trap radiative and radiationless lifetimes on the temperature dependence of trap emission in the equilibrium temperature region have not been discussed. If $N_{tot}$ is the total triplet excited state population, then

$I_\tau \propto N_{tot} \frac{1}{Z(T)}$, where $N_{tot}$ is assumed to be temperature independent. If the total lifetime of the exciton and trap states are equal then the transfer of population between the band and trap does not alter the value of $N_{tot}$. However, if they are not equal, $N_{tot}$ will be temperature dependent, and $I_\tau \propto N_{tot}(T) \frac{1}{Z(T)}$. Hence, both $N_{tot}$ and z are functions of temperature.

$N_{tot}(T)$ can be determined from a system of differential equations assuming steady state. In terms of the parameters in Fig. 12, assuming the ground state concentration, $[S_o]$, remains constant,

$$\frac{d[S^1]}{dt} = P[S^o] - K_{s^1}[S^1] - K^{ISC}[S^1] = 0 \qquad \text{(II.24)}$$

$$\frac{dN_{tot}}{dt} = K^{ISC}[S^1] - K_\tau \chi N_{tot} - K_E(1 - \chi)\, N_{tot} = 0 \qquad \text{(II.25)}$$

$\chi$ is the percentage of population found in the trap. $\chi = 1/Z(T)$, and $(1 - \chi)$ is the percentage of population found in the band at a given temperature. At steady state $N_{tot}(T)$ is found to be

$$N_{tot}(T) = \frac{1}{[K_\tau \chi + K_E(1 - \chi)]} \left( \frac{K^{ISC} P[S^o]}{K_{s^1} + K^{ISC}} \right) \qquad \text{(II.26)}$$

where the only temperature dependent parameter on the right side of the equation is $\chi$. The ratio of the values of $N_{tot}(T)$ at two temperatures is

$$\frac{N_{tot}(T_2)}{N_{tot}(T_1)} = \frac{[K_\tau \chi(T_1) + K_E(1 - \chi(T_1))]}{[K_\tau \chi(T_2) + K_E(1 - \chi(T_2))]} \qquad \text{(II.27)}$$

Eq. (II.27) can be used to obtain $N_{tot}(T)$ relative to the value of $N_{tot}(T_1)$ which may be used to normalize the total population for all other temperatures. Thus, it is not necessary to know the actual value of $N_{tot}(T)$. A similar procedure can be used in the case of more than one trap or for corrections in $N_{tot}$ due to spin-lattice relaxation effects discussed above.

Another point which needs to be mentioned is that it has been tacitly assumed that intersystem crossing takes place from the singlet exciton band to the triplet exciton band and that exciton migration and trapping takes place from the triplet band. However, in some cases after exciting initially into the singlet exciton band, migration and trapping take place before intersystem crossing occurs producing triplet traps. If the triplet traps are in equilibrium with the band, the trap intensity as a function of temperature will reflect the parameters of the triplet system. However, if the time for a trap to transfer its excitation to the band is long compared to its lifetime for decay to the ground state, the triplet trap's population will be determined by the singlet trap's population. In this case, the problem must be considered in terms of the band width and trap depth of the singlet exciton and trap system giving careful consideration to the question of equilibrium. In studying triplet systems, if these complications arise, they can be eliminated to a large extent by suitably filtering the excitation light so that only the first triplet excited state is produced.

D. Qualitative Features of TCB in the Non-Boltzmann Region

The intensity vs temperature data for the two traps in deuterated $D_2$-TCB crystals in the temperature region before Boltzmann equilibration (I) is illustrated in Fig. 11a. The predicted behavior for a system of this type is indeed observed. The shallow trap intensity decreases and the deep trap intensity increases as the temperature increases. The shallow trap HD-TCB and the deep trap $H_2$-TCB are 12.8 $cm^{-1}$ and 23.5 $cm^{-1}$ below the $D_2$-TCB triplet band (k = 0), respectively. Because the Boltzmann factor is small in the temperature region of interest, there is a significant difference in the detrapping rates $K_{so}$ and $K_{do}$. Apart from the phenomenological observation that the temperature dependence of the two traps qualitatively behave in the proper fashion in Region I, several independent experimental observations conclusively demonstrate that $K_{so} >> K_{do}$ for this system. In Fig. 13 the zero field optically detected magnetic resonance (ODMR) spectra[26] for the two traps found in the deuterated TCB are illustrated. These spectra are obtained by monitoring the optical emission to the electronic origin from the two traps separately as a microwave field is swept in frequency.[27] The upper spectrum is the optically detected electron zero field D - |E| transition of the deep trap, $H_2$-TCB. The peak labeled A corresponds to electron spin only transitions while the peaks labeled B and B' are the simultaneous electron spin plus $^{35}Cl$ and $^{37}Cl$ nuclear quadrupole transitions, respectively.[28,29] The B and B' peaks are separated from the center line by the characteristic $^{35}Cl$ and $^{37}Cl$ excited state nuclear quadrupole frequencies. The C peaks correspond to simultaneous electron spin $^{35}Cl$ and $^{37}Cl$ double nuclear quadrupole transitions.[29]

Fig. 13. The optically detected magnetic resonance spectra for the deep trap (upper spectrum) and the shallow trap (lower spectrum) found in deuterated tetrachlorobenzene in the non-Boltzmann temperature Region I. The A peaks are electron only transitions. The B and B' peaks are $Cl^{35}$ and $Cl^{37}$ electron spin plus nuclear quadrupole spin transitions, respectively. The C peaks are electron spin plus $Cl^{35}$ and $Cl^{37}$ double nuclear quadrupole spin transitions. The large peaks in the deep trap spectrum have been truncated to facilitate display. In the deep trap spectrum between peaks B' and C on the low frequency side is a peak going in the opposite direction from the rest of the deep trap spectrum and in the same direction and at the same frequency as the shallow trap electron spin only transition.

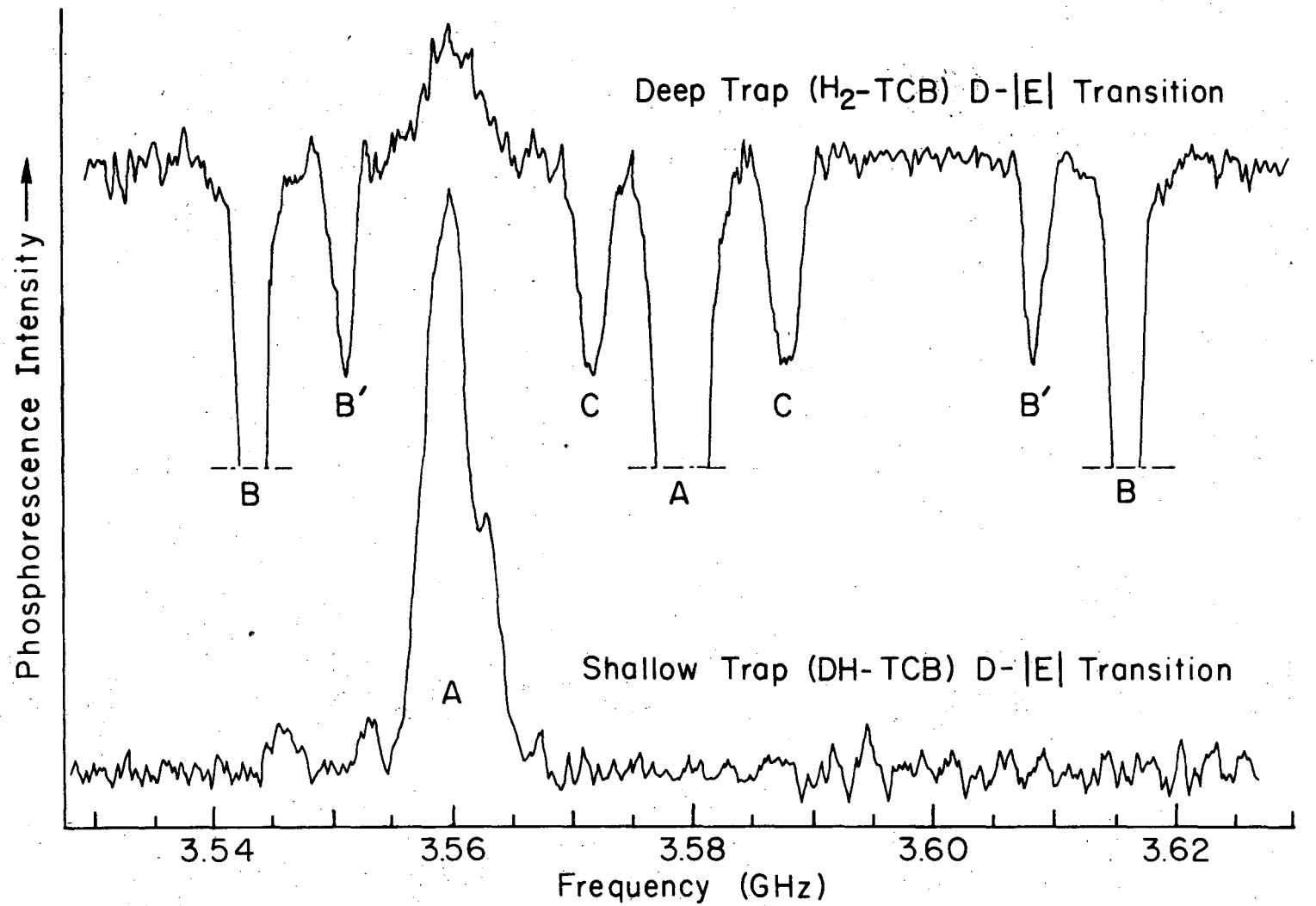


XBL 737-906

Fig. 13

These transitions are split from the electron spin only transition A peak by the difference in the $^{35}Cl$ and $^{37}Cl$ quadrupole frequencies. On the low frequency side of the deep trap spectrum between peaks B' and C is a peak going in the opposite direction from the rest of the spectrum at exactly the frequency associated with the shallow trap D - |E| transition. This will be referred to as the T peak. The major peaks A and B of the deep trap spectrum have been truncated to facilitate display. The lower spectrum in Fig. 14 is the D - |E| transition of the shallow trap, DH-TCB. Only one peak is observed even at moderately high microwave powers at temperatures above 1.3°K. This peak corresponds to the fully allowed electron spin only transition. The change in the light intensity in the shallow trap spectrum is opposite the direction of the change in the light in the deep trap spectrum except for the T peak. These results can be understood as follows.

The spin alignment of the shallow trap is changed by the application of the microwave field at the transition frequency, 3.5600 GHz. This change in spin alignment is at least partially carried into the exciton band by shallow trap detrapping processes. The net result is that the exciton band acquires an altered spin alignment which is carried into the deep traps by the trapping process $K_{di}$. This results in a change in the deep trap light intensity in the same direction and at the same microwave frequency as the shallow trap transition. This is the observed T peak in the deep trap spectrum. Similar effects are observed in $H_2$-TCB when the exciton band spin alignment is altered by a microwave field and the trap emission is monitored.[30] The significant point here

is that there is no corresponding T peak in the shallow trap spectrum even though the deep trap transition is more than an order of magnitude stronger. This implies that the shallow trap excitations are detrapping, migrating and retrapping in deep trap sites, but that deep trap excitations are not transferring population to the shallow trap sites to any significant extent.

A second important observation can be made from the ODMR spectra. Because the electron spin and the nuclear quadrupole eigenstates are coupled by the electron-nuclear hyperfine interaction, only the pure electron transition will be observed in the absence of the hyperfine interaction. If the lifetime of a state is short compared to the inverse frequency associated with the hyperfine interaction, then the triplet state electrons will not be influenced by hyperfine interaction and the coupling of the electron eigenstates to the nuclear eigenstates will vanish, and the quadrupole peaks ($B(Cl^{35})$ and $B'(Cl^{37})$) will be absent from the ODMR. In TCB and similar compounds the hyperfine interaction is on the order of 1 MHz.[29,30] The fact that quadrupole transitions are not observed in the shallow trap ODMR spectrum sets an upper limit of less than 1 μsec for the time an excitation remains trapped in the shallow trap at 1.3°K. On the other hand, the fact that strong quadrupole peaks are observed in the deep trap ODMR spectrum implies that excitations remain in the deep traps for times much longer than 1 μsec. When the temperature is lowered to about 1.2°K to decrease $K_{so}$, weak quadrupole satellites on the shallow trap spectra appear at high microwave power indicating that the detrapping rate constant $K_{so}$ is in fact becoming smaller. Thus, the ODMR data in addition to the temperature dependence of the trap emission data

established that in the temperature Region I immediately before Boltzmann equilibration occurs the shallow trap is detrapping rapidly while the deep trap is detrapping slowly relative to their lifetimes, i.e., $K_{so} >> K_{do}$.

## E. Experimental

1,2,4,5-tetrachlorobenzene (TCB) was purchased from Aldrich Chemical Company, recrystallized from ethanol and vacuum sublimed to remove residual solvent. The recrystallized TCB was vacuum sublimed into a zone refining tube, repeatedly outgassed, and sealed under vacuum in a 10 mm diameter tube. The sample was then zone refined for 600 passes at a rate of 1 cm/hr. Only the center third of the zone refined material was used.

Deuterated TCB was prepared as follows.[31] $D_2O$ and $SO_3$ were reacted to form $D_2SO_4$. $D_2SO_4$ and $H_2$-TCB were then heated for 12 hr in a sealed tube at 150°C. The cold reaction mixture was poured onto cracked ice and the exchange product was filtered off, washed with water and used as the starting material for the next exchange. Five successive exchanges were performed in this manner. The final product was washed thoroughly with water, recrystallized from ethanol, vacuum sublimed, and zone refined for 300 passes. Two separate batches were prepared in this manner.

The percentage deuterium in each sample was determined in the following manner. An accurately weighed sample from each batch of the deuterated TCB was dissolved in a known amount of $CS_2$. Known amounts of dioxane, $C_4H_8O_2$, were added until the concentration of protons from the two species in the $CS_2$ solution were approximately equal. Proton NMR

spectra were then taken and integrated using a Varian model T60 NMR spectrometer. The spectra were also integrated mechanically by taking the area under the spectral peaks. Comparison of these areas allowed the computation of the percent of deuteration of the TCB. As a check on this procedure a second standard was used. A weighed sample of deuterated TCB was dissolved in a known volume of deuterated benzene (95.5%D). The deuterated benzene served as an internal standard in the analysis of the proton NMR spectra. Both of these procedures were repeated 6 times and gave the same result, although the standard deviation was smaller when using the dioxane standard. The deuterated TCB samples contained 97.5±0.1% deuterium.

Since the deuteration procedure is limited by the percent deuteration of the $D_2SO_4$, the deuterated TCB consisted of 3 species, $H_2$-TCB, DH-TCB, and $D_2$-TCB. Assuming that the substitution reaction proceeds with the same probability for exchange of either a hydrogen or deuterium atom with the ring, the percentage of the three species found in the sample can be determined by their statistical probabilities. A sample which contains 97.5% deuterium is composed of 95.06% $D_2$-TCB, 4.88% DH-TCB and 0.06% $H_2$-TCB.

Quantities of both TCB and deuterated TCB were vacuum sublimed into individual crystal growing tubes and outgassed. Single crystals were then grown using the Bridgeman technique. The large single crystals were cleaved, and small transparent pieces were used as experimental samples. The samples were placed in a liquid helium dewar which was cooled slowly to 77°K over a period of 30 min after which liquid He was added. The temperature was monitored by an NRC Equipment

Corporation Alphatron vacuum gauge type 530. The temperature can be read to 0.01°K; however, a small systematic error in temperature measurement may occur if the crystal is not in complete thermal equilibrium with the liquid helium bath. The temperature was varied between 4.2°K and 1.35°K by changing the rate of pumping on the liquid helium.

The samples were illuminated by a 100 watt PEK high pressure mercury arc lamp through a 2800Å interference filter. Excitation takes place into the singlet manifold and after intersystem crossing the first excited triplet state is populated. Phosphorescent emission from the triplet state is detected at right angles to the exciting light using a 3/4 meter Jarrell Ash Czerny-Turner scanning spectrometer with a cooled EMI 6256 photomultiplier tube. The spectrometer is also fitted with a camera which was used for absorption spectra to determine the exciton origin and trap depths. The phosphorescent emission spectrum of the $H_2$-TCB samples consists of two electronic and vibronic origins, one from the exciton band, 3748.2Å, and the other from a trap, 21.3 $cm^{-1}$ lower in energy. A detailed analysis of the phosphorescence spectrum has already been reported.[11,32] Although the exact nature of this trap is unknown doping of impurities into the TCB crystals does not enhance the intensity of this trap, but rather produces another trap of lower energy.[9] The trap is thought to be associated with a crystal lattice defect. At 4.2°K, the $D_2$-TCB spectrum consists of three origins, one from each of the three species found in the deuterated TCB crystal. The $D_2$-TCB triplet exciton emission origin is at 3745Å. The mono-deuterated trap, DH-TCB, is 12.8 $cm^{-1}$ lower in energy, and the diproto trap, $H_2$-TCB, is 23.5 $cm^{-1}$

lower in energy than the exciton origin.

Optically detected magnetic resonance (ODMR) spectra of the trap in the TCB crystals and of the traps in the deuterated TCB crystals gave characteristic tetrachlorobenzene spectra. The details of the TCB trap's ODMR spectra and of the experimental set-up are reported elsewhere.[11]

The results of the trap intensity vs temperature measurement are shown in Fig. 6 for the $H_2$-TCB and in Fig. 11 for the $D_2$-TCB traps. The figures are typical of several sets of data taken on separately prepared TCB single crystals and on single crystals prepared from each of the two batches of deuterated TCB.

Finally, all computer calculations illustrated in the figures and tables were performed on a CDC 7600.

# III. DECAY OF LOCALIZED STATES INTO DELOCALIZED BAND STATES

## A. Introduction

In an attempt to more fully understand the long range transfer of triplet excitation energy between localized states via exciton band[1] intermadiates, an experimental approach has been developed and employed which allows the first step in the indirect transfer process, the phonon assisted promotion of a localized excitation to a delocalized band state, to be isolated and studied. The technique which will be presented here involves the optical detection[33-35] of the loss of electron spin coherence[33] of the localized excitation when the state is spin locked[36] in the rotating frame. In addition, the first experimental data on the temperature dependence of the rate of phonon assisted promotion of localized excitations to band states is reported. Finally, a model which includes the exciton band dispersion and density of states, phonon-localized excitation interactions (including single phonon, Raman, and multiple phonon processes), and the interaction of a localized state with the exciton band is presented and used to describe the promotion process and the radiationless decay of the phonon activated intermediate into the exciton band.

The importance of this initial step in the indirect transfer process cannot be underestimated, for it is one of the essential features which determines whether or not thermal equilibrium between delocalized band states and localized states can be achieved within the lifetime of the excited states and hence determines whether Boltzmann statistics

apply to excited solids at low temperatures.[37] Furthermore, the kinetics of the macroscopic transport of electronic excitation energy in solids also depend in detail upon an understanding of this step, as well as upon the nature of the exciton propagation (coherent vs incoherent) in the band.[8,9,11,13,14]

## B. Discussion

The use of electron spin coherence to study kinetic phenomena associated with excited triplet states can be understood by viewing two of the excited triplet state spin sublevels in a reference frame rotating at the Larmor frequency (the interaction representation). The laboratory frame population of one of the two spin sublevels can be represented as a pseudomagnetization along the positive z-axis of the rotating frame and the laboratory frame population of the other spin sublevel is related to a pseudomagnetization along the negative z-axis of the rotating frame. It has been shown that when the time-dependent density matrix describing the dynamics of the electron spin ensemble is displayed through the electric-dipole transition moment operator responsible for phosphorescence, the projection of the magnetization onto the z-axis in the rotating frame is usually the only observable associated with a change in the intensity of phosphorescent emission.[33,39]

Optically detected electron spin coherence can be used in the measurement of the rate of promotion of a localized state to a delocalized band state by determining the contribution of the promotion process to the loss of electron spin coherence when the spin ensemble is locked in the rotating frame. The loss of the spin locked pseudomagnetization, M, as a function of time, t, can be given by the following equation

$$M(t) = M_o e^{-\left(K^L + K^{T_{1\rho m}} + K^P\right)t} = M_o e^{-K_{T_{1\rho}} t} \qquad \text{(III.1)}$$

where $K^L$ is the average of the rate constants for decay to the ground state of the two spin sublevels involved, $K^{T_{1\rho m}}$ (Ref. 40) is the rate constant for longitudinal spin relaxation along the spin locking field, and $K^P$ is the rate constant for the phonon assisted promotion of localized states to delocalized states. ($K^P$ corresponds to either $K_{so}$ or $K_{do}$ of Chapter II.) The rate constant for the total decay of spin coherence, $K_{T_{1\rho}}$, is the sum of these rate constants.

Specifically by applying a $\pi/2$ microwave pulse to one of the three zero field transitions associated with an ensemble of localized triplet states, two of the spin sublevel populations become saturated in the laboratory frame but are still evolving coherently in time. The pseudomagnetization in the rotating frame is simply tilted 90° into the x-y plane. Spin locking[36] by phase shifting the applied microwave field 90° immediately after the $\pi/2$ pulse prevents the spin coherence from being lost for a time corresponding to $T_{1\rho}$. $T_{1\rho}$ can be measured by turning off the spin locking field and immediately restoring the pseudomagnetization to the z-axis by a final $\pi/2$ pulse having the same phase as the initial pulse and measuring the resulting change in the phosphorescence intensity as a function of the spin locked time.

The uniqueness of spin locking to the measurement of kinetic phenomena is that once the triplet spin states have been locked in the x-y plane, any additional population entering the ensemble of localized states at later times via incoherent processes such as intersystem

crossing or trapping of delocalized band states, enters along the + or - z-axis of the rotating frame because of the random phases of the entering spins relative to the spin locked ensemble. Consequently, this additional population is driven by the microwave field in a plane perpendicular to the x-y plane during the spin lock period. The net effect is that this incoming population results in an incoherent disk of spins in a plane perpendicular to the x-y plane and has no net pseudomagnetization along the z-axis. When the final $\pi/2$ pulse is applied, this disk is tipped into the x-y plane and still has no net projection along the rotating frame z-axis. The result in the laboratory frame is that any population entering the localized state after the initial $\pi/2$ pulse is incoherently and equally distributed between the two spin sublevels. Hence, when the final $\pi/2$ pulse is applied to observe the spin locked population, there will be no change in the phosphorescence intensity due to the non-spin locked population. Thus, population feeding into the ensemble of localized states can be eliminated from consideration, and only those processes which remove population from the ensemble may be isolated and studied. These features are illustrated diagramatically in Fig. 14 and explained in the figure caption.

## C. Experimental

The basic experimental design for optically detected magnetic resonance (ODMR) is similar to that described previously.[28] Microwave pulses of the appropriate phase were obtained as follows. The microwave output of a Hewlett Packard Model 8690B sweep oscillator was amplified by a 1 watt microwave traveling wave amplifier. The output of this amplifier was then divided into two separate parallel channels by use of

Fig. 14. (A) A diagrammatical representation of the rotating frame pseudomagnetization for a system in which intersystem crossing occurs only to one level; (a) pseudomagnetization before the application of microwaves; (b) after initial $\pi/2$ pulse applied along the rotating frame x-axis; (b') the field is shifted 90° to the y-axis spin locking the initial pseudomagnetization. The partial disk indicates incoming population being driven in a plane perpendicular to the spin locked population; (c) a component of pseudomagnetization developing along the negative y-axis due to longitudinal relaxation along the spin locking field is indicated by the double headed arrow. The disk represents entering population after several hundred nanoseconds incoherently distributed and precessing about the spin locking field; (d) after the application of the final $\pi/2$ pulse along the x direction, the remaining spin lock population is restored to the z-axis.

(B) An illustration of the spin sublevel population change in the laboratory frame under the application of the spin locking pulse sequence. (a) All population in the middle spin sublevel; (b) microwaves coupled the middle and bottom sublevel for a time which produces a $\pi/2$ pulse. The sublevel populations are equalized; (b') the system is spin locked. The coherent population is equally distributed between the two spin sublevels but incoherent population beings to enter; (c) the coherent population decreases and the incoherent population becomes equally distributed; (d) the final $\pi/2$ pulse increases the bottom sublevel population. No changes occur due to the incoherent population.

(C) A representation of the microwave pulse sequence.

(D) Illustration of the change in the phosphorescence intensity as observed in an actual experiment due to the spin locking pulse sequence. The change in intensity labelled $\Delta I$ is caused by the application of the final $\pi/2$ pulse and is proportional to the spin locked pseudomagnetization remaining at time $\tau$.

OPTICALLY DETECTED SPIN LOCKING IN THE PRESENCE OF FLUCTUATING SPIN SUBLEVEL POPULATIONS

(The Relationship between the Laboratory Frame and the Interaction Representation)

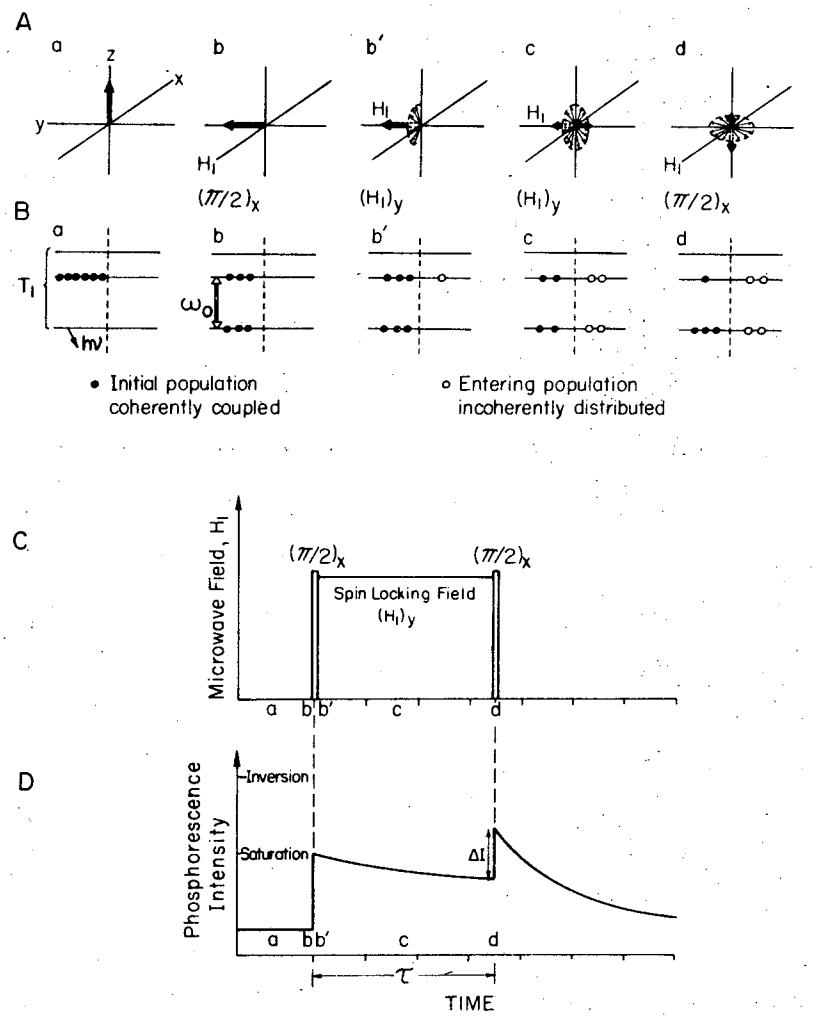


XBL 7311-5594

Fig. 14

Anaren Corp. 90° hybrid coupler. Each channel contained a 10 cm General Radio adjustable sliding coaxial line, a Narda variable attenuator, 20 db isolators, and two Hewlett Packard 33124A PIN diodes in series which were used to produce microwave pulses of the desired duration. The pin diodes were driven by National Semiconductor DH0035CG current drivers which were controlled by TTL logic circuits designed and constructed in this laboratory. The two channels were then combined by an Anaren 180° hybrid coupler, and the resultant microwave pulse sequence was passed through a Hewlett Packard 8430A band pass filter to remove low frequency switching transients. Finally, the microwave pulses were amplified by a 20 watt TWT amplifier whose output was directed into a 50Ω coaxial cable and terminated into a slow wave helix which contained the sample. Phase adjustments were made by observing the response of a crystal diode detector to the incident power from the individual signals when separate channels were switched on and to the resultant signal when two channels were opened concurrently and added together.

The spin lock experiment was performed on two systems, $h_2$-1,2,4,5-tetrachlorobenzene ($h_2$-TCB) in $d_2$-1,2,4,5-tetrachlorobenzene ($d_2$-TCB)[37] and $h_2$-1,2,4,5-tetrachlorobenzene in $h_{14}$-durene,[11,14] which are examples of a "shallow" localized $^3\pi\pi^*$ state and a "deep" localized $^3\pi\pi^*$ state, respectively. The preparation and characterization of the samples are as described earlier (Section II-E). $h_2$-TCB is 23.5 $cm^{-1}$ below the k = 0 state of the $d_2$-TCB triplet exciton band[37] and $h_2$-TCB is 1456 $cm^{-1}$ below the k = 0 state of the $h_{14}$-durene[42] triplet exciton band. The D-E and the 2E transitions were used for these systems respectively. The

transition frequencies for $h_2$-TCB in $d_2$-TCB and $h_2$-TCB in $h_{14}$-durene are 3.578 GHz and 1.746 GHz. The samples were suspended in a liquid helium cryostat in contact with the liquid helium bath. Temperatures below 4.2°K were reached by pumping on the helium, and the bath temperature was obtained from measurements of the vapor pressure of helium gas in the cryostat. In the experiment, the sample was continuously illuminated by a PEK 100 watt Hg-Xe lamp whose light was filtered by a Schott 3100Å interference filter. The intensity of phosphorescence from the electronic origin of each sample was monitored while the spin locking microwave pulse sequence was applied. The change in phosphorescence intensity was time averaged with a Varian Model C-1024 CAT.

## D. Results

Figure 14 illustrates in a purely schematic fashion the relationship of the phosphorescence intensity to state of the electron spin ensemble in the laboratory frame and in the interaction representation. Experimental data for the $h_2$-1,2,4,5-tetrachlorobenzene $\tau_z \rightarrow \tau_y$ transition in a $d_2$-1,2,4,5-tetrachlorbenzene host are presented in Fig. 15. An example of the change in phosphorescence intensity, $\Delta I$ (cf Fig. 14), induced by the final $\pi/2$ pulse as a function of the spin lock time $\tau$ at 1.8°K is presented in the lower portion of Fig. 15. The signal to noise of the data illustrated is representative of 600 time averaged accumulations at a rate of 5 per second. A semilog plot of $\Delta I$ vs the spin lock time $\tau$ reveals an exponential decay with a $T_{1\rho}$ of 4.95 msec at 1.8°K. This is illustrated in the upper portion of Fig. 15. When the same experiment is repeated with $h_2$-TCB doped into $h_{14}$-durene (1% m/m), $T_{1\rho}$ is found to

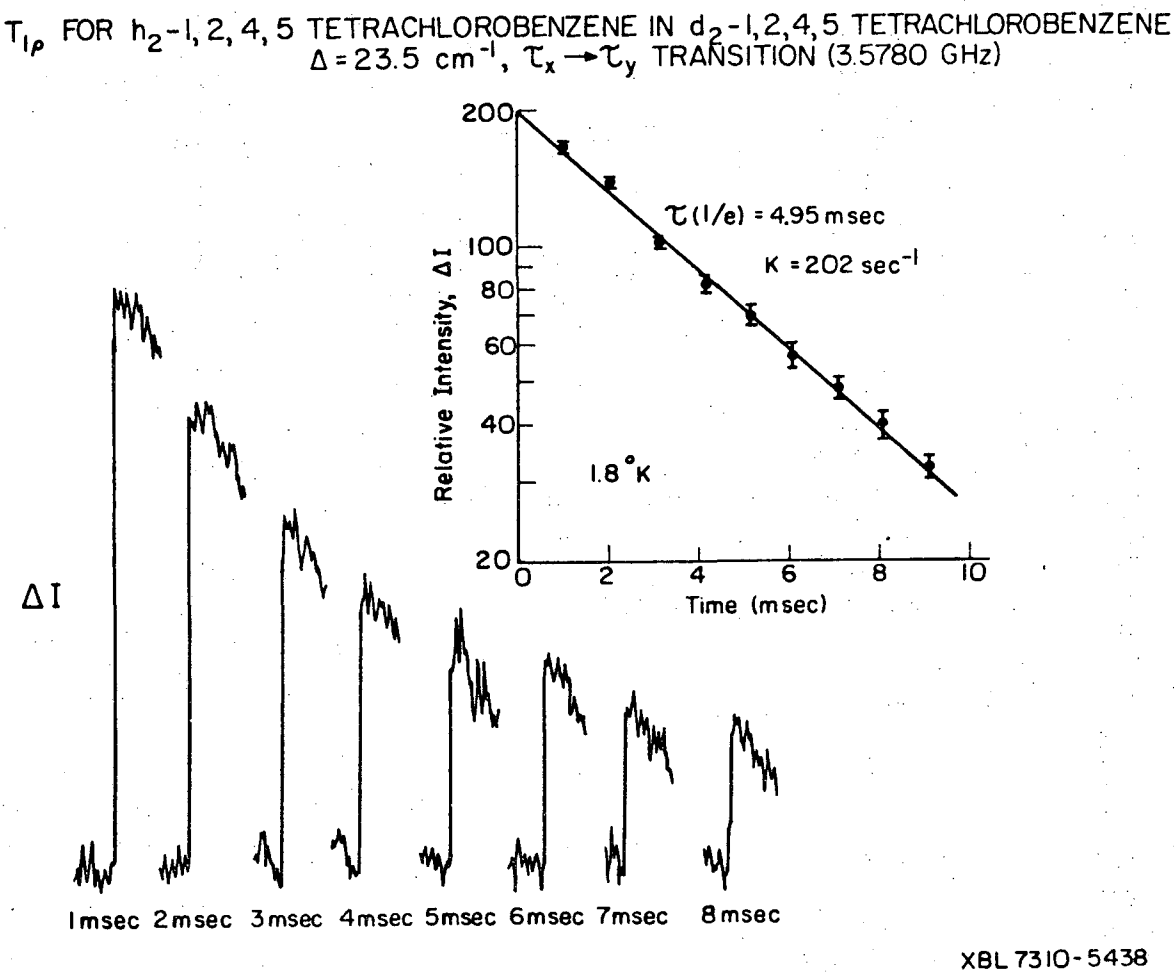


Fig. 15. The lower portion gives typical experimental measurements of the change in the phosphorescence intensity due to the final $\pi/2$ probe pulse at various times. A semilogarithmic plot of these $\Delta I$ values is plotted against time in the upper part of the figure. The decay is exponential.

be significantly longer ($\tau(1/e)$ = 24 ms). Moreover, when the temperature dependence of $h_2$-TCB in $h_{14}$-durene was investigated, $T_{1\rho}$ was found to be invariant within experimential error throughout the range from 4.2°K to 1.5°K. This is illustrated in the lower portion of Fig. 16 in which $K_{T_{1\rho}}$ is plotted against 1/T. On the other hand, for $h_2$-TCB in $d_2$-TCB, the data revealed a dramatic temperature dependence. $T_{1\rho}$ varied more than an order of magnitude in the limited range from 1.4°K to 2.1°K. Due to the unavailability of fast transient averaging equipment, the results of these preliminary experiments could not be extended to higher temperatures. A semilog plot of $K^P$ for $h_2$-TCB in $d_2$-TCB vs 1/T is given in the upper portion of Fig. 16. $K^P$ was obtained by subtracting $K^L$ and $K^{T_{1\rho m}}$ measured in the durene host from $K_{T_{1\rho}}$ measured in $d_2$-TCB. <u>$K^P$, the phonon assisted promotion rate constant, (which corresponds to $K_{do}$ of Chapter II) is seen to be a rapidly changing non-exponential function of temperature</u>.

## E. Model for the Decay of Localized States into Delocalized Band States

In view of the central role the detrapping rate plays in achieving Boltzmann equilibrium, a concrete model for the detrapping process whose details can be verified and tested experimentally is desirable. In this context we develop a model in this section that describes the decay of the localized state into the delocalized exciton band[43,44] in a general way but includes in a well defined manner important considerations such as the phonon dispersions and populations, the exciton dispersion, and phonon-trap interactions. We will only consider phonon single-trap interactions where the decay of the trap into the

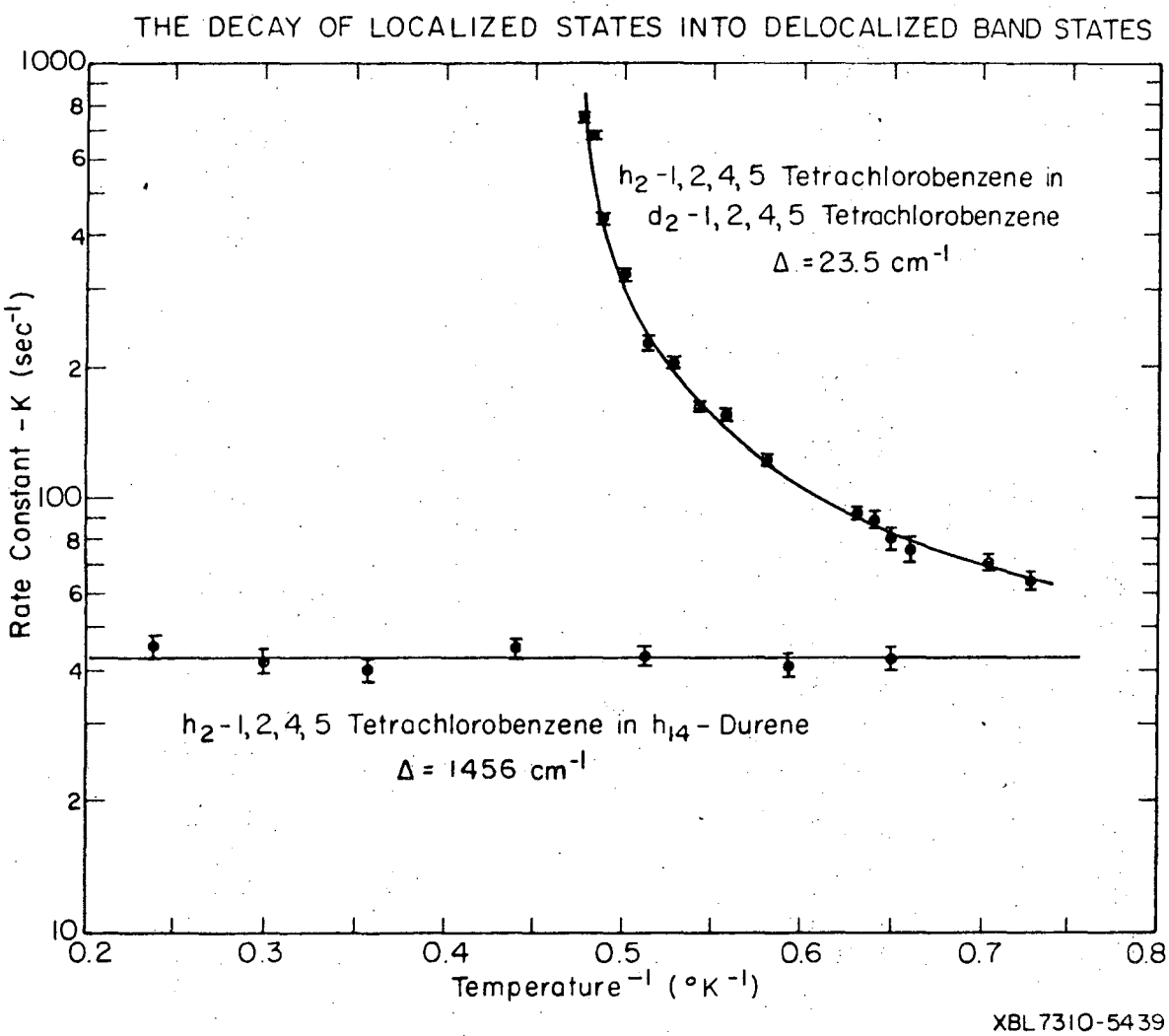


Fig. 16. The lower portion is a semilogarithmic plot of the rate constant for the loss of spin locked population vs 1/T for the $h_2$-1,2,4,5-tetrachlorobenzene in $h_{14}$-durence system. This is and example of a deep localized state ($\Delta \sim 1450$ cm$^{-1}$) and the rate constant is temperature independent. The upper portion is a plot of the rate constant for the loss of the localized state spin locked population due only to the promotion to delocalized band states for $h_2$-TCB in $d_2$-TCB ($\Delta$ = 23.5 cm$^{-1}$). A model for the observed temperature dependence is presented in the text.

band conserves the total momentum and energy of the overall process. Further we shall assume that the initial interaction of a phonon and trap results in an intermediate state that is degenerate with some k state in the band. The decay of the intermediate localized state into the delocalized band states is taken to be a radiationless relaxation process[45] and is displayed in the form of a Golden Rule rate.[46] The assumptions implicit in this model are that the creation of the intermediate state is a stochastic process[47] and that the decay of the intermediate trap state into the band states is irreversible in the sense that recurrence[48] is negligible because of the high density of exciton states in the band and the finite lifetime of k states in the band into which the intermediate has evolved. This is schematically illustrated in Fig. 17.

In this model the probability per unit time of a trap, $\langle \tau|$, interacting with a phonon, $P(\varepsilon)$, of energy $\varepsilon$ and detrapping into a specific band state, $\langle k|$, having momentum $\hbar k$ via an intermediate state, $\tau_i$, is given by

$$K_{\varepsilon k} = (2\pi/\hbar)\,\langle n(\varepsilon)\rangle_T |\langle \tau\, P(\varepsilon)|\mathcal{H}_{TP}|\tau_i\, P(\varepsilon - E_i)\rangle|^2 \qquad \text{(III.2)}$$

$$|\langle \tau_i\, P(\varepsilon - E_i)|\mathcal{H}_{TE}|k\, P(\varepsilon - E_i)\rangle|^2 \rho(E_i)$$

$\langle n(\varepsilon)\rangle$ is the number of phonon states with energy $\varepsilon$; $|\langle \tau\, P(\varepsilon)|\mathcal{H}_{TP}|\tau_i\, P(\varepsilon - E_i)\rangle|^2$ is the probability of creating an intermediate $\tau_i$ which can be identified with $|\tau_i\, P(\varepsilon - E_i)\rangle$. Both direct and Raman[49] trap-phonon interactions are included by $\varepsilon = E_i$ and $\varepsilon > E_i$, respectively. Obviously the initial phonons $P(\varepsilon)$ must have

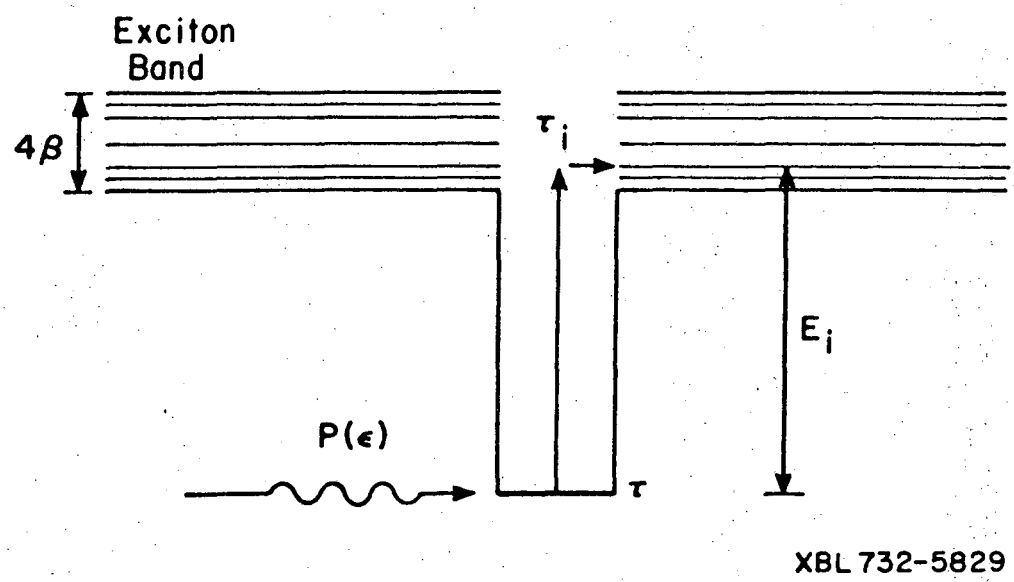


Fig. 17. Schematic representation of the detrapping process. $P(\varepsilon)$ is a phonon of energy $\varepsilon$ interacting with a trapped excitation $\tau$ to produce an excited trap state $\tau_i$ equienergetic with the $i^{th}$ exciton band state. The excitation then decays into the $i^{th}$ band state. $E_i$ is the energy difference between the trap $\tau$ and the band state. The energy of the phonon $P(\varepsilon)$ must obey $\varepsilon \geqslant E_i$.

energies greater than or equal to $E_i$ unless multiphonon processes are included. If the multiple phonon processes are important, then the matrix elements in Eqs. (III.2) and (III.4) are modified to include the interaction of the localized state with the additional phonons. For the two phonon cases, one must include the two phonons, $P(\varepsilon)$ and $P(\varepsilon')$. $\langle n(\varepsilon)\rangle_T$ is replaced with $\langle n(\varepsilon)\rangle_T \langle n(\varepsilon')\rangle_T$ and a summation over all pairs of initial and final phonons which conserve the energy of the overall process must be performed in Eq. (III.4). Extenstion to higher order processes is straighforward. The radiationless decay of the intermediate $\tau_i$ into the exciton manifold whose k states are at energies $E_i$ above the trap is given by $|\langle \tau_i\, P(\varepsilon - E_i)|\mathcal{H}_{TE}|k\, P(\varepsilon - E_i)\rangle|^2\, \rho(E_i)$ where $\rho(E_i)$ is the exciton density of states function evaluated at $E_i$. We will assume that the final phonon, $P(\varepsilon - E_i)$, is not bound to or does not interact with the final exciton k state. With this assumption the intermediate trap-exciton coupling Hamiltonian, $\mathcal{H}_{TE}$, does not depend upon coordinates of the phonon wave vectors and hence only coordinates of the trap and band state need be considered. Although there are many mechanisms (i.e., many forms of $\mathcal{H}_{TE}$) which could describe the coupling of the intermediate trap to the band, in the absence of experimental data it is not clear at this point what the most appropriate choice would be. The coupling matrix elements must certainly, however, reflect the exchange between the trap and band of both electronic energy and the local distortion that is adiabatically propagated with the excited state in the Frenkel limit.

The average number of phonons at energy $\varepsilon$ at temperature T, $\langle n(\varepsilon)\rangle_T$, is given by the Planck distribution function,[50,51]

$$\langle n(\varepsilon)\rangle_T = \frac{1}{e^{\varepsilon/kT} - 1} \tag{III.3}$$

in which the phonon energies $\varepsilon$ are given explicitly by the phonon dispersion of the crystal. The <u>total</u> detrapping probability per unit time which is the detrapping rate constant $K_{so}$ or $K_{do}$ is found by summing over all phonons of energy $\varepsilon \geqslant E_i$ and then summing over all intermediate states $\tau_i$ which have energies $E_i$ greater than or equal to the energy difference between the bottom of the band and the trap, i.e.,

$$K^P = \sum_k \sum_{\varepsilon \geqslant E_i} K_{\varepsilon k} \tag{III.4}$$

When considering the temperature region in which $K^P$ is just becoming nonzero $E_i \gg kT$, the Planck distribution function can be approximated by:

$$\frac{1}{e^{\varepsilon/kT} - 1} \simeq e^{-\varepsilon/kT} \tag{III.5}$$

Further, since the one-dimensional exciton density of states function $\rho(E_i)$ is sharply peaked at $k = 0$ and $k = \pm\pi/a$, we anticipate that intermediate states, $\tau_i$, with energies equal to the energies of the top and bottom of the band might be expected to play the dominant role in the transition probability. If detrapping occurs selectively[14] to one k state, say $k = 0$,[52] then the band width to temperature ratio would

be relatively unimportant. On the other hand, in the absence[53] of a k dependent trap-exciton coupling, if the band width is significant relative to kT, the populations of phonons with energies capable of producing intermediate states at the top of the band will be small compared to the number of phonons available to produce intermediate states at the bottom of the band. In this limit, the expression for $K^P$ can be approximated by considering only one intermediate state at the bottom of the band (which will be k = 0 or k = $\pm\pi/a$ depending upon the sign of $\beta$). In either of these limits, the expression for $K_{so}$ becomes

$$K^P \propto C \sum_{\varepsilon=E_i} (\varepsilon)\, e^{-\varepsilon/kT} = C\rho(E_i)\, e^{-E_i/kT} \qquad \text{(III.6)}$$

where $E_i$ is the energy of the intermediate state $\tau_i$ which coincides with the maximum density of states of the band in one case or to the particular k state (k = 0) in the band in the other. All the non-temperature dependent terms except the density of states function have been collected into the constant C with the assumption that phonon-trap interaction is constant over a range of phonon energies $\varepsilon$ close to $E_i$.

In either of the two above limits the temperature dependence of the detrapping rate would appear as an activated process with an Arrhenius-like activation energy $E_i$. In reality, however, there is no activation, and $E_i$ simply reflects the phonon distribution. Moreover, when the density of k states at the energy of the intermediate trap state differ, as would be the case in different mixed crystals with exciton chains of varying lengths, the absolute value of the detrapping rate $K_{so}$ and $K_{do}$ would change via $\rho(E_i)$ (Eq. (III.6); however, the apparent activation

energy, $E_i$, would stay constant except for small changes resulting from differences in the band dispersions for different finite chain lengths. An experimental investigation into the validity of this model is being pursued using some of the optically detected magnetic resonance techniques described in the previous section.

## F. Conclusions

(1) The fact that the $T_{1\rho}$ for $h_2$-TCB in $h_{14}$-durene is long and temperature independent makes it reasonable to conclude that $K^P$, the phonon assisted promotion rate constant, for this system is zero and that $K_{T_{1\rho}}$ is just the sum of $K^L$ and $K^{T_{1\rho m}}$. This is not surprising in view of the large (1456 $cm^{-1}$)[15] energy difference between the localized $h_2$-TCB $^3\pi\pi^*$ state and the durene triplet band. From an independent measurement of the $\tau_y$ and $\tau_z$ sublevel decay rate constants ($K_y$ = 27.8 $sec^{-1}$; $k_z$ = 26.3 $sec^{-1}$)[11,54] in this system, a value of 27.1 $sec^{-1}$ for $K^L$, the rate constant for decay to the ground state from the spin lock state is obtained. Thus, the spin lattice relaxation time in the rotating frame can be determined from Eq. (III.1) and Fig. 16. $T_{1\rho} = (K^{T_{1\rho m}})^{-1}$ = 67 ms and appears to be temperature independent over the limited range investigated.

(2) In the discussion in Chapter II of the $h_2$-TCB $^3\pi\pi^*$ state in the $d_2$-TCB host it has been shown that in the temperature region 1.38°K to 2.1°K, the phonon assisted promotion of the $h_2$-TCB state to the $d_2$-TCB exciton band is becoming appreciable, although a quantitative measurement of the rate was not determined.[37] This was established from the explicit temperature dependence of the $h_2$-TCB and hd-TCB phosphorescence in a $d_2$-TCB crystal and the relationship of this dependence to the Boltzmann thermal equilibrium between exciton states and multiple trap states in

this system. From these investigations, we have established that in the temperature region 1.3°K to 1.9°K the localized states are not in thermal equilibrium with the $d_2$-TCB band states but that there is promotion to the band and that the phonon assisted promotion rate for $h_2$-TCB to the $d_2$-TCB band must be rapidly increasing with temperature to account for Boltzmann equilibrium between the localized and delocalized states above ~2.4°K. Making the assumption that $K^L$ and $K^{T_{1\rho m}}$ are approximately the same for $h_2$-TCB in the two hosts ($h_{14}$-durene and $d_2$-TCB), $K^P$ can be determined as a function of temperature. This is illustrated by the semilog plot of the data in the upper portion of Fig. 16. Since $K^P$ is large relative to $K^L$ and $K^{T_{1\rho m}}$, changes in these latter two rate constants due to the $d_2$-TCB host will not significantly affect the magnitude of $K^P$ determined at each temperature and will certainly not alter the steep temperature dependence of the promotion rate constant. A significant feature of the temperature dependent promotion rate is that it is clearly non-exponential.

The relation of these preliminary experimental results to the model outlined above has been examined. For the temperatures over which the experiments were performed, it is expected that only the acoustic phonon branches will have appreciable population. Unfortunately, experimental acoustic phonon dispersions are unavailable for this system, and only a limited amount of data is available on other molecular crystals.[55,56] We expect, however, on the basis of the neutron scattering results in $d_8$-napthalene[56] and anthracene,[55] that the acoustic branch is essentially linear up to ~10 $cm^{-1}$; hence, the optic branch and the nonlinear region of the acoustic branch do not significantly change their populations between 1.4 and 2.1°K.

It can be seen from Eqs. (III.2) and (III.4) that the phonon assisted rate of promotion is governed in first order by the phonon distribution function. For temperatures where KT is much less than $\Delta$, the energy difference between the localized state and the exciton band, one expects an exponentially increasing rate constant with temperature when only single phonon processes are considered and when only the linear regions of the acoustic branch are populated. Moreover, when $KT \ll \Delta$, the functional relationship between the rate constant and temperature (exponential vs non-exponential in the range relevant to the experimental data) is relatively insensitive to the exciton band dispersion, and theory predicts an exponential behavior if one assumes that the coupling of the localized state to the phonons is equally probable for all phonon wave vectors q, (i.e., $\langle \tau \cdot P(\varepsilon) | H_p | \tau_i \cdot P(\varepsilon - E_i) \rangle$ is q independent).

The observation of a non-exponential behavior and the steep temperature dependence in this limited temperature range suggests that some or all of the following consideration are important. (a) Multiphonon processes* dominate the promotion process; (b) $d_2$-TCB has an acoustic phonon dispersion that becomes significantly nonlinear at very low energies ($\sim 5\ cm^{-1}$) or (c) the coupling of the phonons to the localized states are strongly q dependent.

---

*If there is a phase transition a soft phonon mode will be produced which will facilitate multi-phonon processes. This possibility is currently being experimentally investigated.

Further experimental data and a detailed comparison of the data to the above model should establish the relative importance of the above considerations.

(c) Although these experiments have demonstrated the temperature dependence of the phonon assisted promotion of localized states to the exciton band, we do not yet know quantitatively what fraction of the promoted intermediates decays radiationlessly into the exciton band, nor do we know whether or not there is a strong k dependence to the process other than the obvious effect of a large exciton density of states at the top and bottom of the triplet band in these systems.[37,57]

In addition to the decay of a localized state into a mobil exciton state, a second possible mechanism for the loss of spin coherence is the creation of a localized bound phonon-exciton state. This bound state can evolve into a mobile state in which case it may be viewed merely as a short-lived intermediate, or it can relax back into the ensemble of non-phonon excited localized states after a time period long enough for it to have lost phase coherence with the spin locked ensemble. The principal factor determining whether electron spin phase coherence is lost, if a bound phonon-exciton intermediate relaxes back into its original lattice site, is the life time of the intermediate. In this system we expect a difference in the D-E transition frequency of the exciton band and the localized trap state to be about 60 MHz; hence phase coherence in these experiments[59] will be lost in the promotion-relaxation process if the excited intermediate has a life time of greater than $\sim 10^{-8}$ sec. Earlier experiments have demonstrated the redistribution of the $h_2$-TCB $^3\pi\pi^*$ state energy to other (hd-TCB)

localized states via the $d_2$-TCB band[6,8] states implying that the production of mobile excitons must account for a significant part of the measured values of $K^P$. Furthermore, a $10^{-8}$ sec lifetime for a vibrationally excited (phonon-excited) intermediate seems very long in view of data available for phonon relaxation rates in solids.[60] To date there is no experimental evidence to demonstrate the existence of bound phonon-exciton states which relax back to the same lattice site. However, if they exist, they will contribute in part to $K^P$. Additional experiments are currently being pursued in this laboratory to determine the extent of these contributions to the magnitude of $K^P$.

## G. Summary of Chapters I, II and III

(1) We have attempted to explain in a general way the mechanism by which thermal equilibrium between localized trap states and delocalized band states in solids is achieved. The essential features of the statistical model which satisfactorially accounts for many experimental observations are that at low temperatures, exciton migration must propagate coherently as a wave packet rather than by a random walk process in order to thermally equilibrate the exciton and trap states within the lifetime of the excited electronic state. A proper description of the process or processes related to the equilibrium populations of trap and band states must include the density of k states, the number of k states comprising the band relative to the number of localized trap states, the detrapping rates which are dependent upon phonon dispersions, the trap depth, the sign and magnitude of the intermolecular interaction which gives rise to the band dispersion and exciton-phonon scattering.

(2) The application of this model to crystals representative of one-dimensional bands allows one to extract from the temperature dependent trap emission the magnitude of the band dispersion, the sign of the intermolecular interaction matrix element and an estimate of the coherence length and average group velocity of the exciton wave packets.

(3) In a crystal characterized by two or more trap states at different energies, below a certain temperature, a "bottleneck" in the Boltzmann distribution between band and trap states results because of the inability of the phonons to detrap the deeper traps at a sufficient rate relative to the radiative and radiationless lifetime of the state. We have solved the coupled differential equation and interpreted the various rate processes in terms of the coherent model.

(4) We have derived a general theory for detrapping which treats the detrapping rate constant as a stochastic radiationless relaxation process in which the trap state once thermally activated decays irreversibly into the density of exciton states.

(5). Finally, we have presented a series of experiments on one-dimensional molecular crystals designed to test the model. Specifically, we have shown how electron spin coherence and optically detected magnetic resonance in localized states can be used to obtain specific information regarding the dynamics of detrapping and the relationship of detrapping to Boltzmann equilibration between trap and band states.

# IV. COHERENT COUPLING WITH FEEDING AND DECAY

## A. Introduction

Perturbation of a two level quantum mechanical system by the application of a coherent radiation field has been extensively treated experimentally and theoretically for proton nuclear magnetic resonance.[61] In the NMR case, a proton is always found in one of its two spin states or in a superposition of the two states and, therefore, the system may be treated rigourously in terms of these two energy levels. However, when considering coherent radiation applied to the excited states of an atom or molecule, such as the coherent microwave perturbation of two magnetic sublevels of an excited triplet state or coherent optical coupling of two excited electronic states in a system such as a four level laser, species will not necessarily be in either of the two states or in a superposition of the two states coupled by the radiation field. Many of the molecules will either be in their ground state or in some excited state other than one of the two being coherently coupled.

To maintain an excited state population, molecules must be continually promoted from their ground states. Also molecules in the excited states are continually relaxing to the ground state. The problem is to consider the coherent coupling of a system composed of two excited states in which there is continual feeding of population into the system and continual decay of population out of the system. A simple example of a physical effect due to feeding and decay is that the total excited state population of the two level system will change upon the application of the radiation field if the excited state life times of the two states differ. This implies that the trace of the density matrix for the two

level system is not constant in time (although the trace of the density matrix for the ground state plus all excited states will of course be constant).

The effects of feeding and decay play a more important role in the two level system than merely modifying the total population. It will be seen that the feeding and decay processes in many instances significantly effect coherent phenomena induced into the two level system by the radiation field. In some cases these processes will be a mechanism for the loss of coherence while in certain special situations it will be shown that incoherent feeding by continually replenishing the coherent state will actually allow coherence to be maintained in the two level system for an extended period of time, in fact, for a period longer than the life times of the excited states.

In the following sections, first the problem of a two level system with decay will be solved by using the time dependent Schrodinger equation. The solutions for the time dependence of the amplitudes of the wavefunctions will be cast into the geometrical representation due to Feynman et al.[62] which allows coherent and incoherent phenomena to be readily distinguished and followed in time. Then feeding will be added to the problem and an analytic solution will be obtained which still permits a geometrical representation. The formulation which is presented allows the effect of any perturbation, such as a sequence of high power pulses or a low power cw spectrum, to be calculated. The problem is initially considered for the case in which the wave length of the radiation field is large relative to the sample size. Several example problems are solved, with special attention being payed to the role of

the feeding process in maintaining a kinetic coherent state of the system. Finally, the treatment is briefly discussed for the case of optical excitations in which the wavelength of the radiation field is small relative to the sample size. In this case, feeding still results in long term kinetic coherence and it is predicted that this kinetic coherent optical state will exhibit long term superradiance.

## B. Mathematical Development

Consider the problem of a radiation field coherently coupling a two level system in which population is continually being fed into the levels and population is continually decaying from the levels. The solution to the two level coherent coupling problem in the absence of feeding and decay is well known.[63] This solution is rigorous when applied to the NMR problem, but when considering coherent coupling in systems composed of excited state levels, which have finite life times and obtain their populations via incoherent feeding, an accurate description must include the feeding and decay processes.

In this section the problem will be solved for the case in which the wavelength of the radiation field is large relative to the dimensions of the crystal, i.e., Vol. $\ll \lambda^3$, where Vol. is the volume of the sample and $\lambda$ is the wavelength of the applied field. Thus the phase of the

perturbing field is constant over the sample. This condition applies to the case of coherent microwave coupling of two of the magnetic spin sublevels of an excited molecular triplet state (cf Chapters II and III). Since we are primarily interested in the triplet state problem in this thesis, the transition will be taken to be magnetic dipole and triplet state operators and matrix elements will be employed.[66] The only loss of generality is in the form of the operators; the rest of the treatment is identical for magnetic and electric dipole transitions. (Electric dipole transitions are briefly discussed in Section IV-B-4).

We wish to perform a model calculation for the following idealized situation. The two spin levels labeled $|y\rangle$ and $|x\rangle$ which are perturbed by the coherent radiation field are also coupled to an infinite bath of spins. Population is transferred from the bath to the y and x levels with constant rates $F_y$ and $F_x$ respectively. The populations found in the y and x levels decay back into the bath with rate constants $k_y$ and $k_x$ respectively. In the absence of an applied field coupling y and x, there is no direct transfer of population between y and x, i.e., there is no $T_1$ process between y and x.

To this point, the above idealized situation corresponds closely to the physical situation found in the microwave perturbation of a molecular triplet state at low temperatures (~4°K). Population is transferred to the y and x spin sublevels from excited singlet states via intersystem crossing. Since, in general the ground state population of the sample is not depleted by the incoherent excitation light, the singlet state populations and, therefore, the feeding rates, $F_y$ and $F_x$, are constant. The decay rate constants, $k_y$ and $k_x$, correspond to the

rate constants for decay to the ground state from the two triplet spin sublevels. These rate constants include both radiative and non-radiative processes. The assumption that $T_1$ processes between x and y are absent is valid for molecular triplet states below 4°K,[24] where the small amount of thermal energy available combined with the weak coupling of a molecular triplet state to the lattice results in a negligable amount of spin lattice relaxation.

We will impose one further condition which is not justified physically. Homogeneous dephasing of the coherent components induced by the radiation field into the ensemble of systems composed of pairs of levels, y and x, will be neglected, i.e., homogeneous $T_2$ processes are neglected. (Dephasing resulting from an inhomogeneous line is discussed at the end of Section IV-B.) Omitting $T_2$ processes simplifies the mathematics but does not alter the qualitative results which are obtained. This will be shown to be true in a paper[78] to be published subsequently in which the following treatment is extended to include $T_2$ and $T_1$ processes. Furthermore, the exclusion of $T_2$ processes is justified for another reason. Since the main thrust of this chapter is to develop the idea of a long term coherent state maintained in the ensemble of two level systems by the radiation field and since this long term coherent state is derived from a component aligned along the static field in the rotating frame; under high power conditions $T_2$ processes do not occur. That is the coherent state is "spin locked".[36] This applies to the optical case (cf Section IV-C-4) in addition to the triplet state magnet resonance case discussed here. This point is discussed in more detail below (cf Section IV-C-3) and will be demonstrated to be a valid

description elsewhere.[78]

The difference in energy between the two levels y and x, is $\hbar\omega_o$. For completeness and to establish the notation which will be used throughout this chapter the equation of motion for the time dependent coefficients of the stationary state eigenfunctions $|y\rangle$ and $|x\rangle$ is obtained in the absence of the feeding and decay processes. The effect of decay to the bath is then added to the equation of motion and a solution is obtained using the Laplace transform technique. Finally, the system is divided into appropriate subensembles which allows the feeding from the bath to be included rigorously and an analytic solution obtained.

1. Equation of Motion in the Absence of Feeding and Decay

Consider the two states $|y\rangle$ and $|x\rangle$ with energy seperation $\hbar\omega_o$ which are connected by a radiation field of frequency $\omega$. The radiation field may be expressed as a time-dependent perturbation[64] given by

$$V(t) = \gamma H_1 S_z \cos\omega t \qquad \text{(IV.1)}$$

Making the rotating field approximation,[64] i.e., resolving the cosine term into two counter rotating circular components and ignoring the off resonance one, the perturbation may be rewritten

$$V(t) = -\frac{\hbar\omega_1}{2} e^{-i\sigma_3\omega t/2} \sigma_2 e^{i\sigma_3\omega t/2} \qquad \text{(IV.2)}$$

where the $\sigma_i$ are the usual Pauli spin matricies,[65] and $\omega_1$ is proportional to the amplitude of the applied field. The matrix elements of V(t) may be either real or imaginary. Here they are taken to be imaginary which corresponds to the triplet state problem.[66] For systems where V(t) would give real matrix elements, $\sigma_2$ should be replaced by $\sigma_1$ and the sign of the expression for V(t) should be changed in Eq. (IV.2). Except for these modifications the development is identical. The total Hamiltonian is

$$\mathcal{H} = \mathcal{H}^o + V(t) = \frac{\hbar\omega_o}{2}\sigma_3 - \frac{\hbar\omega_1}{2} e^{-i\sigma_3\omega t/2} \sigma_2 e^{i\sigma_3\omega t/2} \tag{IV.3}$$

The state of the system at any time t, is given by the wavefunction

$$\psi(t) = y\psi_y^o + x\psi_x^o \tag{IV.4}$$

where y and x are time dependent coefficients. Transforming to a new wavefunction with the unitary operator

$$U^{-1} \equiv e^{i\omega H_o t/\hbar\omega_o} = e^{i\sigma_3\omega t/2} \tag{IV.5}$$

yields

$$\Psi(t) = U^{-1}\psi(t) \tag{IV.6}$$

Expressing $\psi(t)$ as $U\Psi(t)$ and substituting into the time dependent Schrodinger equation for $\psi(t)$ gives

$$i\hbar\left(-\frac{i\omega\sigma_3}{2} U\Psi(t) + U\dot{\Psi}(t)\right) = \hbar\left(\frac{\omega_o}{2}\sigma_3 - \frac{\omega_1}{2} e^{\frac{-i\omega t\sigma_3}{2}} \sigma_2 e^{\frac{i\omega t\sigma_3}{2}} U\Psi(t)\right) \tag{IV.7}$$

Multiplying on the left by $U^{-1}$, collecting terms, and defining $\Delta\omega \equiv \omega_o - \omega$ results in the Schrodinger equation

$$i\hbar\dot{\Psi}(t) = \left(\frac{\hbar\Delta\omega}{2}\sigma_3 - \frac{\hbar\omega_1}{2}\sigma_2\right)\Psi(t) = H^{\ddagger}\Psi(t) \tag{IV.8}$$

where the $\ddagger$ indicates a frame rotating[67] at frequency $\omega$. Any state of the system is given by the rotating frame wavefunction

$$\Psi(t) = y^{\ddagger}\Psi_y^o + x^{\ddagger}\Psi_x^o \tag{IV.9}$$

where $y^{\ddagger}$ and $x^{\ddagger}$ are the rotating frame time dependent coefficients. The problem from this point on will be treated in the rotating frame and therefore the double dagger notation will be dropped.

Substitution of Eq. (IV.9) into Eq. (IV.8) yields

$$i\hbar\left(\dot{y}\Psi_y^o + \dot{x}\Psi_x^o\right) = \left(\frac{\hbar\Delta\omega}{2}\sigma_3 - \frac{\hbar\omega_1}{2}\sigma_2\right)\left(y\Psi_y^o + x\Psi_x^o\right) \tag{IV.10}$$

then projecting out the y coefficient

$$i\hbar\int \dot{y}\ \Psi_y^o\Psi_y^o + \dot{x}\ \Psi_y^o\Psi_x^o\ d\tau =$$

$$\frac{\hbar\Delta\omega}{2}\langle y|\sigma_3|y\rangle\ y - \frac{\hbar\omega_1}{2}\langle y|\sigma_2|y\rangle\ y + \frac{\hbar\Delta\omega}{2}\langle y|\sigma_3|x\rangle\ x \tag{IV.11}$$

$$- \frac{\hbar\omega_1}{2}\langle y|\sigma_2|x\rangle\ x$$

collecting terms and doing the same operation for the x coefficient gives the equations of motion for the y and x probability amplitudes.

$$\dot{y} = -\frac{i\Delta\omega}{2} y + \frac{\omega_1}{2} x \tag{IV.12a}$$

$$\dot{x} = \frac{i\Delta\omega}{2} x - \frac{\omega_1}{2} y \tag{IV.12b}$$

2. Solution of the Equation of Motion with Decay

Loss of population from the two excited state levels is included in the problem by the addition of decay terms[68] to the equations of motion of the probability amplitudes, i.e.,

$$\dot{y} = \left(-\frac{i\Delta\omega}{2} - \frac{k_y}{2}\right) y + \frac{\omega_1}{2} x \tag{IV.13a}$$

$$\dot{x} = \left(\frac{i\Delta\omega}{2} - \frac{k_x}{2}\right) x - \frac{\omega_1}{2} y \tag{IV.13b}$$

It should be noted that in the absence of an applied radiation field, the equations of motion for the applitudes of the states $\Psi_y^o$ and $\Psi_x^o$ become independent and solution of the differential equations results in the probability of the states decaying with their life times $1/k_y$ and $1/k_x$ respectively.

The equations of motion including decay are solved using the Laplace transform[69] method. First the variables are reduced to dimensionless quantities by using the following definitions.

$$\tau \equiv \frac{\omega_1 t}{2} \tag{IV.14a}$$

$$\delta \equiv \frac{\Delta\omega}{\omega_1} \tag{IV.14b}$$

$$K_y \equiv \frac{k_y}{\omega_1} \tag{IV.14c}$$

$$K_x \equiv \frac{k_x}{\omega_1} \tag{IV.14d}$$

In terms of these definitions the differential equations are rewritten as

$$\frac{dy}{d\tau} = -(K_y + i\delta)\, y + x \tag{IV.15a}$$

$$\frac{dx}{d\tau} = -(K_x - i\delta)\, x - y \tag{IV.15b}$$

Taking the Laplace transforms yields

$$S\underline{\bar{Y}} - y^o = -\,(K_y + i\delta)\,\underline{\bar{Y}} + \underline{\bar{X}} \tag{IV.16a}$$

$$S\underline{\bar{X}} - x^o = -\,(K_x + i\delta)\,\underline{\bar{X}} - \underline{\bar{Y}} \tag{IV.16b}$$

where $y^o$ and $x^o$ are the initial values of the time dependent coefficients. These equations have solutions

$$\underline{\bar{Y}} = \frac{y^o S + (K_x - i\delta)\, y^o + x^o}{S^2 + (K_x + K_y)\, S + K_y K_x + i\delta(K_x - K_y) + \delta^2 + 1} \tag{IV.17a}$$

$$\underline{\bar{X}} = \frac{x^o S + (K_y + i\delta)\, x^o - y^o}{S^2 + (K_x + K_y)\, S + K_y K_x + i\delta(K_x - K_y) + \delta^2 + 1} \tag{IV.17b}$$

We need the following standard inverse Laplace transforms

$$\mathcal{L}^{-1}\,\frac{s}{s^2 + bs + c} = \frac{-be^{-bt/2}}{2\hat{\omega}}\sin(\hat{\omega}t) + e^{-bt/2}\cos(\hat{\omega}t) \tag{IV.18}$$

$$\mathcal{L}^{-1}\,\frac{1}{s^2 + bs + c} = \frac{e^{-bt/2}}{2\hat{\omega}}\sin(\hat{\omega}t) \tag{IV.19}$$

where

$$b = (K_x + K_y) \tag{IV.20a}$$

$$c = K_y K_x + i\delta(K_x - K_y) + \delta^2 + 1 \tag{IV.20b}$$

and

$$\hat{\omega} = \left(c - \frac{b^2}{4}\right)^{1/2} = \left[1 + \left(\delta + i\,\frac{(K_x - K_y)}{2}\right)^2\right]^{1/2} \tag{IV-20c}$$

Replacing the dimensionless quantities with their counterparts (cf Eq. (IV.14a-d) and defining the following quantities

$$k_A \equiv \frac{k_x + k_y}{2} \tag{IV.21a}$$

$$k_D \equiv \frac{k_x - k_y}{2} \tag{IV.21b}$$

$$\bar{\omega} \equiv [\omega_1^2 + (\Delta\omega + ik_D)^2]^{1/2} \tag{IV.21c}$$

we obtain the inverse Laplace transforms

$$y = e^{-k_A t/2}\left(y^o \cos\frac{\bar{\omega}t}{2} + \frac{y^o k_D + x^o\omega_1 - iy^o\Delta\omega}{\bar{\omega}}\sin\frac{\bar{\omega}t}{2}\right) \tag{IV.22a}$$

$$x = e^{-k_A t/2}\left(x^o \cos\frac{\bar{\omega}t}{2} - \frac{x^o k_D + y^o\omega_1 - ix^o\Delta\omega}{\bar{\omega}}\sin\frac{\bar{\omega}t}{2}\right) \tag{IV.22b}$$

The solutions given in Eqs. (IV.22a) and (IV.22b) are valid provided $\bar{\omega} \neq 0$, which corresponds to the under damped and over damped cases. However, if $\Delta\omega = 0$ and $\omega_1 = k_D$, then $\bar{\omega} = 0$, and the critically damped case occurs. The solutions are obtained by substituting the critically damped conditions into the Laplace transforms, Eqs. (IV.17a) and IV.17b), collecting terms, and taking the inverse Laplace transform.

These are given by

$$y_{CD} = e^{-\frac{k_A t}{2}} \left[ y^o + \frac{y^o t}{2} k_D + \frac{\omega_1 t}{2} x^o \right] \tag{IV.22c}$$

$$x_{CD} = e^{-\frac{k_A t}{2}} \left[ x^o - \frac{x^o t k_D}{2} - \frac{\omega_1 t}{2} y^o \right] \tag{IV.22d}$$

where the subscript CD indicates that these are the critically damped solutions only. Since these solutions only occur for one particular set of experimental conditions, they will not be discussed in the following sections, although they may be treated in a manner analogous to the more general underdamped and overdamped cases.

Equations (IV.22a) and (IV.22b) give the time dependence of the probability amplitudes of the states $\psi_y^o$ and $\psi_x^o$ which are coupled by a coherent radiation field and whose populations are irreversibly decaying with rate constants $k_y$ and $k_x$ respectively. Since we are dealing with coherent coupling, the Equation of motion for a single species is the same as that for N identical species. The effects due to inhomogenious broadening, will be discussed later. The time t = 0 coefficients $y^o$ and $x^o$ are, therefore, normalized such that $y^o y^{o*}$ and $x^o x^{o*}$ give the t = 0 populations of the y and x levels, i.e.,

$$y^o y^{o*} = N_y^o \tag{IV.23a}$$

$$x^o x^{o*} = N_x^o \tag{IV.23b}$$

The total initial population of the two level system is $N^o = N_y^o + N_x^o$.

Now that the time dependence of the amplitudes of the wavefunctions has been determined, it is possible to take appropriate combinations of these amplitudes and form a geometrical representation[62] of the state of the two level systems which allows physical observables to be readily calculated. The quantities of interest are

$$r_y = yy^* \tag{IV.24a}$$

$$r_x = xx^* \tag{IV.24b}$$

$$r_1 = yx^* + xy^* \tag{IV.24c}$$

$$r_2 = i(yx^* - xy^*) \tag{IV.24d}$$

$r_y$ and $r_x$ are the time dependent populations of the y and x levels. $r_1$ and $r_2$ are the out of phase and in phase coherent components introduced into the ensemble of identical two level systems by the radiation field. They correspond to the out of phase and in phase components of the transverse magnitization in an NMR experiment.[70] Other quantities of interest are

$$r_3 = r_y - r_x \tag{IV.25a}$$

$$N = r_y + r_x \tag{IV.25b}$$

where $r_3$ is the time dependent difference in the populations of the y and x levels and N is the time dependent total population found in the ensemble of two level systems. $r_1$, $r_2$ and $r_3$ together are the components of the Feynman r-vector. The total coherent component is $(r_1^2 + r_2^2)^{1/2}$. It should be pointed out that $r_y$ and $r_x$ are the diagonal elements of the density matrix and that $(r_1 + ir_2)$ and $(r_1 + ir_2)^*$ are the off diagonal elements of the density matrix and therefore determination of these

quantities is sufficient to completely characterize the system.

Calculation of the quantities in Eqs. (IV.24a-d) from Eqs. (IV.22a-b) is straight-forward but exceedingly lengthy. The general form is

$$r_g = \frac{e^{-k_A t}}{2(\alpha^2 + \beta^2)} (A\cos\alpha t + B\sin\alpha t + C\cosh\beta t + D\sinh\beta t) \qquad \text{(IV.26)}$$

where g is y, x, 1 or 2 and

$$\bar{\omega} = \alpha + i\beta \qquad \text{(IV.27a)}$$

$$\alpha = \left\{ \frac{\left[\left(\omega_1^2 + \Delta\omega^2 - k_D^2\right)^2 + 4\Delta\omega^2 k_D^2\right]^{1/2} + \left(\omega_1^2 + \Delta\omega^2 - k_D^2\right)}{2} \right\}^{1/2} \qquad \text{(IV.27b)}$$

$$\beta = \left\{ \frac{\left[\left(\omega_1^2 + \Delta\omega^2 - k_D^2\right)^2 + 4\Delta\omega^2 k_D^2\right]^{1/2} - \left(\omega_1^2 + \Delta\omega^2 - k_D^2\right)}{2} \right\}^{1/2} \qquad \text{(IV.27c)}$$

The coefficients A, B, C and D for each expression $r_g$ are tabulated in Table IV. To determine the time dependence of a component $r_g$, simply determine the coefficients A, B, C and D by inserting the particular set of experimental conditions into the tabulated forms. Once the coefficients are evaluated, they are inserted into Eq. (IV.26) and $r_g$ is determined. Several example calculations will be presented after feeding of population into the ensemble of excited two level-systems is discussed in the next section.

3. Inclusion of Entering Population into the Geometrical Representation

In this section we will obtain the time dependence of the r-vector equations discussed in the previous section for the case in which there is population feeding into the ensemble of excited two level systems. The problem is made tractable by partitioning all the

Table IV. General form.

$$r_g = \frac{e^{-k_A t}}{2(\alpha^2 + \beta^2)} \left(A\cos\alpha t + B\sin\alpha t + C\cosh\beta t + D\sinh\beta t\right)$$

$$k_A = \frac{k_x + k_y}{2} \qquad k_D = \frac{k_x - k_y}{2} \qquad \alpha + i\beta = \left[\omega_1^2 + (\Delta\omega + ik_D)^2\right]^{1/2}$$

| Component | A | B | C | D |
|---|---|---|---|---|
| $yy^*$ $r_y$ | $(\alpha^2 + \beta^2 - k_D^2 - \Delta\omega^2)\, r_y^o$ $-(\omega_1^2)\, r_x^o - (k_D\omega_1)\, r_1^o$ $+ (\omega_1\Delta\omega)\, r_2^o$ | $2(k_D\alpha - \Delta\omega\beta)\, r_y^o$ $+ (\omega_1\alpha)\, r_1^o$ $+ (\omega_1\beta)\, r_2^o$ | $(\alpha^2 + \beta^2 + k_D^2 + \Delta\omega^2)\, r_y^o$ $+ (\omega_1^2)\, r_x^o + (k_D\omega_1)\, r_1^o$ $- (\omega_1\Delta\omega)\, r_2^o$ | $2(\Delta\omega\alpha + k_D\beta)\, r_y^o$ $+ (\omega_1\beta)\, r_1^o$ $- (\omega_1\alpha)\, r_2^o$ |
| $xx^*$ $r_x$ | $(\alpha^2 + \beta^2 - k_D^2 - \Delta\omega^2)\, r_x^o$ $-(\omega_1^2)\, r_y^o - (k_D\omega_1)\, r_1^o$ $- (\omega_1\Delta\omega)\, r_2^o$ | $-2(k_D\alpha - \Delta\omega\beta)\, r_x^o$ $- (\omega_1\alpha)\, r_1^o$ $+ (\omega_1\beta)\, r_2^o$ | $(\alpha^2 + \beta^2 + k_D^2 + \Delta\omega^2)\, r_x^o$ $+ (\omega_1^2)\, r_y^o + (k_D\omega_1)\, r_1^o$ $+ (\omega_1\Delta\omega)\, r_2^o$ | $-2(\Delta\omega\alpha + k_D\beta)\, r_x^o$ $- (\omega_1\beta)\, r_1^o$ $- (\omega_1\alpha)\, r_2^o$ |
| $(yx^* + xy^*)$ $r_1$ | $(\alpha^2 + \beta^2 + k_D^2 + \Delta\omega^2 + \omega_1^2)\, r_1^o$ $+ (2k_D\omega_1)\, r_y^o + (2k_D\omega_1) r_x^o$ | $-2(\Delta\omega\alpha + k_D\beta)\, r_2^o$ $- (2\omega_1\alpha)\, r_y^o$ $+ (2\omega_1\alpha)\, r_x^o$ | $(\alpha^2 + \beta^2 - k_D^2 - \Delta\omega^2 - \omega_1^2)\, r_1^o$ $- (2\omega_1 k_D)\, r_y^o - (2\omega_1 k_D)\, r_x^o$ | $2(k_D\alpha - \Delta\omega\beta)\, r_2^o$ $- (\omega_1\beta)\, r_y^o$ $+ (\omega_1\beta)\, r_x^o$ |
| $(yx^* - xy^*)$ $r_2$ | $(\alpha^2 + \beta^2 + k_D^2 + \Delta\omega^2 - \omega_1^2)\, r_2^o$ $+ (2\omega_1\Delta\omega)\, r_y^o - (2\omega_1\Delta\omega)\, r_x^o$ | $2(\Delta\omega\alpha + k_D\beta)\, r_1^o$ $+ (2\omega_1\beta)\, r_y^o$ $+ (2\omega_1\beta)\, r_x^o$ | $(\alpha^2 + \beta^2 - k_D^2 - \Delta\omega^2 + \omega_1^2)\, r_2^o$ $- (2\omega_1\Delta\omega)\, r_y^o + (2\omega_1\Delta\omega)\, r_x^o$ | $-2(k_D\alpha - \Delta\omega\beta)\, r_1^o$ $- (2\omega_1\alpha)\, r_x^o$ $- (2\omega_1\alpha)\, r_x^o$ |

molecules in a sample into carefully chosen independent subensembles. Qualitatively the procedure is as follows. At some instant of time $t = 0$, some of the molecules in the sample are in the two excited state levels under consideration while a large number of molecules are in other states. Those molecules in the two level system form one subensemble. This subensemble, which is excited at $t = 0$, will follow the equations of the previous section. During a small interval of time after $t = 0$, other molecules will become excited. These newly excited molecules form another subensemble. The behavior of this subensemble also follows the treatment of the previous section, however, it is necessary to keep track of the phase relationship between the $t = 0$ subensemble and this newly created ensemble. At some later time, more population will be fed into the two excited levels under consideration. This population forms another subensemble. Thus, the procedure is to follow the behavior of each of these subensembles and to determine the properties of the total ensemble of excited two level systems by summing the properties of the individual subensembles. The significant point is that each subensemble interacts independently with the radiation field and, therefore, the basic problem amounts to keeping track of the behavior of the various pieces relative to each other. It should be pointed out that the $t = 0$ subensemble may be empty if $t = 0$ is chosen before the incoherent source which produces excited states is turned on. Also, if the excitation light is turned off at $t = 0$, the treatment in Section IV-B-3 is exact since population will not be fed into the two level system. In the following discussion the number of excited molecules is taken to be small relative to the total number of molecules in the system. This implies that the feeding

rates $F_y$ and $F_x$ are independent of the state of coherent coupling of the ensemble of excited two level systems. $F_y$ and $F_x$ are therefore constants for a given rate of incoherent pumping. The case where $F_y$ and $F_x$ are not constants may be treated in a manner which is analogous to the following.

To include the effects of feeding into the ensemble of excited two level systems which are coupled by a coherent radiation field, we must partition the entire system into subensembles by the following method.

1. Divide the sample into excited and unexcited subensembles at any time t. Obviously feeding can only occur to the unexcited subensemble.

2. Further subdivide the unexcited subensemble into two classes:

   $\hat{y}$ Those molecules whose y levels become populated in a small increment of time $\delta t$.

   $\hat{x}$ Those molecules whose x levels become populated during the same time. There still exist a large number of molecules which are unexcited.

The $\hat{y}$ and $\hat{x}$ classes are treated as follows. The $\hat{y}$ class follows the equations given in Table IV of the previous section with the initial conditions

$$r_1^o = r_2^o = r_x^o = 0 \tag{IV.28a}$$

$$r_y^o = F_y \delta t \tag{IV.28b}$$

where $F_y$ is a constant feeding rate.

The $\hat{x}$ class also follows the equations in Table IV but with initial conditions

$$r_1^o = r_2^o = r_y^o = 0 \tag{IV.29a}$$

$$r_x^o = F_x \delta t \tag{IV.29b}$$

In general, we begin with a certain excited population in the ensemble of two level systems under consideration which may have nonzero values for any component $r_g$. This population evolves in time in the manner given by Table IV for each small increment of time $\delta t$. Furthermore, any additional population which is fed in will have the initial $r_g$ values given above for the $\hat{y}$ and $\hat{x}$ classes. Let $f_g^o(t)$ be the function describing the time behavior of the component $r_g$ with initial value $r_g^o$, and let $f_g^y(t)$ be the specialized function for the population entering the y level. An expression for the behavior of all subensembles can be built in increments of $\delta t$.

$$t = 0 \quad r_g = r_g^o \tag{IV.30a}$$

$$t = \delta t \quad r_g = f_g^o(\delta t) + F_y \delta t f_g^y(o) \tag{IV.30b}$$

$$t = 2\delta t \quad r_g = f_g^o(2\delta t) + F_y \delta t f_g^y(\delta t) + F_y \delta t f_g^y(o) \tag{IV.30c}$$

$$t = m\delta t \quad r_g = f_g^o(t) + F_y \delta t \sum_{\ell=1}^{m} f_g^y[(m - \ell)\ \delta t] \tag{IV.30d}$$

At time $t = 0$, $r_g$ is equal to its $t = 0$ value $r_g^o$. At $t = \delta t$, the $t = 0$ population has evolved in time according to the equations of Table IV,

i.e., $f_g^o(\delta t)$. In addition population $F_y \delta t$ has been fed into the y level and contributes $F_y \delta t f_g^y(o)$ to the value of $r_g$. (For the moment we are ignoring possible feeding into the x level.) At $t = 2\delta t$, the $t = 0$ population has evolved in a manner described by $f_g^o(2\delta t)$. The population which entered during $t = \delta t$ has evolved according to $f_g^y(\delta t)$ and the population which has just entered contributes $F_y \delta t f_g^y(o)$ to $r_g$. For any time $t = m\delta t$ we have the value of $r_g$ given by Eq. (IV.30d). It is important to keep in mind that the function $f_g^o(t)$ is normalized to the total number of states in the system at time $t = 0$, while the function $f_g^y(t)$ represents the time evolution of a single state with the total number of states being explicitly written as $F_y \delta t$.

Changing dummy variables in Eq. (IV.30d) such that $n = m - \ell$, the equation may be written

$$r_g = f_g^o(t) + F_y \delta t \sum_{n=0}^{m=1} f_g^y(n\delta t) \qquad \text{(IV.31)}$$

letting $\delta t \to 0$ and $m \to \infty$ the sum becomes an integral

$$r_g = f_g^o(t) + F_y \int_0^t f_g^y(\tau)\, d\tau \qquad \text{(IV.32)}$$

Since $f_g^y(t)$ has the form

$$\frac{e^{-k_A T}}{2(\alpha^2 + \beta^2)} (A_y \cos\alpha t + B_y \sin\alpha t + C_y \cosh\beta t + D_y \sinh\beta t)$$

identical to Eq. (IV.26) of Section IV-B-2 C except that the subscript y has been added to the coefficients which are given in Table IV to keep

track of the special initial conditions for the $\hat{y}$ class, i.e., Eqs. (IV.28) and (IV.29), we only needed the following integrals

$$I = \int_0^t e^{-k_A\tau} \cos\alpha\tau d\tau = \frac{1}{k_A^2 + \alpha^2}\left(k_A + e^{-k_A t}\left[\alpha\sin\alpha t - k_A\cos\alpha t\right]\right) \quad \text{(IV.33a)}$$

$$II = \int_0^t e^{-k_A\tau} \sin\alpha\tau d\tau = \frac{1}{k_A^2 + \alpha^2}\left(\alpha - e^{-k_A t}\left[k_A\sin\alpha t + \alpha\cos\alpha t\right]\right) \quad \text{(IV.33b)}$$

$$III = \int_0^t e^{-k_A\tau} \cosh\beta\tau d\tau = \frac{1}{k_A^2 - \beta^2}\left(k_A - e^{-k_A t}\left[\beta\sinh\beta t + k_A\cosh\beta t\right]\right) \quad \text{(IV.33c)}$$

$$IV = \int_0^t e^{-k_A\tau} \sinh\beta\tau d\tau = \frac{1}{k_A^2 - \beta^2}\left(\beta - e^{-k_A t}\left[k_A\sinh\beta t + \beta\cosh\beta t\right]\right) \quad \text{(IV.33d)}$$

To include the effect of population feeding into the x level an identical procedure is followed using the function $f_g^x(t)$. Combining the above results gives the most general form for any component $r_g$.

$$r_g = \left[\frac{e^{-k_A t}}{2(\alpha^2 + \beta^2)}(A\cos\alpha t + B\sin\alpha t + C\cosh\beta t + D\sinh\beta t)\right] \quad \text{(IV.34)}$$
$$+ \left[\frac{F_y}{2(\alpha^2 + \beta^2)}(A_y I + B_y II + C_y III + D_y IV)\right]$$
$$+ \left[\frac{F_x}{2(\alpha^2 + \beta^2)}(A_x I + B_x II + C_x III + D_x IV)\right]$$

The first bracketed expression is due to the t = 0 excited subensemble. The second bracketed expression is due to the $\hat{y}$ class and the third bracketed expression is due to the $\hat{x}$ class subensemble. The coefficients A, B,

C and D are obtained from Table IV for a given set of experimental conditions. The subscripts y and x on these coefficients indicate the initial conditions given in Eqs. (IV.28a) and (IV.29a) are used when determining the values of the coefficients from Table IV. (Note that for determining $A_y$, $B_y$, $C_y$ and $D_y$, $r_y^o$ is set equal to one since $F_y \delta t$ has been taken into the integrals. Similarly $r_x^o$ is set equal to one when determining $A_x$, $B_x$, $C_x$ and $D_x$.) I, II, III and IV are defined above in Eqs. (IV.33a-b) and the other parameters are defined earlier.

Equation (IV.34) is the general equation which permits the effect of the application of a coherent radiation field to a two level system with feeding and decay to be determined. The coherent pertrubation does not have to be continuous. The general equation will allow the effect of any pulse sequence to be calculated in the following manner. At the end of the first pulse, the components $r_g$ are determined. These are then used as initial conditions in the determination of the effect of the next pulse. A period between pulses in which no power is applied is considered to be a pulse with $\omega_1 = 0$. The general equation, Eq. (IV.34), is used to determine the $r_g$ components at the end of this zero power pulse. These $r_g$ components are then the initial values for the calculation of the effect of the next pulse. In this way, the results of the application of any pulse sequence may be examined.

The general equation is valid for a single homogeneous line. To treat inhomogeneous lines, Eq. (IV.34) is used to determine the effect of the coherent radiation field on each isochromat in the inhomogeneous line. $r_g$ can be calculated for each component of the inhomogeneous line

and the results added. Thus, an inhomogeneous line may be readily treated using the above formulation.

$T_2$ and $T_1$ processes have not been included in the above mathematical development, however, these processes will be added using the general treatment due to Redfield[71] and the many other workers[72] in the field of coherent coupling in two level systems in a subsequent paper.[78] The purpose of this treatment is to develop a mathematical formulation for and to illustrate the effects of feeding and decay in a coherently coupled two level system. Some of these effects, which appear as if they are conventional $T_2$ and $T_1$ processes, are more graphically demonstrated using the above hypothetical model in which $T_2$ and $T_1$ processes are absent. In the following section the above formulation will be applied to several concrete examples.

## C. Physical Applications

In this section, the mathematical formulation developed above will be applied to several examples of physical significance. The examples will illustrate the manner in which a problem is treated, in addition to demonstrating significant features which are introduced into a coherently coupled two level system by the feeding and decay processes. The problems examined are; the transient nutation,[73] the high and low power CW spectrum, and the production of long term kinetic coherence. The role played by feeding and decay will be emphasized in each of these. Conventional $T_1$ and $T_2$ processes have been omitted so

that the contributions from feeding and decay may be clearly examined.

1. Transient Nutation

First consider a transient nutation[73] in the absence of feeding and decay. For the two level system in which the x and y levels have initial populations $r_x^o$ and $r_y^o$ respectively, the initial population difference is $r_3^o = r_y^o - r_x^o$. These two levels are then coupled by a coherent radiation field applied at the transition frequency. We wish to determine the time evolution of the population difference, $r_3 = r_y - r_x$. For a sample composed of identical two level systems which do not experience $T_1$ or $T_2$ relaxation processes and for a homogeneous applied field of amplitude $\omega_1$, the time evolution is simply given by

$$r_3 = r_3^o \cos\omega_1 t \tag{IV.35}$$

The population difference oscillates indefinitely between values of $r_3^o$ and $-r_3^o$ with a period of $2\pi\omega_1$.

To treat the above problem, but to include the effects of population feeding into and decaying from the two levels, the general equation (Eq. (IV.34)) of Section IV-B-3 is employed. It is first necessary to define the values of the parameters which apply to the transient nutation. Since the radiation field of amplitude $\omega_1$ is applied on resonance,

$$\Delta\omega = 0 \tag{IV.36}$$

and therefore, from Eqs. (IV.21) and (IV.27)

$$\bar{\omega} \equiv \alpha + i\beta = \sqrt{\omega_1^2 - k_D^2} \quad .$$

As mentioned in Section IV-B-2 there are three possible solutions depending upon the relative magnitudes of $k_D$ and $\omega_1$. We will only solve the problem analytically for the under damped case, i.e., $\omega_1 > k_D$. In the under damped case $\alpha \neq 0$ and $\beta = 0$. However in the over damped case $\alpha = 0$ and $\beta \neq 0$. Separate solutions must be obtained for these two cases. For the underdamped case, taking

$$\omega_1 > k_D \tag{IV.37}$$

the following values of $\alpha$ and $\beta$ are determined from Eqs. (IV.27b-c)

$$\alpha = (\omega_1^2 - k_D^2)^{1/2} \tag{IV.38a}$$

$$\beta = 0 \tag{IV.38b}$$

Since $\alpha = \bar{\omega}$ for the case under consideration, we define the parameter, $\bar{\omega}_{or}$, i.e.,

$$\bar{\omega}_{or} \equiv \alpha = (\omega_1^2 - k_D^2)^{1/2} \tag{IV.39}$$

where the subscript, or, stands for on resonance. The other necessary parameters are the zero time subensemble initial populations of the x and y levels, i.e., $r_x^o$ and $r_y^o$ respectively, and $r_1^o = r_2^o = 0$.

Remembering the special initial conditions for the $\hat{y}$ subensemble

$$r_x^o = r_1^o = r_2^o = 0 \tag{IV.39a}$$

$$r_y^o = 1 \tag{IV.39b}$$

and for the $\hat{x}$ subensemble

$$r_y^o = r_1^o = r_2^o = 0 \tag{IV.40a}$$

$$r_x^o = 1 \tag{IV.40b}$$

the coefficients ($A$, $A_y$, $A_x$, $B$, $B_y$, $B_x$, $C$, $C_y$, $C_x$, $D$, $D_y$, $D_x$) in the general equation can be determined from Table IV. The coefficients for $r_y$ and $r_x$ which are the components of interest are given in Table V. The coefficients for the overdamped case in which $\alpha = 0$ and $\beta = (\omega_1^2 - k_D^2)^{1/2}$ for other components, or for other sets of experimental conditions can be determined in an analogous manner.

Using the coefficients listed in Table V, the time evolution of $r_x$ and $r_y$ is obtained from the general equation (Eq. (IV.34)). Subtracting $r_x$ from $r_y$ and collecting terms yields the time evolution of $r_3$.

$$r_3 = \left[\left(r_3^o \cos\bar{\omega}_{or}t + \frac{k_D(r_x^o + r_y^o)}{\bar{\omega}_{or}} \sin\bar{\omega}_{or}t\right) e^{-k_A t}\right] \tag{IV.41}$$

$$- \frac{(F_x - F_y)}{k_A^2 + \bar{\omega}_{or}^2} \left[k_A + e^{-k_A t} (\bar{\omega}_{or}\sin\bar{\omega}_{or}t - k_A\cos\bar{\omega}_{or}t)\right]$$

$$+ \frac{(F_x + F_y)\, k_D}{\bar{\omega}_{or}(k_A^2 + \bar{\omega}_{or}^2)} \left[\bar{\omega}_{or} - e^{-k_A t}(k_A\sin\bar{\omega}_{or}t + \bar{\omega}_{or}\cos\bar{\omega}_{or}t)\right]$$

The first term in square brackets is due to the zero time subensemble, while the other terms are due to population fed into the x and y levels after $t = 0$. Rearranging this expression we obtain,

$$r_3 = e^{-k_A t}\left[\left(r_3^o - \frac{F_y k_x - F_x k_y}{\omega_1^2 + k_x k_y}\right)\cos(\bar{\omega}_{or}t)\right. \tag{IV.42}$$

$$\left. + \left(\frac{(r_x^o + r_y^o)\, k_D}{\bar{\omega}_{or}} - \frac{(F_x - F_y)\,\bar{\omega}_{or}}{\omega_1^2 + k_x k_y} - \frac{(F_x + F_y)\, k_D k_A}{(\omega_1^2 + k_x k_y)\,\bar{\omega}_{or}}\right)\sin(\bar{\omega}_{or}t)\right] + \frac{F_y k_x - F_x k_y}{\omega_1^2 + k_x k_y}.$$

Table V. On resonance transient nutation under damped case.

| Zero Time Subensemble | $\hat{y}$ Subensemble | $\hat{x}$ Subensemble |
|---|---|---|
| $r_y$ | | |
| $A = (\bar{\omega}_{or}^2 - k_D^2)\, r_y^o - \omega_1^2 r_x^o$ | $A_y = \bar{\omega}_{or}^2 - k_D^2$ | $A_x = -\omega_1^2$ |
| $B = 2k_D\bar{\omega}_{or} r_y^o$ | $B_y = 2k_D\bar{\omega}_{or}$ | $B_x = 0$ |
| $C = \omega_1^2 r_y^o + \omega_1^2 r_x^o$ | $C_y = \omega_1^2$ | $C_x = \omega_1^2$ |
| $D = 0$ | $D_y = 0$ | $D_x = 0$ |
| $r_x$ | | |
| $A = (\bar{\omega}_{or}^2 - k_D^2)\, r_x^o - \omega_1^2 r_y^o$ | $A_y = -\omega_1^2$ | $A_x = \bar{\omega}_{or}^2 - k_D^2$ |
| $B = -2k_D\bar{\omega}_{or} r_x^o$ | $B_y = 0$ | $B_x = -2k_D\bar{\omega}_{or}$ |
| $C = \omega_1^2 r_x^o + \omega_1^2 r_y^o$ | $C_y = \omega_1^2$ | $C_x = \omega_1^2$ |
| $D = 0$ | $D_y = 0$ | $D_x = 0$ |

There are several interesting features to note in Eqs. (IV.41) and (IV.42). First, if $r_x^o$ and $r_y^o$ are zero, i.e., there is no excited state population in the ensemble of two level systems under consideration at time t = 0, the contribution to $r_3$ from the zero time subensemble vanishes. There is, however, still an oscillatory behavior in $r_3$ which occurs due to population being incoherently fed into the system provided that either $k_x \neq k_y$ or $F_x \neq F_y$ (cf Eq. (IV.41)). Second, it can be seen from Eq. (IV.42) that all of the oscillatory terms are multiplied by the decay exponential $e^{-k_A t}$ and therefore even in the absence of other relaxation processes the oscillatory behavior of $r_3$ is damped. At long times $r_3$ goes to a steady state constant value given by the last term in Eq. (IV.42). Third, given the proper values, the parameters in Eq. (IV.42) will make the term multiplied by $\sin(\bar{\omega}_{or} t)$ finite. This results in a phase shift in the oscillations relative to those given by the simple transient nutation of Eq. (IV.35). Finally, unlike Eq. (IV.35), the oscillations in Eq. (IV.42) do not occur at frequency $\omega_1$, but rather at frequency $(\omega_1^2 - k_D^2)^{1/2}$. For the under damped case which we are considering here, in most situations the deviation from $\omega_1$ will not be significant. However, if $k_A$ is large, then $k_D^2$ can take on values approaching $\omega_1^2$. For $k_A$ large, the total oscillatory behavior will be damped out rapidly, but those oscillations which do occur will be at a frequency significantly different from $\omega_1$. (If $k_D > \omega_1$, the over damped case occurs, and the expression for $r_3$ is in terms of sinh and cosh. In this case of course no oscillatory behavior occurs.)

To this point we have been considering perfect experimental conditions. If the applied coherent radiation field is inhomogeneous in amplitude over the size of the sample, the oscillatory terms may be damped out at a rate considerably faster than $\exp(-k_A t)$. At times long relative to the inhomogeneous field damping but short enough to keep $\exp(-k_A t)$ finite, the time evolution of the total population in the ensemble of two level systems, $N = r_x + r_y$, is given by the following equation.

$$N = \frac{\omega_1^2}{\bar{\omega}^2 k_A} [(r_y^o + r_x^o)\, k_A - (F_y + F_x)]\, e^{-k_A t} + \left[\frac{F_y k_x + F_x k_y + \frac{\omega_1^2}{k_A}(F_y + F_x)}{\omega_1^2 + k_x k_y}\right] \tag{IV.43}$$

The total population evolves exponentially in time with a rate constant given by the average of the life times of the two levels involved. It reaches a new steady state value given by the last term in square brackets in Eq. (IV.43). This should be compared to the steady state population in the absence of the applied radiation field, i.e., $N = \frac{F_x}{k_x} + \frac{F_y}{k_y}$.

2. <u>The CW Spectrum</u>

Another important physical example is the CW spectrum. Here again we will solve the problem in the absence of conventional $T_1$ and $T_2$ processes. The solution is obtained from the general equation (Eq. (IV.34)) by taking the terms which survive when $t \to \infty$. These are the time-independent terms of the $\hat{y}$ and $\hat{x}$ feeding subensembles. Any component $r_g$ is given by

$$r_g \underset{t\to\infty}{=} F_y\left(\frac{A_y k_A + B_y \alpha}{k_A^2 + \alpha^2} + \frac{C_y k_A + D_y \beta}{k_A^2 - \beta^2}\right) + F_x\left(\frac{A_x k_A + B_x \alpha}{k_A^2 + \alpha^2} + \frac{C_x k_A + D_x \beta}{k_A^2 - \beta^2}\right) \tag{IV.44}$$

The coefficients ($A_y$ through $D_x$) are given in Table IV and the other parameters are defined above. Using Eq. (IV.44), the $r_y$ and $r_x$ components are obtained after extensive algebra.

$$r_y = \frac{F_y k_x\left(1 + \frac{\Delta\omega^2}{k_A^2}\right) + \frac{\omega_1^2}{k_A}\left(\frac{F_x + F_y}{2}\right)}{\omega_1^2 + k_x k_y\left(1 + \frac{\Delta\omega^2}{k_A^2}\right)} \tag{IV.45a}$$

$$r_x = \frac{F_x k_y\left(1 + \frac{\Delta\omega^2}{k_A^2}\right) + \frac{\omega_1^2}{k_A}\left(\frac{F_x + F_y}{2}\right)}{\omega_1^2 + k_x k_y\left(1 + \frac{\Delta\omega^2}{k_A^2}\right)} \tag{IV.45b}$$

Note that for $\omega_1 = 0$, $r_y$ and $r_x$ go to their steady state values, i.e., $r_y = \frac{F_y}{k_y}$ and $r_x = \frac{F_x}{k_x}$.

To compute the CW spectrum, we only need $r_3 = r_y - r_x$,

$$r_3 = \frac{\left(\frac{F_y k_x - F_x k_y}{k_x k_y}\right)\left(1 + \frac{\Delta\omega^2}{k_A^2}\right)}{1 + \frac{\Delta\omega^2}{k_A^2} + \frac{\omega_1^2}{k_x k_y}} \tag{IV.46}$$

Defining

$$r_3^o \equiv (F_y k_x - F_x k_y)/k_x k_y \tag{IV.47a}$$

yields

$$r_3 = \frac{r_3^o\left(1 + \frac{\Delta\omega^2}{k_A^2}\right)}{1 + \frac{\Delta\omega^2}{k_A^2} + \frac{\omega_1^2}{k_x k_y}} \tag{IV.47b}$$

This expression can be cast into a familiar form by making the additional definitions,

$$T_{2k} \equiv \frac{1}{k_A} \tag{IV.48a}$$

$$T_{1k} \equiv \frac{k_A}{k_x k_y} \tag{IV.48b}$$

The subscript k is to distinguish the parameters defined in Eqs. (IV.48a-b) form the conventional $T_1$ and $T_2$. In terms of $T_{1k}$ and $T_{2k}$, the expression for $r_3$ becomes

$$r_3 = \frac{r_3^o(1 + \Delta\omega^2 T_{2k}^2)}{1 + \Delta\omega^2 T_{2k}^2 + T_{1k}T_{2k}\omega_1^2} \tag{IV.49}$$

where $T_{1k}T_{2k}\omega_1^2$ is the "saturation term"[74] which appears to broaden the line at high powers (large $\omega_1$). At low power, the line shape is given by

$$r_3 = r_3^o\left(1 - \frac{{}^2T_{1k}T_{2k}}{1 + \Delta\omega^2 T_{2k}^2}\right) \tag{IV.50}$$

Equation (IV.50) gives the normal Lonentz line shape.[74] In a two level system without feeding and decay, $T_1$ processes maintain the population difference which is a necessary condition for a CW spectrum. However, in the systems under consideration, a combination of feeding and decay processes maintain the necessary population difference. In the special case of equal feeding and decay, $r_3^o = 0$ and the CW spectrum vanishes.

3. Kinetic Coherence

Using Eq. (IV.44) of the last section, the CW $r_1$ and $r_2$ components of the ensemble of excited state two level systems can be obtained.

$$r_1 = \frac{\frac{\omega_1}{k_A}(F_x k_y - F_y k_x)}{\omega_1^2 + k_x k_y\left(1 + \frac{\Delta\omega^2}{k_A^2}\right)} \tag{IV.51a}$$

$$r_2 = \frac{\frac{\omega_1 \Delta\omega}{k_A^2}(F_x k_y - F_y k_x)}{\omega_1^2 + k_y k_x\left(1 + \frac{\Delta\omega^2}{k_A^2}\right)} \tag{IV.51b}$$

These components represent the long lived coherent state maintained in the ensemble by the radiation field. This type of effect is also manifest in conventional magnetic resonance systems,[64] however it is very small, due to the inability of $T_1$ processes competing with the applied radiation field to maintain a sizeable population difference. It is important to remember that the radiation field is applied along the $r_2$ axis (Eq. (IV.2) and therefore the $r_2$ component is in phase with the applied field and the $r_1$ component is out of phase.

The maximum values of $r_1$ and $r_2$ can be readily calculated under various conditions of feeding, decay and power. First consider $r_1$. From Eq. (IV.51a) it can be seen that $r_1$ has a maximum value on-resonance ($\Delta\omega = 0$), and so we consider the expression

$$r_1 = \frac{\frac{\omega_1}{k_A}(F_x k_y - F_y k_x)}{\omega_1^2 + k_y k_x} \tag{IV.52}$$

This expression vanishes for both low and high power, and therefore it must have a maximum in between. Taking the derivative of Eq. (IV.52) with respect to $\omega_1$ and equating the results to zero, indicates that $r_1$ has a maximum when

$$\omega_1^2 = k_x k_y \tag{IV.53}$$

Thus the maximum value of $r_1$ is given by

$$r_1^{max} = \frac{(F_x k_y - F_y k_x)(k_x k_y)^{1/2}}{k_x k_y (k_x + k_y)} = \frac{-r_3^o (k_x k_y)^{1/2}}{(k_x + k_y)} \tag{IV.54}$$

Now consider $r_2$. First $r_2$ is maximized with respect to $\Delta\omega$ by taking the partial derivative of Eq. (IV.51b) with respect to $\Delta\omega$ and equating the resulting expression to zero. This gives the value of $\Delta\omega$ for which $r_2$, also is maximum.

$$\Delta\omega^{max} = k_A\left(1 + \frac{\omega_1^2}{k_x k_y}\right)^{1/2} \tag{IV.55}$$

$r_2$ has a maximum value when the applied radiation field is $\Delta\omega^{max}$ off resonance. Substituting this expression into Eq. (IV.51b) for $r_2$ yields,

$$r_2 = \frac{\dfrac{(F_x k_y - F_y k_x)}{k_x k_y}\,\omega_1\left(1 + \dfrac{\omega_1^2}{k_x k_y}\right)}{(k_x + k_y)\left(1 + \dfrac{\omega_1^2}{k_x k_y}\right)} \tag{IV.56}$$

$r_2$ has no maximum with respect to power, but it does approach a asymtotic value for large values of $\omega_1$, i.e., $\omega_1^2/k_x k_y >> 1$. With this condition, $r_2^{max}$ is obtained.

$$r_2^{max} = \frac{(F_x k_y - F_y k_x)^{1/2}}{k_x k_y (k_x + k_y)} = \frac{-r_3^o (k_x k_y)^{1/2}}{(k_x + k_y)} \tag{IV.57}$$

If $k_x = k_y$, then both $r_1^{max}$ and $r_2^{max}$ are equal to $r_3^o/2$, where $r_3^o$ is determined by the feeding and decay rates (cf Eq. (IV.47a). $r_3^o$ can be quite large if the incoherent source used to produce the excited states is intense and if there is a large difference in the feeding or decay rates of the two levels. This will result in large coherent components being maintained in the ensemble of excited state systems.

Qualitatively, the production of long term coherence can be viewed as follows. For the $r_1$ component the maximum value occurs on resonance, so we will consider the on resonance case. Initially, there is some population difference, $r_3^o$. When the levels are coupled coherently by turning on the radiation field, the $r_3^o$ vector will precess around the $r_2$ axis in the $r_1$, $r_3$ plane. Since there is continual decay to the ground state, the $r_3^o$ vector decreases in length as it executes a transient nutation about the $r_2$ axis. When it is along the $r_1$ direction it has some magnitude. By the time it reaches the $-r_1$ direction it has decreased in size. As discussed in Section IV-B-3, the population being

fed into the system behaves similarly to the initial population except for phase differences. Population fed into the system at some time t also precesses about the $r_2$ direction, and the vector created at time t also decreases in length as it goes around the circle. When the system has reached steady state, there is a continuous set of vectors precessing about the $r_2$ direction. If there were no decay from the system, this set of vectors would form a disc in the $r_1$, $r_3$ plane and there would be no net $r_1$ component. However, owing to decay, each vector shrinks as it precesses and therefore the vectors on one side of the "disc" are always shorter than those on the other side. Taking the projection of these vectors onto the $r_1$ axis results in a larger component along the possitive $r_1$ axis then along negative $r_1$ axis giving rise to a net $r_1$ component.

In the expression for $r_1^{max}$, conventional $T_2$ processes have not been considered. As population which enters the system along the $r_3$ axis precesses about the applied field, a $r_1$ component develops. This in-plane component will be reduced by $T_2$ and, therefore, the magnitude of the coherent component developed along the $r_1$ axis will be restricted. However, this does not present a problem for the production of long term kinetic coherence along the $r_2$ axis. This point is discussed below.

The production of long term coherence along the $r_2$ axis has a somewhat different mechanism than the $r_1$ case. The long term $r_2$ coherent component occurs when the radiation field is applied off resonance. The initial $r_3^o$ vector precesses around the effective field which is in the $r_2$, $r_3$ plane due to the off resonance condition. The motion of

the vector describes a cone around the effective field. Owing either to field inhomogeneity or sample inhomogeneity the $r_3^o$ vector will fan out around the conical path producing a thin cone of vectors precessing around the effective field. (This is not central to the argument for even with a homogeneous field and sample, the feeding process itself will cause this fan of vectors.) This cone of vectors has a net projection along the effective field direction which can be resolved into an $r_3$ component and an $r_2$ component. This $r_2$ component is the coherent component produced by the initial $r_3^o$ population in the system. This component will decay due to relaxation of the excited states to the ground state. However, as this initial population decays, additional population is fed into the system which forms an identical cone with a colinear $r_2$ component. Thus as the $r_2$ vector due to the first cone decays, it is replaced by the $r_2$ vector from the next cone. Through continual feeding, the cone and therefore the coherent $r_2$ vector is constantly replenished.

The result is that a coherent state is maintained in the excited ensemble for times longer than the life times of the excited states. In fact, it will remain as long as the radiation field remains coherent and population continues to be fed into the system by incoherent pumping. The magnitude of the $r_2$ component is controlled both by the effective field angle (i.e., $\tan\theta = \Delta\omega/\omega_1$) which determines the amount of the vector aligned along the effective field which is projected onto the $r_2$ axis, and by the incoherent pumping rate which determines the amount of population in the cone and therefore the size of the

vector aligned along the effective field. The advantage of the $r_2$ component over the $r_1$ component in an attempt to produce long term coherence is that the vector which gives rise to the $r_2$ component is aligned along the effective field and therefore it is "spin locked",[36] i.e., the $r_2$ component does not suffer the dephasing processes which tend to reduce the $r_1$ component because $r_2$ is derived from a vector which is aligned along the rotating frame static field.

4. The Optical Case: Long Term Superradiance

To this point, coherent coupling in two level systems with feeding and decay has only been discussed for the case in which the wavelength of the radiation field is large relative to the size of the sample. This condition implies that the phase of the radiation field is constant over the size of the sample, and, therefore, each molecule is considered to have an identical time dependent Hamiltonian.

In this section it is demonstrated that the development of the previous sections applies to the case in which the wavelength of the radiation field is small relative to the size of the sample. Under this condition, the time dependent Hamiltonian which describes the coherent perturbation, contains a spatially dependent phase factor, and therefore each molecule experiences a perturbation Hamiltonian given by

$$V^{j}(t) = \hbar\omega_1 \cos(\omega t - \vec{k}\cdot\vec{r}_j) \qquad \text{(IV.58)}$$

where j labels a particular molecule, $\omega_1 = \vec{\mu}\cdot\vec{E}_1$ where $E_1$ is the amplitude of the applied field, $\omega$ is the frequency of the applied field and $\vec{k}$ is the wave vector of the applied field. $\vec{r}_j$ describes the

location of the jth molecule. As discussed in reference to Eqs. (IV.1) through (IV.3), we make the rotating field approximation, and write the total Hamiltonian as

$$\mathcal{H}^j = \mathcal{H}^o + V^j(t) = \frac{\hbar\omega_o}{2}\,\sigma_3 + \frac{\hbar\omega_1}{2}\,e^{-i\sigma_3(\omega t-\vec{k}\cdot\vec{r}_j)}\,\sigma_1 e^{i\sigma_3(\omega t-\vec{k}\cdot\vec{r}_j)} \tag{IV.59}$$

Here, the matrix elements of the perturbation have been taken to be real, corresponding to optical transitions. In a fashion identical to that described in Eqs. (IV.4) through (IV.8), we transform into a frame rotating at frequency $\omega$, i.e., the Schrödinger equation becomes

$$i\hbar\dot{\Psi}(t) = \left(\frac{\hbar\Delta\omega}{2}\,\sigma_3 + \frac{\hbar\omega_1}{2}\,e^{i\sigma_3\vec{k}\cdot\vec{r}_j/2}\,\sigma_1 e^{-i\sigma_3\vec{k}\cdot\vec{r}_j}\right)\Psi(t) = \mathcal{H}^{j\ddagger}\Psi(t) \tag{IV.60}$$

where the $\ddagger$ indicates the rotating frame and $\Psi(t)$ is given by Eq. (IV.9).

In analogy to the rotating frame transformation, we will now transform into a $\vec{k}$ frame. We construct the unitary operator

$$T_{kj}^{-1} = e^{-i\sigma_3\vec{k}\cdot\vec{r}_j/2} \tag{IV.61}$$

with

$$\phi(t) = T_{kj}^{-1}\Psi(t) \tag{IV.62}$$

Substituting

$$\Psi(t) = T_{kj}\phi(t) \tag{IV.63}$$

into Eq. (IV.60) and taking the indicated derivative yields

$$i\hbar T_{kj}\dot{\phi}(t) = \left(\frac{\hbar\Delta\omega}{2}\,\sigma_3 + \frac{\hbar\omega_1}{2}\,e^{i\sigma_3\vec{k}\cdot\vec{r}_j/2}\,\sigma_1 e^{-i\sigma_3\vec{k}\cdot\vec{r}_j}\right)T_{kj}\phi(t) \tag{IV.64}$$

Multiplying both sides of Eq. (IV.64) by $T_{kj}^{-1}$ and substituting the definition of $T_{kj}^{-1}$ given in Eq. (IV.61) gives

$$i\hbar\dot{\phi}(t) = \left(e^{-i\sigma_3\vec{k}\cdot\vec{r}_j}\,\frac{\hbar\Delta\omega}{2}\,\sigma_3 e^{i\sigma_3\vec{k}\cdot\vec{r}_j}\right. \tag{IV.65}$$

$$\left. + \frac{\hbar\omega_1}{2}\, e^{-i\sigma_3\vec{k}\cdot\vec{r}_j}\, e^{i\sigma_3\vec{k}\cdot\vec{r}_j}\,\sigma_1 e^{-i\sigma_3\vec{k}\cdot\vec{r}_j}\, e^{i\sigma_3\vec{k}\cdot\vec{r}_j}\right)\phi(t)$$

and therefore

$$i\hbar\dot{\phi}(t) = \left(\frac{\hbar\Delta\omega}{2}\,\sigma_3 + \frac{\hbar\omega_1}{2}\,\sigma_1\right)\phi(t) = \mathcal{H}_k^{\ddagger}\phi(t) \tag{IV.66}$$

where $\mathcal{H}_k^{\ddagger}$ is the Hamiltonian in the double transformed frame and $\phi(t)$ is given by

$$\phi(t) = y_k^{\ddagger}\phi_y^o + x_k^{\ddagger}\phi_x^o \tag{IV.67}$$

where $y_k^{\ddagger}$ and $x_k^{\ddagger}$ are the rotating frame, k frame time dependent coefficients.

Equation (IV.66) has two significant features. First, it is identical for each molecule. In the k frame, the $\vec{r}_j$ dependence has vanished. Second, Eq. (IV.66) is just the equation of motion which was solved in Section IV-2-B (except for the real matrix elements of the perturbation which do not affect the solution. Compare Eqs. (IV.8) and (IV.66)). These two facts imply that the results obtained in the previous sections for the large wavelength case can be carried over completely to the short wavelength optical case when it is treated in the k frame. In the earlier sections we employed a rotating frame to simplify the solution. To determine the observables in the laboratory frame, an inverse transformation must be preformed to take us from the rotating

frame to the lab frame. Thus the coherent component $r_2$ calculated to be stationary in the rotating frame of frequency $\omega$ (cf Section IV-C-3), will precess at frequency $\omega$ in the lab frame. In this section we have used a rotating frame and a k frame. To determine the observables in the lab frame, we must make two inverse tranformations to return to the lab frame.

In the last section, it was demonstrated that a long term in-phase coherent component could be maintained in an ensemble of excited two level systems with feeding and decay by off resonance coherent coupling of the two levels. This result also applies to the optical case where the two levels would be capable of undergoing optical transitions and would obtain their population via incoherent feeding. Coherent optical radiation applied off resonance will maintain a coherent component in the ensemble. This coherent component is a precessing macroscopic electric dipole, and as in other methods for producing a coherent optical state such as the photon echo experiment,[75] this coherent ensemble will exhibit superradiance,[76] i.e., enhanced spontaneous emission, which was first discussed by Dicke.[77] In the photon echo and other current experiments, it is impossible to maintain the coherent state, and therefore the superradiance is short lived. However, the theory presented above embodies an experimental technique capable of producing long term superradiance through the maintenance of the kinetic coherent state.

It will be demonstrated in detail elsewhere[78] that superradiant emission in this type of experiment will have the usual directional properties. That is, for an infinite sample size, coherent light will only be emitted in the $\vec{k}$ direction, and that for a finite sample size,

coherent light will be emitted with an angular distribution given by a zeroth order spherical Bessel function centered about the $\vec{k}$ direction. However, this emission will not occur at the natural transition frequency of the two levels $\omega_o$, but rather at the frequency of the applied field $\omega$. This is because the coherent component precesses in the lab frame at the frequency of the rotating frame, i.e., the frequency of the applied field. The emitted radiation is spontaneous emission, but not spontaneous emission at the natural wavelength of the transition. It is in effect "off resonance" spontaneous emission.

Another point which should be made is that by varying either $\Delta\omega$ or $\omega_1$, the angle of the effective field may be changed and therefore an ensemble may be maintained and studied which has a particular cooperation number.[77] The cooperation number, which is related to the magnitude of the coherent component, determines the extent to which normal spontaneous emission is amplified.[79]

Finally, it is important to mention the possibility that the production of long term superradiance can lead to a useful device if the many experimental obstacles can be over come. Since the intenstiy of coherent light emitted by the long term kinetic coherent state is determined by the rate of incoherent pumping and the life times of the states in addition to the amplitude of the applied coherent radiation field, in principal a carefully chosen system could exhibit gain, and therefore act as coherent light amplifier. This amplifier is tunable over the spectral region in which gain occurs. Further, if a system is found which exhibits gain, the amplified emission could be fed back in phase into the superradiant amplifier and the applied coherent field

removed. If the gain is great enough to overcome the loses in the feed-back cavity, the superradiant amplifier will go into a self-sustaining continuous mode emitting coherent light at the wavelength of initial applied field.

## D. Summary of Chapter IV

1. The problem of coherent coupling in two level systems in which population is continually being fed into the systems and population is continually decaying from the systems is considered. The problem is solved analytically and cast into a geometrical representation which allows coherent and incoherent phenomena to be readily distinguished.

2. A general equation is obtained which allows the effect of coherent perturbation to be calculated for any set of experimental conditions. Feeding and decay play a central role in this equation and therefore in determining the effects of the perturbation on the ensemble of two level systems.

3. Several sample calculations are performed to illustrate the use of the mathematical formulation and to illustrate the role played by feeding and decay. In particular it is demonstrated that a long term coherent component, which may be quite large, can be maintained in an ensemble of excited two level systems and that this component is effectively "spin locked" even for systems involving optical transitions.

4. Finally, it is shown that this long term kinetic coherent state in optical systems will give rise to long term superradiant emission and that it may be possible to use this effect to produce a new type of coherent light amplifying device.

## ACKNOWLEDGEMENTS

I would like to thank Professor Charles B. Harris for his valuable assistance in all aspects of this work. He provided the necessary personal encouragement in addition to supplying a vast wealth of experimental and theoretical ideas. His unlimited energy and wide ranging knowledge of modern physical science has guided me to the beginning of my path through the scientific world.

I would also like to thank my many friends and colleagues in the Chemistry Department for their professional and non-professional assistance in making my time here enjoyable. Professor H. Strauss, in particular, has been friendly and encouraging at times when I needed a friend and encouragement.

Finally, I would like to thank my family, William and Frieda Fayer, Caroline and Robert Altman and Terri Fayer, for their unwavering faith in me and for just putting up with me over the past years.

This work was supported in part by a grant from the National Science Foundation and in part by the Inorganic Materials Research Division of the Lawrence Berkeley Laboratory under the auspices of the U. S. Atomic Energy Commission.

# APPENDIX. COMPUTER PROGRAMS

## 1. Program TRAPS

Program TRAPS calculates the probability of finding an excitation of a system, composed of a low energy trap state and a one domensional exciton band, in the trap (cf Chapter I). One data card with format (3F10.4) must be read for each calculation. The data card contains in the first 10 spaces, Beta, the value of the nearest neighbor interaction matrix element which is 1/4 of the bandwidth in ergs. The sign of BETA must also be included. Positive BETA implies K = 0 is at the top of the exciton band and negitive Beta indicates K = 0 is at the bottom of the band. In the second 10 spaces is DEPTH, the difference in energy between the K = 0 level of the exciton band and the trap level, in ergs. In the third 10 spaces is AN, 1/2 the number of K states in the band. The last card listed in the program print out is an example of a data card. If more than one set of data is to be run, merely stack the data cards. The program will automatically terminate after running the last set of data.

As the program is written now, the trap probability is calculated at 4.3°K and at every 0.3°K down to 1.0°K. The starting temperature can be changed by changing the card T = 4.3 to the desired starting temperature. The increment of temperature change can be controlled by altering the card T = T - 0.3 to the desired increment. The lowest temperature may be changed by changing the card. If (T.GT. 0.99) GO TO 110 to slightly below the desired final temperature.

```
TRAPS,7,160,60000,400512, MIKE FAYER
*7600
*USERPR
RUN(S)
LINK(X)
-
      PROGRAM TRAPS (INPUT,OUTPUT,TAPE5=INPUT)
      REAL KB
      PI=3.1416
      KB=1.38E-16
90    READ700,BETA,DEPTH,AN
      IF(EOF,5) 600,95
95    PRINT500
      PRINT720, BETA, DEPTH
      PRINT550
100   T=4.3
110   SUM1=1.+EXP(-1.*(DEPTH)/(KB*T))
      N=AN+.1
      I=0
1000  I=I+1
      C=COS(PI*(FLOAT(I)/AN))
      E=EXP(-1.*(DEPTH-2.*BETA*(1.-C))/(KB*T))
      SUM1=SUM1+2.*E
      IF(I.LT.N) GO TO 1000
      PT=1/SUM1
      PRINT710,T,AN,PT
      IF(PT.GT.0.998) GO TO 120
      T=T-0.3
      IF(T.GT.0.99) GO TO 110
120   CONTINUE
      GO TO 90
600   CONTINUE
500   FORMAT(///,10X,*BETA EQUALS    DEPTH EQUALS*,/)
550   FORMAT(///,10X,*TEMP.          STATES/2      TRAP PROB.*,/)
700   FORMAT(3F10.4)
710   FORMAT(10X,3F12.5)
720   FORMAT(10X,2(4X,E12.4))
      END

2.484E-16 4.111E-15   20000.0
```

2. Program DEEP2

Program DEEP2 calculates the probabilities of finding an excitation in either a deep trap or a shallow trap in a system composed of a deep trap, a shallow trap, and a one dimensional exciton band (cf Chapter II). The first data card with format (2F10.4) reads in B and G. B determines how many different values of Beta will be read in for each set of parameters G1, G2 and AN. G tells how many different sets of G1, G2 and AN will be read in. The second data card with format (2F10.4) contains in the first 10 spaces DEPTH1, the difference in energy between the deep trap and the shallow trap in ergs, and in the second 10 spaces DEPTH 2, the difference in energy between the deep trap and the K = 0 level of the exciton band in ergs. The third data card with format (3F10.4) contains in the first 10 spaces G1, the number of shallow traps relative to one deep trap; in the second 10 spaces G2, the number of exciton chains relative to one deep trap; and AN, 1/2 the number of K states in the average length exciton chain (cf Chapter II). The fourth data card with format (1F10.4) contains BETA, the value of the nearest neighbor interaction matrix element which is 1/4 of the bandwidth, in ergs. If several calculations, with different values of BETA but with the same values of G1, G2 and AN are desired, simply stack a series of individual BETA cards. The number of BETA cards must be specified by B on data card 1. If several different sets of G1, G2 and AN are desired, each new data card of this type is placed after the last BETA card of the previous data set. Another set of BETA cards are then placed after each G1, G2 and AN card. The number of G1, G2 and AN cards must be specified by G on the first

data card. An example of data cards is given in the last four lines of the program printout. The temperature range is controlled in a manner identical to that described in the section on Program TRAPS.

```
DEEP2,7,40,60000,400512, MIKE FAYER
*7600
*USERPR
RUN(S)
LINK(X)
-
      PROGRAM DEEP2 (INPUT,OUTPUT)
      REAL KB
      PI=3.1416
      KB=1.38E-16
      READ685,B,G
      READ690, DEPTH1, DEPTH2
      J=0
89    READ695,G1,G2,AN
      J=J+1
      M=0
90    READ700, BETA
      M=M+1
95    PRINT500
      PRINT720,BETA,DEPTH1,DEPTH2,G1,G2,AN
      PRINT550
100   T=4.3
110   SUM1=1.+G1*EXP(-1.*(DEPTH1)/(KB*T))+G2*EXP(-1.*(DEPTH2)/
     1(KB*T))
      N=AN+.1
      I=0
1000  I=I+1
      C=COS(PI*(FLOAT(I)/AN))
      E=EXP(-1.*(DEPTH2-2.*BETA*(1.-C))/(KB*T))
      SUM1=SUM1+G2*2.0*E
      IF(I.LT.N) GO TO 1000
      PT1=1/SUM1
      PT2=G1*EXP(-1.*(DEPTH1)/(KB*T))/SUM1
      PEX=1.0-(PT1+PT2)
      PRINT710,T,AN,PT1,PT2,PEX
      T=T-0.3
      IF(T.GT.0.99) GO TO 110
      IF(B.GT.M) GO TO 90
      IF(G.GT.J) GO TO 89
      CONTINUE
500   FORMAT(///,10X,*BETA EQUALS    DEPTH1 EQUALS DEPTH2 EQUALS
     1  G1 EQUALS    G2 EQUALS    AN EQUALS*,/)
550   FORMAT(///,14X,*TEMP.        STATES/2     T1 PROB.       T2 PROB.
     1  EX PROB.*,/)
685   FORMAT(2F10.4)
690   FORMAT(2F10.4)
695   FORMAT(3F10.4)
700   FORMAT(1F10.4)
710   FORMAT(10X,5F12.5)
720   FORMAT(6X,6(4X,E12.4))
      END
```

```
      30.9        0.9
  25.4E-16   46.7E-16
      62.0       62.0        8.0
 .497E-16
```

3. Program GVELO

Program GVELO calculates the average group velocity in one direction of an ensemble of one dimensional excitons (cf Chapter I). Each data card with format (F10.4) contains BETA, the nearest neighbor interaction matrix element which is 1/4 of the bandwidth, in ergs. The parameter A must be set equal to the lattice spacing in centimeters along the one dimensional axis. The parameter AN is set equal to 1/2 the number of molecules in the average length exciton chain. If it is desired to make the calculation using the same value of BETA but different values of AN, the parameter STOP is set for the largest value of AN desired with the condition that AN will be doubled each time until AN is greater than STOP. If only one value of AN is desired for each BETA, set STOP equal to the same number which AN is set equal to. The program will automatically terminate after the last BETA data card is used. The group velocities are printed in centimeters. Control of the temperature range is given in the section on Program TRAPS.

```
GVELO,7,400,60000.400512. MIKE FAYER
*7600
*USERPR
RUN(S)
LINK(X)

      PROGRAM GVELO (INPUT,OUTPUT, TAPE5=INPUT)
      REAL KB
      PI=3.1416
      A=3.76E-8
      STOP=13000.0
      KB=1.38E-16
      H=1.054E-27
90    READ700,BETA
      IF(EOF,5) 600,95
95    PRINT500
      PRINT720,BETA
      PRINT550
      AN=50.0
100   T=4.3
110   SUM1=0
      SUM2=0
      N=AN+.1
      I=0
1000  C=COS(PI*(FLOAT(I)/AN))
      S=SIN(PI*(FLOAT(I)/AN))
      E=EXP(-1.*((42.3E-16)-2.*BETA*(1.-C))/(KB*T))
      SUM1=SUM1+S*E
      SUM2=SUM2+E
      I=I+1
      IF(I.LT.N) GO TO 1000
      VGK=-2.*BETA*A*SUM1/(SUM2*H)
      PRINT710,T,AN,VGK
      T=T-0.3
      IF(T.GT.0.99) GO TO 110
      AN=2.*AN
      IF(AN.LT.STOP) GO TO 100
      GO TO 90
600   CONTINUE
500   FORMAT(///,10X,*BETA EQUALS*,/)
720   FORMAT(10X,E12.4)
700   FORMAT(F10.4)
550   FORMAT(///,10X,*TEMP.          STATES/2      GROUP VELO.*,/)
710   FORMAT(10X,3F12.5)
      END
```

4. Program TWODI

Program TWODI calculates the probability of an excitation being found in a low energy trap level in a system composed of a trap level and a two dimensional exciton band (cf Chapter I). The data card with format (3F10.4) contains in the first 10 spaces BA, the value of the nearest neighbor interaction matrix element along one of the two dimensional axes in ergs. In the second 10 spaces is BB, the value of the nearest neighbor interaction matrix element along the other axis, in ergs. In the third 10 spaces is DEPTH, the difference in energy between the trap level and the K = 0 level of the exciton band. On this data card it is very important to specify the signs of BA and BB. AM is set equal to 1/2 the number of K states along the BA axis and AN specifies 1/2 the number of K states along the BB axis. If it is desired to calculate the trap probability for only one set of AM, AN for each value of BETA then set STOP equal to the value assigned to AM. If STOP is set greater than AM, AN and AM will be doupled after each calculation until AM becomes greater than STOP. When AM becomes greater than STOP a new value of BETA is read in from the data cards. The program will terminate automatically when the BETA data cards are exhausted. Control of the temperature range of the calculation is described in the section on Program TRAPS. The last card in the program printout is an example of a data card.

```
TWODI,7,200,60000,400512. MIKE FAYER
*7600
*USERPR
RUN(S)
LINK(X)
-
      PROGRAM TWODI (INPUT,OUTPUT,TAPE5=INPUT)
      REAL KB
      PI=3.1416
      KB=1.38E-16
      STOP=55
90    READ700,BA,BB,DEPTH
      IF(EOF,5) 600,95
95    PRINT500
      PRINT720,BA,BB,DEPTH
      PRINT550
      AM=40.0
      AN=40.0
100   T=4.3
110   SUM1=1.+EXP(-1.*(DEPTH)/(KB*T))
      N=AN+.1
      I=0
1000  I=I+1
      CI=COS(PI*(FLOAT(I)/AN))
      EI=EXP(-1.*(DEPTH-2.*BA*(1.-CI))/(KB*T))
      SUM1=SUM1+2.*EI
      IF(I.LT.N) GO TO 1000
      M=AM+.1
      J=0
2000  J=J+1
      CJ=COS(PI*(FLOAT(J)/AN))
      EJ=EXP(-1.*(DEPTH-2.*BB*(1.-CJ))/(KB*T))
      SUM1=SUM1+2.*EJ
      IF(J.LT.M) GO TO 2000
      I=0
3000  I=I+1
      J=0
4000  J=J+1
      EIJ=EXP(-1.*(DEPTH-2.*BA*(1.-CI)-2.*BB*(1.-CJ))/(KB*T))
      SUM1=SUM1+4.*EIJ
      IF(J.LT.M) GO TO 4000
      IF(I.LT.N) GO TO 3000
      PT=1./SUM1
      PRINT710,T,AN,AM,PT
      IF(PT.GT.0.998) GO TO 120
      T=T-0.3
      IF(T.GT.0.991) GO TO 110
120   AN=2.*AN
      AM=2.*AM
      IF(AN.LT.STOP) GO TO 100
      GO TO 90
600   CONTINUE
500   FORMAT(///,10X,*BA EQUALS BB EQUALS DEPTH EQUALS*,/)
720   FORMAT(8X,3(10X,E12.4))
550   FORMAT(///,10X,*TEMP.        AN            AM            TRAP PROB*/)
710   FORMAT(10X,4F12.5)
700   FORMAT(3F10.4)
      END

-4.96E-16  2.48E-16  42.3E-16
```

REFERENCES

1. J. Frenkel, Phys. Rev. 37, 17, 1276 (1931).

2. A. Sommerfeld and L. Waldmann, Hand- und Jahrbuch der Chemischen Physik--Die Boltzmannsche Statistik und Ihre Modifikation Durch die Quantentheorie, Akademische Verlagsgesellschaft, m.b.H., Leipzig, 1939; R. C. Tolman, The Principles of Statistical Mechanics (Oxford University Press, Oxford, 1967).

3. A. S. Davydov, Theory of Molecular Excitons (McGraw-Hill, New York, 1962).

4. The singularities in the density of states function at $k = 0$ and $\pm\pi/a$ for infinite one dimensional bands is not a problem when the number of exciton k states is limited by a finite number of molecules in the chain.

5. R. S. Knox and A. Gold, Symmetry in the Solid State (Benjamin, New York, 1964).

6. L. Pauling and E. B. Wilson, Introduction to Quantum Mechanics (McGraw-Hill, New York, 1935).

7. L. van Hove, Phys. Rev. 89, 1189 (1953).

8. A. H. Francis and C. B. Harris, Chem. Phys. Lett 9, 181 (1971).

9. A. H. Francis and C. B. Harris, Chem. Phys. Lett. 9, 188 (1971).

10. R. M. Hochstrasser and J. D. Whiteman, J. Chem. Phys. 56, 5945 (1972).

11. A. H. Francis and C. B. Harris, J. Chem. Phys. 57, 1050 (1972).

12a. G. F. Koster and J. C. Slater, Phys. Rev. 95, 1167 (1954); 96, 1208 (1954); V. L. Broude and E. I. Rashba, Sov. Phys. Solid State 3, 1415 (1962); E. I. Rashba, Sov. Phys. Solid State 5, 757 (1963); V. L. Broude and S. M. Kochubei, Sov. Phys. Solid State 6, 285 (1964).

12b. J. Hoshen and J. Jortner, J. Chem. Phys. 56, 933; 4138; 5550 (1972); P. Soven, Phys. Rev. 156, 809 (1967); 178, 1136 (1969); B2, 4715 (1970); H. K. Hong and G. W. Robinson, J. Chem. Phys. 52, 825 (1970); 54, 1369 (1970); H. K. Hong and R. Kopelman, J. Chem. Phys. 55, 5380 (1971); D. P. Craig and M. R. Philpott, Proc. Roy, Soc. A290, 583; 602; A293, 213 (1966).

13. T. Holstein, Ann. Phys. (N.Y.) 8, 343 (1959); M. Grover and R. Silbey, J. Chem. Phys. 54, 4843 (1971).

14. R. W. Munn and W. Seibrand, J. Chem. Phys. 52, 47 (1970).

15. W. Feller, An Introduction to Probability Theory and Its Applications (Wiley, New York, 1966), Vol. II.

16. M. D. Fayer and C. B. Harris, Phys. Rev. BX , XXX (1974).

17. G. W. Robinson and R. P. Frosch, J. Chem. Phys. 37, 1962 (1962).

18. C. Dean, M. Pollak, B. M. Craven and G. A. Jeffrey, Acta Cryst. 11, 710 (1958).

19. E. Kreyszig, Advanced Engineering Mathematics (Wiley, New York, 1967).

20. C. A. Hutchison, Jr. and B. W. Mangum, J. Chem. Phys. 34, 908 (1961).

21. A. C. Albrecht, J. Chem. Phys. 38, 354 (1963).

22. D. S. McClure, J. Chem. Phys. 17, 665 (1949).

23. A. A. Manenkov and R. Orbach, Spin Lattice Relaxation in Ionic Solids (Harper Row, New York, 1966).

24. J. P. Wolfe, Chem. Phys. Lett. 10, 212 (1971); U. Konzelman and M. Schwoerer, Chem. Phys. Lett. 18, 143 (1973).

25. M. D. Fayer and C. B. Harris, unpublished results.

26. J. Schmidt and J. H. van der Waals, Chem. Phys. Lett. 2, 640 (1968).

27. D. S. Tinti, M. A. El-Sayed, A. H. Maki and C. B. Harris, Chem. Phys. Lett. 3, 343 (1969).

28. M. J. Buckley and C. B. Harris, J. Chem. Phys. 56, 137 (1972).

29. M. J. Buckley and C. B. Harris, Chem. Phys. Lett 5, 205 (1970).

30. A. H. Francis and C. B. Harris, J. Chem. Phys. 55, 3595 (1971).

31. R. N. Renaud, D. Kovachic and L. C. Leitch, Can. J. Chem. 39, 21 (1961).

32. G. A. George and G. C. Morris, Mol. Cryst. and Liquid Cryst. 11, 61 (1970).

33. C. B. Harris, J. Chem. Phys. 54, 972 (1971).
E. L. Hahn, Phys. Rev. 80, 580 (1950).

34. W. G. Breiland, C. B. Harris and A. Pines, Phys. Rev. Lett. 30, 158 (1973).

35. C. B. Harris, R. L. Schlupp and H. Schuch, Phys. Rev. Lett 30, 1010 (1973).

36. A. G. Redfield, Phys. Rev. 98, 1787 (1955); I. Solomon, Compt. rend. 248, 92 (1959).
I. Solomon, Phys. Rev. Lett. 2, 301 (1959).

37. M. D. Fayer and C. B. Harris, Phys. Rev. B9, 748 (1974).

38. P. Reineker and H. Haken, Z. Physik 250, 300 (1972); H. Haken and P. Reineker, Z. Physik 249, 253 (1972).

39. If the two spin sublevels coupled by the microwave field have the same phosphorescent emission polarization, then, in principle, the emitted radiation will have a quantum beat modulation at the larmor frequency as discussed in Ref. 33.

40. $K^{T_{1\rho m}}$ is the rate constant for the loss of spin locked pseudomagnetization due to relaxation along the rotating frame magnetic field and is to be distinguished from $K_{T_{1\rho}}$ which is the total rate constant for the loss of spin locked population due to all mechanisms.

41. M. A. El-Sayed and C. R. Chen, Chem. Phys. Lett. 10, 313 (1971).

42. R. V. Nauman, Ph. D. Thesis, University of California, Berkeley, California (1947).

43. Delocalized exciton band is taken to mean any linear combination of the stationary k states of the exciton band. In general, the decay will take place into an admixture of a small number of k states which form a mobile wave packet state. However, the possibility exists that the admixture will contain all k states and therefore will be described by a Wannier function which is centered about a particular lattice site.

44. G. H. Wannier, Phys. Rev. 52, 191 (1937); J. C. Slater, Phys. Rev. 76, 1552 (1949); J. C. Slater, Phys. Rev. 87, 807 (1952).

45. R. Kubo, Phys. Rev. 86, 929 (1952); S. H. Lin, J. Chem. Phys. 44, 3759 (1966); M. Bixon and J. Jortner, J. Chem. Phys. 48, 715 (1968); 50, 4061 (1969); D. M. Burland and G. W. Robinson, Proc. Nat. Acad. Sci. 66, 257 (1970).

46. M. L. Goldberger and K. M. Watson, Collision Theory (Wiley, New York, 1964), Chapter 8.

47. W. Feller, An Introduction to Probability Theory and Its Applications (Wiley, New York, 1966, Vol. I.

48. H. Poincaré, Acta Meth. 13, 67 (1890); R. M. Mazo, The International Encyclopedia of Physical Chemistry and Chemical Physics. Vol. I.

Statistical Mechanical Theories of Transport Processes (Pergamon Press, Oxford, 1967); W. Siebrand, Chem. Phys. Lett. 14, 23 (1972).

49. R. de L. Krönig, Physica 6, 33 (1939); J. H. Van Vleck, Phys. Rev. 57, 426, 1052 (1940).

50. R. C. Tolman, The Principles of Statistical Mechanics (Oxford University Press, Oxford, 1967), p. 512.

51. The Planck distribution function may be employed, provided that anharmonic contributions to the phonon potential are not large, and is certainly adequate for a first order calculation.

52. A model for selective k dependent detrapping can be developed using partially localized crystal eigenfunctions which are solutions to the perturbed periodic potential problem (cf Ref. 12a).

53. In substitutionally disordered crystals where the k states are appreciably mixed, one might have decay of the localized trap state into many k states of the band. Because of the high density of exciton states at $k = 0$ and $k = \pm\pi/a$, the rate of decay of the trap into the band might still be preferential to these states.

54. W. G. Breiland and C. B. Harris, Chem. Phys. Lett. 18, 309 (1973).

55. John W. White, Excitons, Magnons and Phonons Beirut Symposium 1968, A. B. Zahlan, ed. (Cambridge University Press, Cambridge, 1968).

56. G. S. Pawley and E. A. Yeats, Solid State Commun. 7, 385 (1969).

57. The peaking of the density of states function at the top and bottom of the exciton band occurs for one dimensional bands; cf. L. van Hove, Phys. Rev. 89, 1189 (1953) 27. Crystals of $h_2$-1,2,4,5-tetrachlorobenzene and 1,4-dibromonaphthalene have been shown to have one dimensional band structures (cf Refs. 8,9,11,37,58). For $d_2$-1,2,4,5-tetrachlorobenzene

discussed in this paper, it is reasonable to assume a one dimensional band since deuteration will not greatly alter the crystal structure.

58. R. M. Hochstrasser and J. D. Whiteman, J. Chem. Phys. 56, 5945 (1972).

59. The time dependence of the loss of electron spin coherence with the spin locked ensemble is determined by the difference in the larmor frequencies of the two states relative to the life time of the bound phonon-exciton intermediate. In these experiments $\gamma H_1 \simeq 5$MHz while the difference between the band and localized states larmor frequencies ($\Delta\omega$) is about 60 MHz (unpublished results; C. B. Harris). Thus the spin when promoted will dephase with the ensemble in a time of the order of $\Delta\omega^{-1}$ provided $\gamma H_1 < \Delta\omega$. This is the case in these experiments.

60. R. R. Alfano and S. L. Shapiro, Phys. Rev. Lett. 26, 1247 (1971).

61. E. L. Hahn, Phys. Rev. 80, 580 (1950)
H. Y. Carr and E. M. Purcell, Phys. Rev. 94, 630 (1954).
I. Solomon, Phys. Rev. Lett. 2, 301 (1959).
I. Solomon, C. R. Acad, Sci. Paris, 248, 92 (1959).
J. S. Waugh, L. M. Huber, U. Haeberlen, Phys. Rev. Lett, 20, 180 (1968).
J. C. Farrar and E. D. Becker, Pulse and Fourier Transform NMR (Academic Press, New York, 1971).

62. R. P. Feynman, F. L. Vernon and R. W. Hellwarth, J. Applied Physics 28, 49 (1957).

63. E. Merzbacher, Quantum Mechanics (Wiley, New York, 1970), Chapter 13.

64. C. P. Slichter, Principles of Magnetic Resonance (Harper Row, New York, 1963), Chapters 1 and 2.

65. R. H. Dicke and J. P. Wiffke, Introduction to Quantum Mechanics (Addison-Wesley, Reading, 1960), Chapter 12.

66. A. Carrington and A. D. McLachlan, Introduction to Magnetic Resonance (Harper Row, New York, 1967), Chapter 8.

67. A. Abragam, The Principles of Nuclear Magnetism (Oxford University Press, London, 1961), Chapter 2.

68. V. Weisskopf, Ann. Physik 9, 23 (1931).
G. Breit, Rev. mod. Phys. 5, 91 (1933).
P. A. Franken, Phys. Rev. 121, 508 (1961).
M. E. Rose and R. L. Corovillano, Phys. Rev. 122, 1185 (1961).
H. Wieder and T. G. Eck, Phys. Rev. 153, 103 (1967).
R. L. Kelley, Phys. Rev. 147, 376 (1966).
M. Bixon, J. Jortner and Y. Dothan, Mol. Phys. 17, 109 (1969).

69. M. Abramowitz and I. A. Stegun, Handbook of Mathematical Functions (Dover, New York, 1965).
E. Kreyszig, Advanced Engineering Mathematics (Wiley, New York, 1967), Chapter 4.

70. A. Abragam, Op. Cit., Chapters 3 and 12.

71. A. G. Redfield, IBM J. Research Development 1, 19 (1957).

72. F. Bloch, Phys. Rev. 70, 460 (1946).
R. K. Wangsness and F. Bloch, Phys. Rev. 89, 728 (1953).
N. Bloembergen, E. M. Purcell and R. V. Pound, Phys. Rev. 73, 677 (1948).

73. H. C. Torrey, Phys. Rev. 76, 1059 (1949).

74. A. Carrington, Op. Cit., Chapter 11.

75. I. D. Abella, N. A. Kurnit and S. R. Hartmann, Phys. Rev. 141, 391 (1966).

S. R. Hartman, IEEE J. Quantum Electronics 4, 802 (1968).

R. G. Brewer and R. L. Shoemaker, Phys. Rev. Lett. 27, 631 (1971).

76. R. H. Dicke, Phys. Rev. 93, 99 (1954).

R. H. Dicke and R. H. Romer, Rev. of Scientific Instr. 76, 915 (1955).

E. R. Buley and F. W. Cummings, Phys. Rev. 134, A1454 (1964).

I. P. Herman, J. C. MacGillivray, N. Skribanowitz and M. S. Feld, Proceedings of the Vail Conference on Laser Spectroscopy (Plenum Press, 1973).

J. H. Eberly and N. E. Rehler, Phys. Lett. 29A, 142 (1969).

L. Allen and G. I. Peters, Phys. Lett. 31A, 95 (1970).

P. S. Lee, Y. C. Lee, C. T. Chang, Phys. Rev. A 8, 722 (1973).

R. H. Picard and C. R. Willis, Phys. Rev. A 8, 1536 (1973).

77. R. H. Dicke, Phys. Rev. 93, 99 (1954).

78. W. G. Breiland, M. D. Fayer and C. B. Harris, Phys. Rev. A X, XXX (1974).

79. E. R. Buley and F. W. Cummings, Phys. Rev. A134, 1454 (1964).

LEGAL NOTICE

*This report was prepared as an account of work sponsored by the United States Government. Neither the United States nor the United States Atomic Energy Commission, nor any of their employees, nor any of their contractors, subcontractors, or their employees, makes any warranty, express or implied, or assumes any legal liability or responsibility for the accuracy, completeness or usefulness of any information, apparatus, product or process disclosed, or represents that its use would not infringe privately owned rights.*

*TECHNICAL INFORMATION DIVISION*
*LAWRENCE BERKELEY LABORATORY*
*UNIVERSITY OF CALIFORNIA*
*BERKELEY, CALIFORNIA 94720*